Tactile Arrays for Virtual Textures

Submitted by Alan Christopher Brady, to the University of Exeter as a thesis for the degree of Doctor of Philosophy in Physics, September 2010.

I certify that all material contained in this thesis which is not my own work has been identified and that no material has been previously submitted and approved for the award of a degree at this or any other university.

(Signature) .....

Abstract

This thesis describes the development of three new tactile stimulators for active touch, i.e. devices to deliver virtual touch stimuli to the fingertip in response to exploratory movements by the user. All three stimulators are designed to provide spatiotemporal patterns of mechanical input to the skin via an array of contactors, each under individual computer control. Drive mechanisms are based on piezoelectric bimorphs in a cantilever geometry.

The first of these is a 25-contactor array (5 $\times$ 5 contactors at 2 mm spacing). It is a rugged design with a compact drive system and is capable of producing strong stimuli when running from low voltage supplies. Combined with a PC mouse, it can be used for active exploration tasks. Pilot studies were performed which demonstrated that subjects could successfully use the device for discrimination of line orientation, simple shape identification and line following tasks.

A 24-contactor stimulator (6 $\times$ 4 contactors at 2 mm spacing) with improved bandwidth was then developed. This features control electronics designed to transmit arbitrary waveforms to each channel (generated on-the-fly, in real time) and software for rapid development of experiments. It is built around a graphics tablet, giving high precision position capability over a large 2D workspace. Experiments using two-component stimuli (components at 40 Hz and 320 Hz) indicate that spectral balance within active stimuli is discriminable independent of overall intensity, and that the spatial variation (texture) within the target is easier to detect at 320 Hz that at 40 Hz.

The third system developed (again 6 $\times$ 4 contactors at 2 mm spacing) was a

lightweight modular stimulator developed for fingertip and thumb grasping tasks; furthermore it was integrated with force-feedback on each digit and a complex graphical display, forming a multi-modal Virtual Reality device for the display of virtual textiles. It is capable of broadband stimulation with real-time generated outputs derived from a physical model of the fabric surface. In an evaluation study, virtual textiles generated from physical measurements of real textiles were ranked in categories reflecting key mechanical and textural properties. The results were compared with a similar study performed on the real fabrics from which the virtual textiles had been derived. There was good agreement between the ratings of the virtual textiles and the real textiles, indicating that the virtual textiles are a good representation of the real textiles and that the system is delivering appropriate cues to the user.

Contents

List of Tables

List of Figures

Acknowledgements

First and foremost I owe a huge debt of gratitude to my supervisor, Dr Ian Summers for all of his help, support, ideas, knowledge and general cajoling over all of the time we have worked together.

My colleagues in Biomedical Physics Research Group over the years provided both comradeship and a ready supply of willing volunteers to undergo the sometimes rather lengthy experimental tasks. I am also very grateful to the support staff and technicians in the School of Physics and EXAT, without whom some of the manufacturing and programming issues might have proved insurmountable. Co-workers ENACTIVE network of excellence and HapTex project

My final thank you is to Annie, whose patience and encouragement have got me through.

Chapter 1

Introduction

The massive increase in the popularity and availability of small electronic devices over the last few years has provided a springboard for mass adoption of tactile interfaces into consumer devices. Simple push-button operation of devices or keyboard and mouse interaction with computers was the norm, but now we routinely see touchscreen interaction with powerful handheld mini-computers such as the iPhone and gesture-driven (and even body-posture controlled) gaming, spearheaded by the Nintendo Wii. Device manufacturers are now starting to seriously experiment with tactile feedback. Car manufacturers have long invested significantly in the tactile aesthetics of their interiors, and more recently in the feel of their switchgear and door hinges. Premium manufacturers such as Jaguar and BMW have taken this further and have implemented active, electronically controlled profiling of the feeling of some of the key controls and even the steering (e.g. see [3]). Away from the consumer arena, it is now widely appreciated that a degree of tactile and proprioceptive feedback is of great benefit to improve the performance of tele-operation tasks [4] such as hazardous environment work and robot-assisted surgery [5].

Touch research has a long history in the Physics department at Exeter, starting in the early 1980s with the development of the "TAM". This was a wrist worn aid for the deaf which was originally intended to provide the user with a way of being aware of environmental sounds, but which also showed promise as an aid

to lip reading [6]. Over the years, successively more advanced and more complex instrumentation and strategies for tactile aids were developed [7] [8]. In the late 1990s Craig Chanter built the state of the art Tactile Array described in [9], a pure research tool which marked a departure from the development of targeted tactile aid devices. This thesis charts the development of tactile displays at Exeter over a number of years following on from Chanter's work. The work described comes from a range of projects and target applications, with valuable contributions from a number of co-workers - their input is acknowledged in the relevant sections.

The work described herein was not a single project and did not have a single definite objective. Some of the work was performed in parallel. There were multiple revisions, evolutionary dead-ends and more than a little interaction between the development of the hardware, software and experimental ideas in each of the project streams. As a consequence, this thesis does not provide a chronological account. Instead, the work has been grouped into the history of three devices; in each case its development is described, followed by some examples of the experimental work performed on it. In some ways this is a rather artificial presentation as the simpler devices constantly evolved and were used as test platforms for the later devices, and experimental results and software development from the most complex device were then used to improve the older devices. Some of these details have been deliberately omitted for the sake of narrative clarity.

Before we begin looking at the design and development of tactile displays, it is important to first gain some understanding of the complexities of the sense of touch, and to appreciate the good and bad aspects of some other tactile devices. This is the subject of the next chapter. General design considerations are discussed in the following chapter (chapter 3). The three principal research lines are then described, with one chapter for each (chapters 4, 5 and 6). Overall conclusions are drawn in chapter 7.

The material in Chapter 4 relates to an EPSRC-funded project in which all the research was carried out by the author, with his supervisor providing valuable

discussion. The material in Chapter 5 relates partly to the same EPSRC-funded project, and partly the to the EC-funded ENACTIVE and HAPTEX projects. In these EC-funded projects, the Exeter Group was responsible for tactile workpackages in which the great majority of the work was carried out by the author (a second research assistant contributed in building and tesing devices in the HAPTEX project), again with his supervisor providing valuable discussion.

The material in Chapter 6 relates entirely to the HAPTEX project, in which workers from five research groups collaborated to develop a complex multi-modal virtual reality system. As previously mentioned the Exeter Group was responsible for tactile workpackages; the author was responsible for majority of the design, construction and testing of the tactile mechanical hardware described in section 6.4.2, with valuable contributions from a second research assistant and his supervisor, and was a key partner (with workers from Hannover and Pisa) in integrating the complete system. The author also provided the intial schematics and layouts for the electronic drive hardware described in section 6.4.1, and collaborated with the Hannover group to develop and build the design. Along with his supervisor, he played an instrumental role in developing the concepts underlying the rendering algorithms implemented by the Hannover group (outlined in section 6.4.1) and in assembling the system testing strategies described in section 6.5.

Chapter 2

A review of the literature

In this chapter we will consider the sense of touch in some detail, and look into the underlying science behind touch research. This will lead us to some of the devices which have been built for tactile research.

2.1 The sense of touch

Touch is perhaps the most pervasive of the senses. However, its pervasive nature means that touch is probably also the most overlooked. It comprises a series of parallel physiological processes which are processed in a complex manner by the nervous system and brain to create what we experience as tactile perception.

The skin is the largest sense organ in the body - almost 2 m^2 in an adult – and is suffused over its whole area by populations of modified nerve endings. In addition to the cutaneous sensory system, receptors are to be found the tendons, muscles and joints. These, the so called kinesthetic (also known as proprioceptive) receptors, monitor the movement and forces experienced by our limbs, and inform our knowledge of their position in space. When used to actively explore the environment, the sensation arising from the fusion of the various cutaneous and proprioceptive neural inputs is commonly known as haptic touch – a concept originally developed in experimental psychology.

In order to properly appreciate how much the tactile sense completely pervades

our existence, it is worth considering what life might be like without it. Fortunately, medical cases in which the sense of touch has been completely lost are very rare. Gabriel Robles-De-La-Torre describes [10] two such patients who have lost sensory input from below the neck but retain voluntary muscular control. In these cases, the patients were forced to learn to control their limbs using sight to compensate for the missing sense of touch. Even with sight, their movements are ponderous and clumsy, and they tend to use excessive force in manual tasks. Only one of the patients managed to relearn to walk, and it took him considerably longer (and extreme physical effort) to learn how to prevent himself from falling down if the lights go out. If you have experienced a 'ghost limb' from sleeping on top of your arm, you have had a small taste of the complete disorientation that these people must experience every day of their lives.

This thesis is primarily concerned with cutaneous touch. This sense is required to experience the detail of surface texture, curvature, fine contact pressure (particularly of deformable objects) and friction. It is also important for shape detail such as edges and corners. That this is the case can be demonstrated using local anaesthesia to numb the fingertip, or more easily with a thimble. Jansson [11] emphasises that providing spatially distributed information over an extended contact area on the skin is more important than increasing the number of areas that are discretely addressed. This is an important consideration when considering virtual environments.

2.1.1 Communication through touch

The potential of touch as means of communication has long been apparent - Gault [12] and Geldard [13] have both suggested it as an alternative channel of communication which could supplement or replace another diminished or absent sense. Most readers will be at least passingly familiar with Braille – the system of writing developed for the blind. Originally characters were represented by a 2 by 3 array of raised dots embossed on paper. Nowadays, Braille is often used on computer

peripherals called refreshable Braille displays, and a fourth row has been added to encode extra characters. An experienced Braille user can read text at up to 150 words per minute – about half the rate typically reported for print reading. Proficiency in Braille requires extensive training.

A lesser known and less widespread (but equally successful) form of tactile communication is the Tadoma technique used by deaf-blind to understand speech at normal rates, using the hands placed so as to monitor the lip movement and the vibrations of vocal chords of the speaker.

In an attempt to utilise the "neglected sense of communication", Geldard [13] developed a tactile "language" called "Vibratese". This was based on a set of 45 clearly distinguishable stimuli, consisting of 3 intensities and 3 durations of stimuli presented at 5 locations on the subject's chest. With training, rates of 35-60 words per minute could be achieved – substantially better than an expert Morse code reader. Vibratese was an excellent example of what can be achieved when understanding and careful design are applied to a problem. Unfortunately it seems to have disappeared and is only remembered as an academic exercise. A more recent tactile communication device is Tan's "Tactuator" [14] – a handheld device designed for optimum discriminability and which could be used with minimal training. Data rates of up to 12 bits/s were claimed - comparable to Tadoma.

In contrast to the studies above which used stimulation at multiple body sites to improve discriminability, Bliss' Optacon [15] - a device for converting text or line drawings into tactile stimuli – used multiple contactors on a single fingertip, yet was still capable of enabling reading rates in excess of 100 words per minute for an experienced user. The design and construction is relevant to the work in this thesis so it is described in detail in section 2.3.2.

Tactile displays can be used to grab attention, to indicate sense of urgency, or to provide information in a manner which reduces the cognitive load of the user. Van Erp has been at the forefront of pushing tactile displays into high stress, information critical environments, such as providing navigational information to

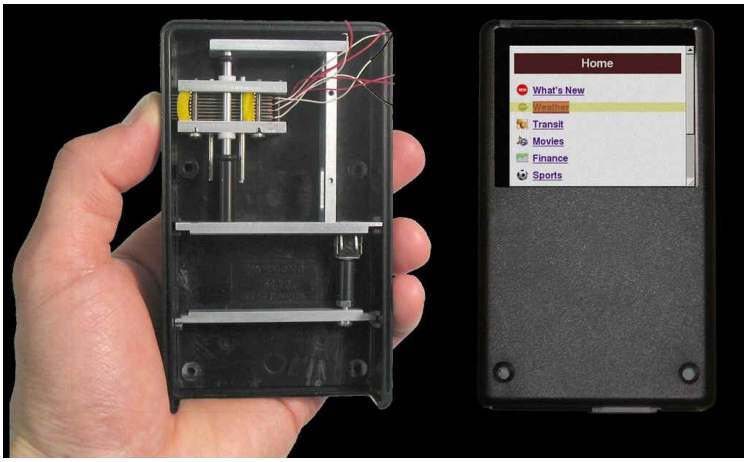

Figure 2.1: The McGill THMB device (*image source: McGill University*)

military helicopter pilots (see for example [16]). Similar work has also been carried out by Cholewiak [17] in collaboration with the US Air Force.

Not everybody is a fighter pilot, but modern life is loading us up with more and more portable electronic devices which clamour for our attention with beeps and buzzes. There is a serious danger that these signals can lose their meaning and become distracting or annoying. Tactile encoding to provide context, intensity and richness of content is being investigated by a number of groups – recent examples are the work of Brown [18] and Chan et. al. [19] . Another approach to contextualisation has recently been demonstrated by Nokia with touchscreen devices (e.g. the Nokia 5230) incorporating tactile feedback.

In order to overcome the limitations of a single vibrator, it will be necessary to make use of a distributed tactile display. The McGill THMB [20] is a simplified version of their Virtual Braille Display (see section 2.3.3). This is an exciting concept which looks like it could be incorporated into a mobile device using existing actuator technologies and batteries.

2.2 The Physiology of the Sense of Touch

In order to design a tactile display it is necessary to know something about the processes involved in the sense of touch; that is to say it is very useful to understand how a stimulation of the skin (be it mechanical, thermal, electrical or some other interaction) is translated into perception. We will focus on mechanical stimulation, although other modes follow similar steps. A mechanical event on the surface of the skin, which itself has a very elaborate structure with complex mechanical interactions (see figure 2.2), triggers a chain of events:

- The skin and underlying tissue essentially form an extended visco-elastic matrix through which mechanical impulses can propogate. The spreading stimulus will then interact with any mechanoreceptors it encounters. The types of receptors are described further in section 2.2.1)

- Any mechanoreceptors which are triggered by the stimulus will begin to send out a train of nerve impulses. Whether this occurs or not will depend on a number of factors including the nature of the stimulus, the type of mechanoreceptor and the recent stimulation history of the mechanoreceptor. Even the simplest of contacts will spread through a reasonably large volume of tissue and will encompass a variety of mechanoreceptors, and so will cause complex patterns of nerve activity from the region.

- The nerve impulses travel from the periphery along nerve fibres. These disparate fibres form bundles as they head up towards the spinal cord and then on to the brain stem. Whilst the processes are not fully understood, it is clear that there is some degree of interaction between the nerve signals in the Central Nervous System, and it appears that a degree of pre-processing occurs in the Dorsal Column Nuclei before the nerve impulses are transmitted to the brain[1].

[1]Studying this neural processing and encoding was one of the goals of the ROSANA project, described further in Appendix B.

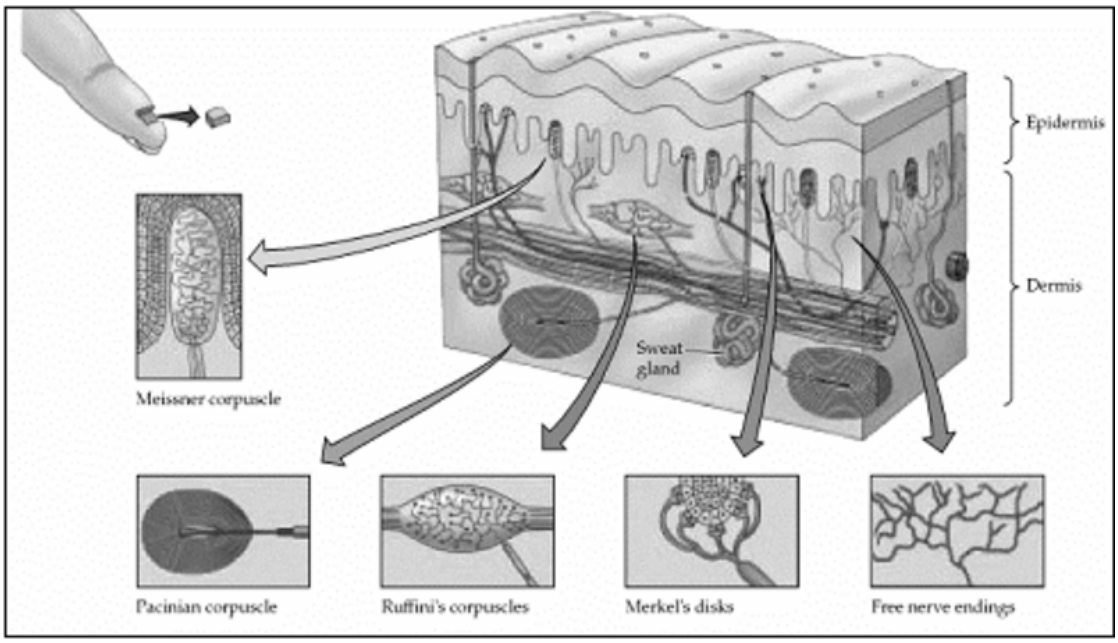

Figure 2.2: The structure of glabrous skin (*Image source: WikiCommons Image*)

- The processed neural signals are responsible for the activation of a number of regions in the cerebral cortex, most notably the primary somatosensory cortex SI and the secondary somatosensory cortex SII (each of which is located bilaterally) [21].

- The sum of this neurological activity is what we understand as perception.

Which of these steps can we understand? If we cannot understand the whole, what use can we make of the parts that we do? Most pertinently, can we use this knowledge to simplify the design of a display or to enable us to interact with the perceptual processes in useful ways?

2.2.1 The structure of skin & its touch receptors

Human skin has a complex layered structure [22] (see figure 2.2). The outer layer (the epidermis) is itself multi layered, consisting of a horny outer layer (the stratum corneum), granular cell and spinous cell layers, and finally the basal layer which may be ridged. Overall the epidermis is between 0.1 to 1 mm thick. Underlying the

epidermis and loosely bound to it is the dermis. This is a (mainly) collagen-elastin matrix, and is typically about 4 times thicker than the epidermis. Within the dermis can be found blood vessels, hair follicles, sweat glands and nerve structures. These are of particular relevance to this discussion and are described in more detail below. Finally, separating the dermis from the underlying tissues, is a layer of subcutaneous fat. This is a gel like matrix of adipose tissue which drastically varies in thickness across the body and between individuals.

The mechanical properties of the skin with regards to impulses and vibration depend on the transmission of energy between and along the layers. This is complicated by the presence of hair, ridges and other surface variations, the hydration of the epidermis, the state of the collagen matrix in the dermis, the thickness of fat layer and the nature of underlying tissue, whether it be muscle, bone or otherwise. In other words, whilst it is possible to construct simple models of the skin (e.g. see the work of Manschot & Brakkee [23]), these are only valid for a given localised region of the body, and it is likely that the parameters within the model will vary from individual to individual and even from day to day. This is not to say that models cannot provide very useful information and insight; it is important to realise the limitations of such models and not to draw over-generalised inferences from them.

As mentioned above, there exist within the skin a number of types of sensory structures referred to by the general name mechanoreceptors, and these can be very abundant in sensitive areas. For example, there are on average 17000 skin receptors in the human hand [24]. The simplest of these are nerve fibres with free nerve endings – the others feature various kinds of encapsulation which modify the mechanical sensitivity. Although there is evidence which suggests a good degree of specificity in the roles of particular classes of mechanoreceptor, there has been some difficulty of correlating the structures with sensory modalities [25]. This is presumably because there is a degree of overlap between the sensitivities of the different classes of receptors.

The classes of mechanoreceptor are as follows:

- Free nerve endings (figure 2.3a) are a group of different types of unmyelinated nerve endings that respond to mechanical, thermal or noxious stimulation.

- Hair Follicle Endings (figure 2.3b) can be found wrapped around hair follicles in hairy skin. They respond to hair displacement, and are very important for some mammals.

- Merkel (figure 2.3e) cells are are found in the stratum basale (at the bottom of sweat duct ridges) of the epidermis. They are usually associated with sensory nerve endings; in this state they are known as Merkel nerve endings. Their somewhat rigid structure, and the fact that they are not encapsulated, causes them to have a sustained response to mechanical deflection of the tissue. They are the most sensitive of the four main types of mechanoreceptors to vibrations at low frequencies, around 5–15 Hz. Merkel nerve endings are extremely sensitive to tissue displacement, and may respond to displacements of less than 1 μm.

- Meissner corpuscles (figure 2.3d) are primarily located just beneath the epidermis within the dermal papillae of glabrous skin. They consist of unmyelinated nerve supported by horizontal lamellae surrounded by a connective tissue capsule. They respond to vibration, and are most sensitive in the 20–40 Hz range.

- Ruffini Endings (figure 2.3f) are spindle-shaped receptors found in the deep layers of the dermis of both hairy and glabrous skin which are sensitive to skin stretch and pressure on the skin. They are thought to contribute to the kinesthetic sense of and control of finger position and movement; in this way they are used for monitoring slippage of objects along the surface of the skin, allowing the modulation of the grip on an object. However, some authors have expressed doubt about the role of Ruffini endings in humans because of the lack of histological evidence that they exist in sufficient numbers [26].

- Pacinian corpuscles (figure 2.3c) are multi layered onion-like structures consisting of 20 to 60 concentric lamellae composed of fibrous connective tissue and fibroblasts and separated by gelatinous material surrounding the central unmyelinated nerve. They are found in the deep layers of the dermis in both hairy and glabrous skin. They respond to vibration, and are most sensitive in the 150–300 Hz range. This is thought to be due to mechanical filtering by the structure; fluid flow within the structure very rapidly allows the environment around the neuron to return to it's equilibrium state. This means that Pacinian corpuscles react mainly only to changing stimuli as they rapidly adapt to static pressures [27].

- Finally, and of less relevance to this thesis, Krause (bulbous) endings are bulbous structures which are primarily located in the mucous membranes and the genitals. They are formed by the expansion of the connective-tissue sheath of a medullated fibre. They are primarily sensitive to low frequency vibrations, but have also been linked to temperature [28].

We have considered the physical make up of the organs of touch, and the presumed role of the mechanoreceptors. In the next section, we will consider what happens after a mechanoreceptor has been stimulated.

2.2.2 Neurophysiology

The physical interaction of a stimulus with a mechanoreceptor is mediated by the mechanical environment and by the structure of the receptor. The response of the receptor can be seen as action potentials or spikes in the nerve fibres connected to it. Multiple mechanoreceptors can be attached to a single fibre. These excitations can be studied by electronic recording (discussed below). Neurophysiologists have noted that the firing rate in some nerve fibres drops off very rapidly after the application of a stimulus, whereas others maintain their rate at a high plateau for many (tens of) minutes after the initial stimulus. These two groups are respectively classified as Rapidly Adapting (RA) and Slowly Adapting (SA) fibres. Additionally

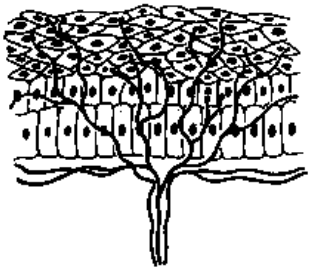

(a) Free Nerve Endings.

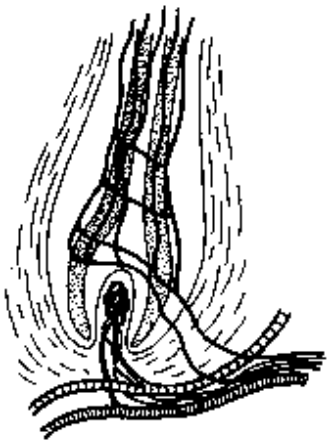

(b) A Hair Follicle Ending.

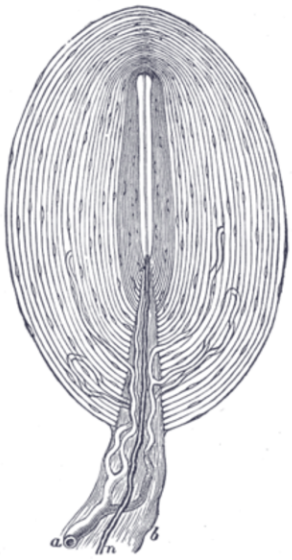

(c) A Pacinian Corpuscle.

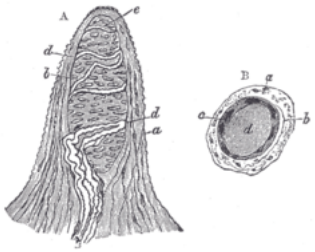

(d) A Meissner Corpuscle.

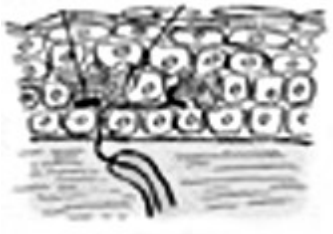

(e) Merkel Cells in the epidermis.

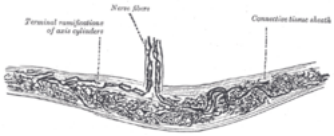

(f) A Ruffini Corpuscle.

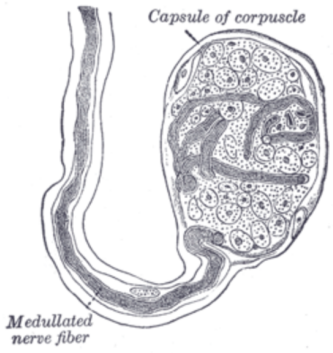

(g) A Krause corpuscle.

Figure 2.3: Structures of the touch receptors found in the skin. (*Images from WikiCommons.*)

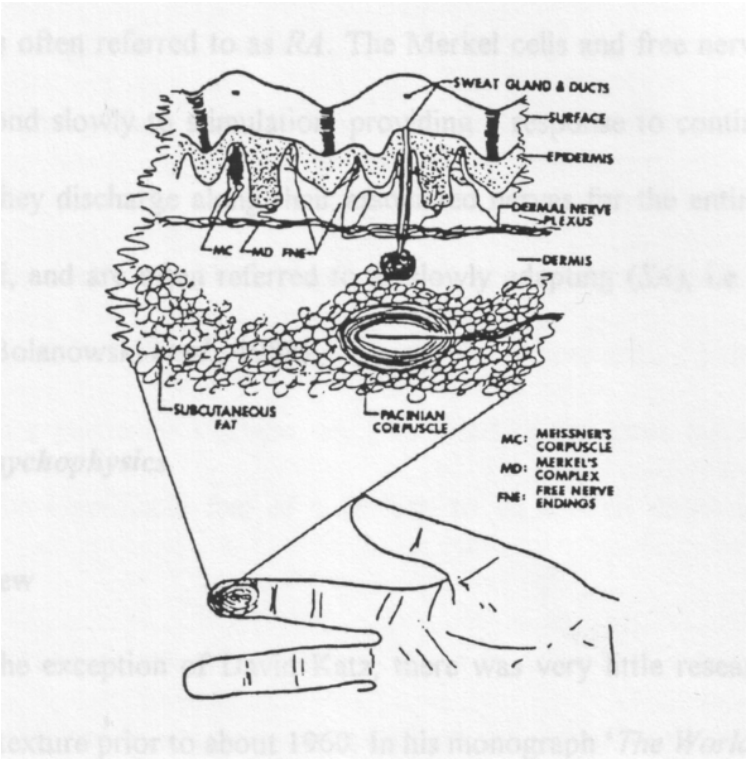

Figure 2.4: Location of mechanoreceptors in the fingertip. (*After* [2])

it has been noted that some fibres only respond to stimuli applied to a very localised area of the skin, whereas others respond over a much larger area - up to several tens of square millimetres. These latter fibres are said to have a larger receptive field and are classified as type II fibres. Several studies (e.g. [29])indicate that type I fibres (those with a small receptive field) mediate high resolution tactile discrimination, and are responsible for the ability of our finger tips to feel fine detailed surface patterns (e.g. for reading Braille). These observations can be rationalised by assuming that type I fibres are associated with receptors close to the skin surface, whilst type II fibres are more deeply connected - it seems reasonable to assume that a deeply seated receptor will experience stimuli from a larger area of the skin. Using this inference it is reasonable to suggest that Merkel endings are associated with SAI nerve fibres and Ruffini endings with SAII. By the same logic, hair follicle cells and Meissner corpuscles should be associated with RAI fibres, leaving Pacinian Corpuscles associated with the RAIIs. Free nerve endings may

be slow, intermediate or rapidly adapting. Whilst some do respond to mechanical stimulus, their role in tactile perception is unclear.

The observations and classifications above are the result of direct recordings of nerve activity, made using cuff, hook or needle electrodes around (or in the case of the needle, into) nerve bundles. Several of these studies have been directly related to tactile perception. These have mainly used primate subjects, although there are a few groups e.g. Johansson's who have had success with humans [30]. Of particular relevance to this thesis are the moving dot studies by carried out by Johnson [31], Lamotte [32] and Philips [33]. Philips also investigated the effect of scanning velocity on afferent response, showing that the mean afferent response rate increased with velocity but that response per dot increases with decreased velocity. In the latter study, nerve bundle recordings were made in a primate whilst the subject's finger was exposed to moving dot patterns. These recordings were used to generate spatial event plots, and showed encoding of spatial information within the afferent responses. Analysis of these data suggest that afferent spatial resolution is comparatively coarse – of the order of 1.5 mm.

The neural encoding of tactile movement has been studied by Gardner [34] [35] and Ruiz [36]. In the same study, Gardner compares activity in cutaneous afferents with activation of the somatosensory cortex and concludes that there is no coding in channels associated with Pacinian afferents. NB The ROSANA project described in appendix B attempted a more detailed study comparing the neural response to complex tactile stimuli in both peripheral nerves and in the cortex.

In this section we have seen how a mechanical stimulus is converted into a complex pattern of neurological events and how the overlapping sensitivity of neighbouring afferents leads to the concept of receptive fields. However, in order to understand how these might relate to perception, it is necessary to actually study the perception of an individual as they experience a stimulus. Some techniques and results using this approach are described in the next section.

2.2.3 Psychophysics of touch perception

Psychophysics is a discipline within psychology which treats the perceptual process as a "black box", and is based heavily on signal detection theory. It was described by Gescheider [37] as the scientific study of the relation between stimulus and sensation. The basis of the approach is to plot out "psychometric functions" of the relationship between a quantifiable parameter of a physical stimulus and the responses of a person who has to decide about a certain aspect of that stimulus. A number of techniques are used, but almost all are based on the use of detection thresholds, scaling or just noticeable differences to map out the "perceptual space".(See also [38].)

With the exception of some early studies by Katz during the 1920s, serious interest in tactile psychophysics research did not begin until the 1960s. Since then, a large body of work has amassed. Some of these studies have looked at tactile analogues of what would normally be considered to be visual tasks, for example the examination of the perception of form, size, orientation and spatial localisation [39] [40] [41]. In other studies, a number of groups (e.g. Lederman [42]) have explored the crossover of the tactile sense with visual and auditory stimuli, and Srinivasan's group has investigated [43] the tactile interpretation of curved surfaces. Of more interest to this discussion are studies that focused on perceptual processes which could be described as more overtly in the tactile domain such as cutaneous texture.

Lederman [44] and Taylor [45] examined various aspects of the perception of gratings (for example effects on roughness from variations of the macroscopic geometry and from varying contact force). Subjective roughness was found to depend strongly on the groove width, but much less so on the land width or the spatial frequency. Counter-intuitively, perceived roughness was found not to be a function of friction coefficient [46]. Patterns of dots and other embossed surfaces used to evoke sensations of roughness have been studied by a number of workers, e.g. Tanaka [47], Lamb [48] and Irwin [49]. Perhaps the most important observa-

tion was made by Connor and Johnson who noted that roughness is not a simple function of spatial period [50].

All of the studies described above were based on the perception of real objects; in many cases this has been custom made apparatus. Katz suggested that roughness perception is mediated by vibrations [51]. This is a very reasonable supposition; it is straightforward to show how motion can translate a spatial pattern into a temporally varying stimulus, and we have already seen that the mechanoreceptors are sensitive across a range of frequencies. These ideas have been developed by Hollins and co-workers([52] [53]). This raises some important questions: what is the role of motion in perception, and how are vibrations perceived? The relative motion between the skin and an object generates the vibrations that Katz described, but is the motion a necessary part of the perception? It has been posited that tactile perception is an active process, i.e. that it is enhanced by conscious exploration by the subject (e.g. see [54]). However, Lederman showed that the rate of hand motion is unrelated to the roughness perception of gratings [55] and Craig [56] made use of the Optacon (see 2.3.2) to compare scanned dot patterns to static ones, noting that the static patterns were easier to identify, particularly at short presentation times.

There is an extensive amount of research documented in the literature which is exclusively focused on the perception of vibratory stimuli, covering such topics as sensitivity as a function of frequency, effect of contactor size, spatial and temporal summation as well as a whole wealth of interpretations and direct applications. Perhaps the first question to address is the frequency range and sensitivity of the human tactile sense.

Figure 2.5 shows the 4 channel model proposed by Bolanowski [57]. In this model, the tactile afferents are grouped into four classes as previously described in section 2.2.2. The thresholds of the four individual channels is shown along with their implied combined threshold. There is excellent agreement with the measured overall detection threshold. It is important to remember that this study

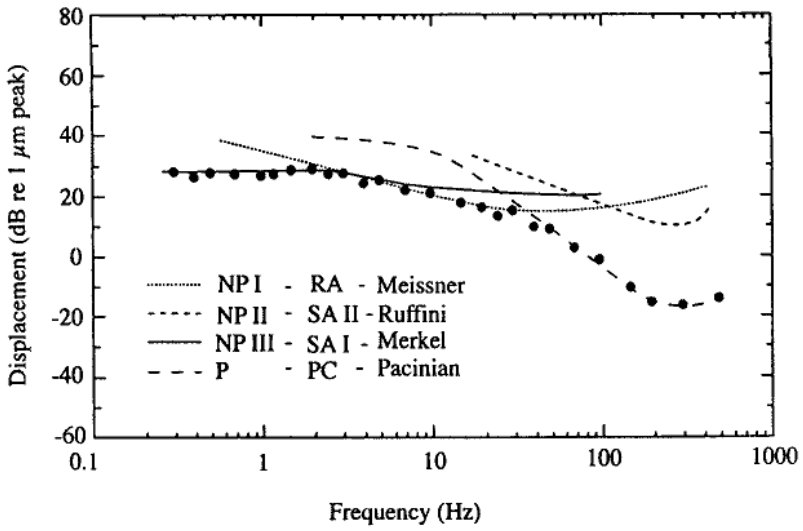

Figure 2.5: The four channel model of tactile perception as proposed by Bolanowski (*After Bolanowski et al.*)

(as with most described here) was performed using psychophysics techniques at the threshold of perception; in contrast, the majority of tactile perception occurs at supra-threshold levels. The perceptual processes involved are likely to result from the balance of excitation across the afferent populations and not from any single receptor type. This supposition is supported by Van Doren [58]. In a model based on strains in the dermis, he suggests that temporal tuning (i.e. the local frequency sensitivity) is a property of the individual receptor (in agreement with other authors, e.g. Bolanowski) whereas spatial properties (e.g. the apparent spatial acuity) are due to the mechanical influence of the surrounding tissue.

Figure 2.6 shows a plot of equal-sensation contours mapped out by Verrillo et al. [59] using a ≈ 1 cm^2 contactor on the thenar eminence (a body of muscle on the palm of the hand just beneath the thumb). It can be seen that at threshold, the sensitivity increases with increasing frequency to reach a peak at around 250 Hz before dropping away again. Above threshold, the high frequency fall-off is less pronounced. The frequency response curve exhibits two domains: a reasonably flat region at low frequencies, and a U-shaped curve peaking at about 250 Hz at higher frequencies. This has been interpreted on the basis that the mechanisms

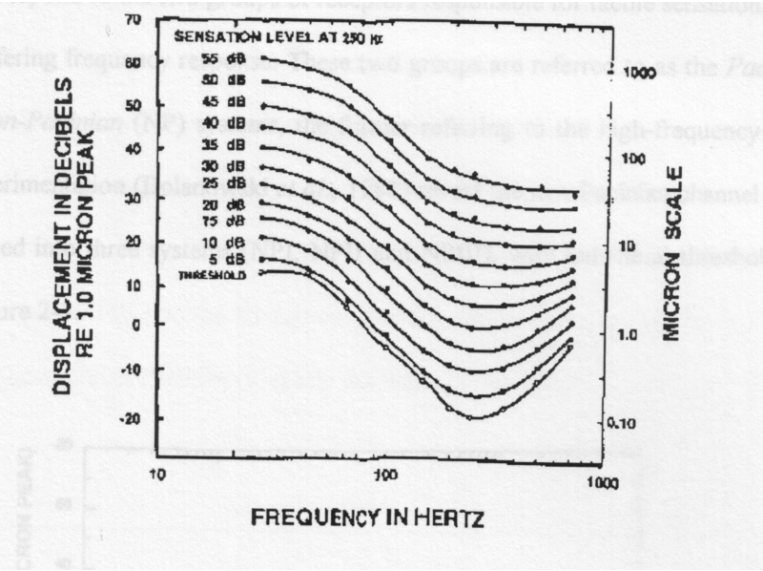

Figure 2.6: Equal sensation curves as a function of intensity and frequency, as mapped out by Verrillo et al. (*After Verrillo et al.*)

responsible for tactile sensation fall into two groups with differing response to frequencies. These have historically been referred to as the Pacinian (PC) and non-Pacinian (nPC) systems; whilst the nomenclature might not be strictly correct, the two channel model is useful and one to which we shall return later. It has been observed by Van Doren [60] that isolation of regions of skin uniformly raises the perceptual thresholds within the area without changing the tuning - this implies that individual receptors are not spatially and temporally independent.

The size of a vibrating contactor is clearly a potential factor in how a stimulus can be perceived, as increasing the size potentially recruits additional receptors. Spatial summation - that is to say the effect that a change in contactor size has on the sensitivity - has been studied by Craig [61] and Verillo [62]. Figure 2.7 shows that for small contactors the perceptual threshold is effectively independent of the frequency whilst the larger contactors show a 3 dB increase in sensitivity per doubling of the contactor area at frequencies above 40 Hz. It is also worth noting that stimuli applied by closely spaced small contactors will be perceived in the same way as a single larger contactor. This means that a variable contact area can be represented by the number of active elements in an array of smaller contactors

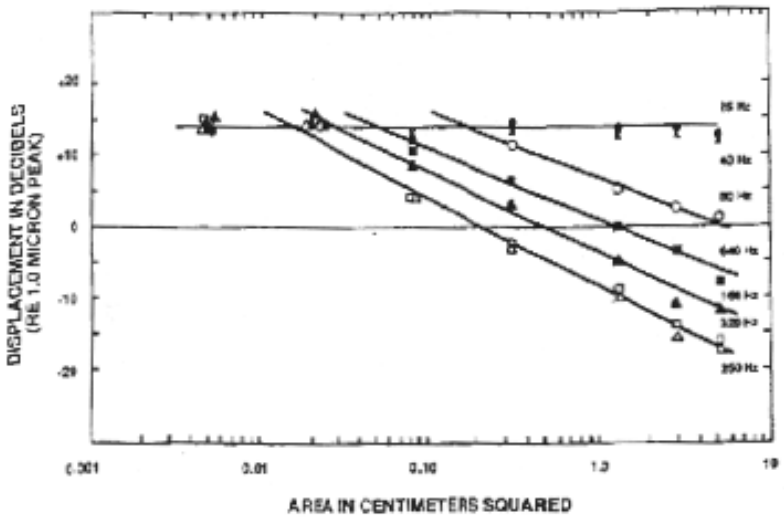

Figure 2.7: Detection thresholds for different contactor sizes, as mapped out by Verrillo et al. (*After Verrillo et al.*)

and has important implications for the design of tactile arrays. Mujiser [63] reports that spatial summation is not present in Pacinian channel, implying that the RAI channel is where the spatial summation is occurring. However, most authors (e.g. Bolanowski and Verillo) prefer the explanation that the Pacinian channel is the one capable of spatial summation. Whilst it is beyond the scope of this thesis to attempt to explain this discrepancy, it will be discussed further in chapter 5.

Humans are able to discriminate very fine textures with structure sizes well below the resolution of the SAI receptors, so these cannot be the only receptors responsible for the perception of roughness. The importance of the fingerprints for the perception of fine textures has been investigated by Scheibert [64]. Two sensors imitating the geometrical and mechanical properties of the human fingertip were developed. Only one sensor surface was patterned with ridges mimicking the fingerprints. Comparing the frequency responses of the sensors, the sensor with ridges shows a reduced damping in a frequency range that corresponds to the sensitivity range of the PC sensors at a typical exploration velocity of 12-15 cm/sec. The authors conclude that the fingerprints play an important role in the perception of fine surface textures.

With a mean receptor spacing of around 1.3 mm in the fingertip, it is perhaps not surprising that the spatial acuity of the fingertip is of the order 1 to 2 mm, and that this is frequency dependent [33] [65]; this is smaller than the average 2 point discrimination threshold [66].

In addition to spatial and frequency effects, the duration of stimuli and the inter-stimulus temporal spacing have an influence on perception. A touch receptor may fire multiple times during the lifetime of a stimulus pulse; these events might be integrated by the Central Nervous System (CNS). Similarly it is reasonable to suppose that there is a finite time-window associated with a detection event, and that therefore stimuli that are too close together in time cannot be discriminated. This was considered in some theoretical detail for the auditory case by Zwislocki [67], who proposed a theoretical framework describing temporal summation. This model correctly predicts the observed 3 dB lowering of threshold for each doubling of stimulus duration and was applied to the tactile system by Verillo [68]. Verillo also showed that temporal summation effects can be observed for up to 1000 ms. Gescheider and Verillo [69] examined the effects of enhancement and suppression of one stimulus by another at the same and different body sites, and Lederman [70] showed that two 1 ms pulse stimuli need to be separated by 5.5 ms to be resolved.

The nature of the temporal response of the tactile sense can be exploited to generate tactile and vibrotactile illusions such as saltation (mislocalisation of stimuli) and apparent motion described by numerous workers including Sherrick and Cholewiak [2] and Geldard [13]. One such example is the "Cutaneous rabbit". In this illusion, a series of short (2 ms) taps are presented at two body sites. If the timing parameters are correct, this is experienced as stimulus hopping discretely across the skin between the presentation sites, "like a tiny rabbit". Whilst this is similar to apparent motion, it is considered as a separate effect because in apparent motion the sensation is continuous. Cholewiak and Collins claim that the quality of a saltatory presentation is comparable to a real physical stimulus.

In this section we have seen how the tactile sense is investigated, and had a taste of how knowledge of its workings can be exploited to present complex sensations with relatively simple stimuli. The sensations experienced through touch can be structurally complex over relatively short length scales, and moreover these are experienced in parallel. Therefore, in order to create a tactile display capable of providing feature-rich sensations to the skin, it is necessary to produce a distributed display, i.e. one that can present varying stimuli across its surface, ideally over length scales comparable to the tactile acuity of the subject. In the next section we will look at some of the devices that have been made to do just this.

2.3 Tactile Displays - state of the art

2.3.1 Approaches for distributed displays

This section describes a selection of the devices and technologies that have been built as tactile displays. Whilst this thesis is focused on the development of displays for presenting vibratory stimuli, there are other mechanisms which have been exploited to transfer information to the touch receptors. One of these is to make use of the stretch of the skin - this is described in greater detail in section 2.3.3.

Another strategy is to directly stimulate the peripheral nerves using electric currents – examples of such devices have been reported by various workers, for example [71], [72]. (A more recent example is that presented by Kajimoto [73]). These devices are appealing because they could theoretically reproduce precisely correct signals in each nerve fibre to elicit a given percept. However, this would rely on the electrodes being directly coupled into the nerves, and whilst such research is being carried out (e.g. CyberHand, IST-FET Project #2001-35094), most of the devices that have been made are affixed to electrodes on the skin surface. This causes two major drawbacks. Firstly, there is no control over which nerve fibres are stimulated, so at best the stimuli will not feel like a real object because of the lack of temporal cues across the different perceptual channels, and at worst the

perception generated is one of pain! The second problem arises from the variations of skin/electrode impedance. Even with constant-current drive signals it is very difficult to set a comfortable level. In the author's experience of such devices, there tends to a be an unpleasant positive feedback loop in which an uncomfortable stimulus creates some slight anxiety in the subject, expressed in the form of resistance-reducing perspiration and stronger stimulation.

Some displays try to represent macroscopic shapes and surfaces. This is an excellent way of conveying dimensions, curvature and mechanical properties, but is not so useful for the display of complex shapes or fine details. They typically use electric motors [74] [75] for their drive, and some make clever use of haptic illusions, but these are beyond the scope of this review. There have even been shape displays demonstrated which use electro- or magneto-rheological materials [76], [77], [78] to create the forms. These devices require a substantial amount of associated hardware (and often involve hazardous compounds) to create what can at best be described as unconvincing virtual objects. In their defence these have been early prototypes, but it is hard to envisage a future for such technologies in tactile displays.

There have also been attempts to produce thermal displays using peltier heat pumps [79], although at the time of writing the author is unaware of any multiple-contactor devices that have been successful. The addition of a thermal dimension would certainly improve both the information carrying aspect and the believability of a tactile display device, as temperature can provide important cues to material properties. (For example, wood feels warmer than stone which in turn feels warmer than metal.)

Moving on to displays intended to display textures or patterns to the skin, there have been a number of actuation technologies employed. Devices have been reported which generate vibrations at the surface of the skin indirectly using Surface Acoustic Waves (SAW) [80] or the radiation pressure from ultrasonic transducers [81]. These show great innovation, but at present seem to lack in power and as

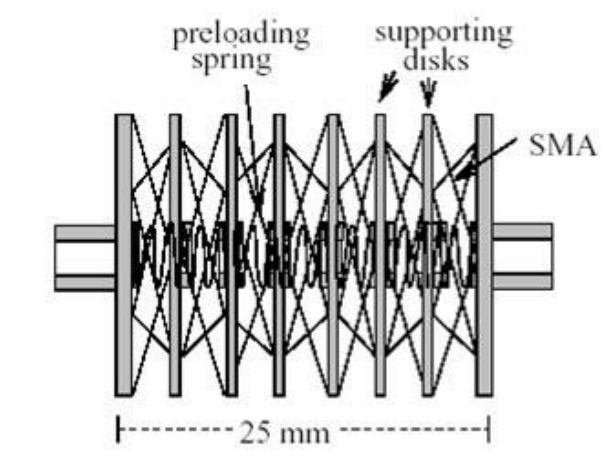

Figure 2.8: Schematic of a Shape-Memory Alloy based display (*After Taylor et al.*)

yet are little more than single contactor devices. Somewhat more successful have been devices based on direct or indirect pneumatic interaction with the skin, via air jets [82], suction plates [83] and inflatable bladders [84]. These devices do actually function as true distributed displays, successfully transmitting simple patterns. However, with pneumatic systems the combination of valves, dead volumes, compliance in pipes etc. mean that they typically have insufficient operating bandwidth to cover the full tactile spectrum.

The most successful distributed displays have been those which directly address the skin with moving contactors. Electric motors can deliver very precise control and achieve high bandwidths, but a device to address a fingertip via multiple contactors is very expensive and complex to make. An excellent example of the type was reported by Schneider [85]. This device used jacketed cables to connect 400 linear motors to the 400 contactor elements at 0.5 mm spacing.

Shape memory alloys, which can be used to make powerful yet compact actuators as shown in figure 2.8, have been used to overcome the complexity hurdle (Taylor [86]). Unfortunately such devices are limited by their ability to dissipate heat – timescales associated with cooling the elements between strokes limit the stimulus repetition rate.

Direct electromechanical drive would seem to be the best solution, both in terms of reducing complexity and increasing the bandwidth of the device. Miniature voice coils have been developed by Hafez [87], and a device based on Micro-electromechanical systems (MEMS) is under development by Talbi [88]. These have the potential to become viable, dense broadband displays, although there is still a question mark remaining over whether such devices are capable of delivering sufficient displacement amplitudes with acceptable power consumption.

The most widely used technology for tactile display devices is based on piezo-ceramic bimorph actuators, described in detail in 3. The form of these devices (see figure 2.9) creates an intrinsic mechanical amplifier which can convert high bandwidth drive signals into large displacements and relatively large forces. Their down-side is that they require high voltages to operate and their relatively large footprint can lead to complex device geometries. Nevertheless, the piezoelectric bimorph dominates the landscape of distributed tactile displays. Pin arrays driven by them are at the heart of commercial refreshable Braille cells such as those produced by UBI (California) or Metec (Stuttgart) (see figure 2.10). They are also at the heart of the Optacon (see 2.3.2 below) and the Exeter Tactile Array (see 2.4 below) as well as more recent devices by Kyung et al. [89] and Shigeki [90]. It is also possible to contact the finger directly with the end of a stack of bimorphs, as was shown by van Doren [91]. A similar approach is utilised in the McGill VBD and StreSS devices (see 2.3.3 below).

The design of piezoelectric bimorph driven pin-arrays will be discussed in more detail in Chapter 3. In the following sections we will look in more depth at three successful tactile displays.

2.3.2 The Optacon

The Optacon (**OP**tical to **TA**ctile **CON**verter) is not state-of-the-art in the conventional sense as it was developed in the 1960s [15] [92], but it was the original compact distributed tactile display, and is the benchmark for all subsequent de-

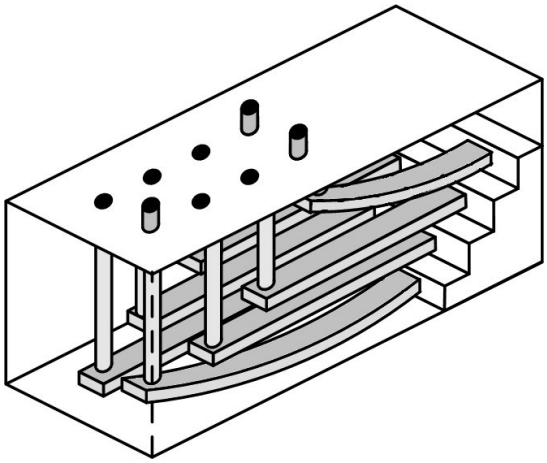

Figure 2.9: Schematic representation of a Braille cell (*Image source: McGill University*)

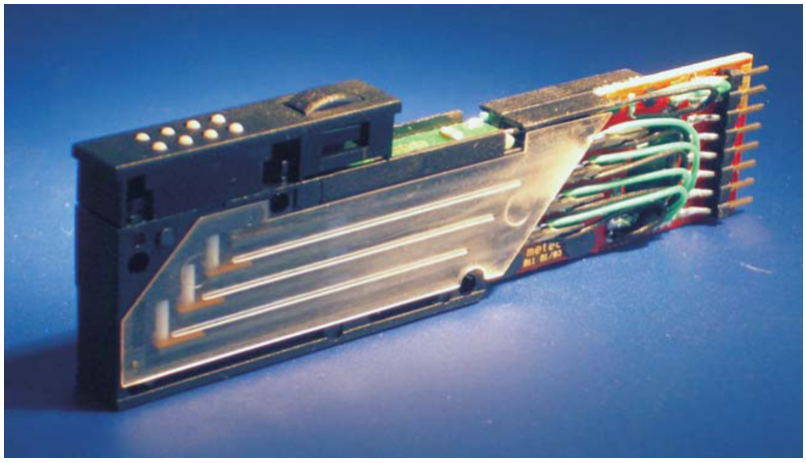

Figure 2.10: A commercial Braille cell from Metec (*Image source: Metec AG*)

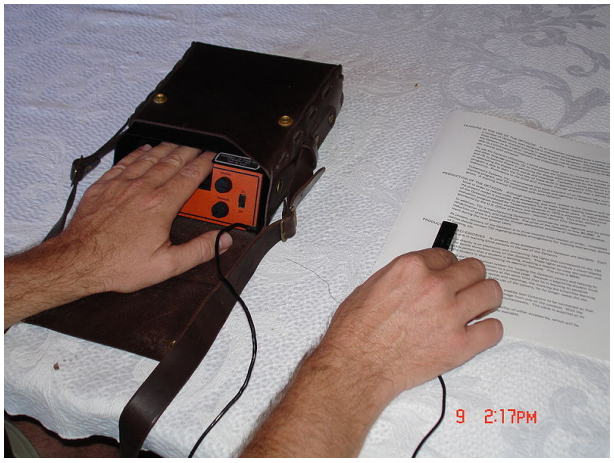

Figure 2.11: The Optacon in use (*Image source: Wikimedia Commons*)

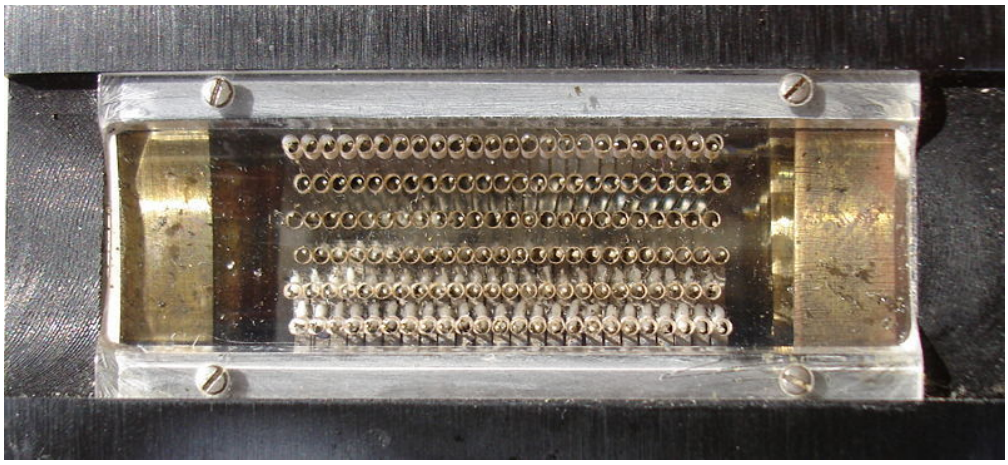

Figure 2.12: The surface of the Optacon

vices. In 1962 John Linvill (Stanford) visited an IBM laboratory in Germany and saw a printer based on an array of pin-hammers. Inspired by this, he set out to develop a device for his blind daughter Candy. The machine he created was designed to display text read by array of photocells into a pattern displayed on a grid of metal pins. U.S. Patent 3,229,387 was granted in January 1966.

The display itself consists of a 24 (1 mm) × 6 (2 mm) array of pins driven by piezoelectric bimorphs.

Linvill calculated that for reading rates of 100 words per minute, vibration rates of at least are 200 Hz required – in practice the bimorphs are driven at their resonant frequency 238 Hz. Skilled users can read at half the speed of a skilled Braille

reader (approximately one tenth the speed of sighted reading). This shows both the tremendous skill at tactile pattern recognition of the users, and the high information transfer rate possible through the device. Bliss' data [15] showing useful reading with 144 stimulators on a fingertip appears to be in conflict Geldard's research using vibrators distributed over the body (see section 2.1.1). The difference is between communicating using two dimensional tactile images versus an 8 point code. Both Bliss and Geldard were reporting similar reading rates, but in the days before high accuracy optical character recognition, the Optacon approach was much more practical. The Optacon remained in production between 1971 and 1996. At its peak, some 15000 were in use, and there is still an active community of users. The excellent display has also been adapted for use in psychophysics experiments([56] [93]). The primary limitation of the Optacon as a psychophysics tool or more general tactile display, apart from its general scarcity these days, is its single frequency on-resonance drive. This means that even if completely new control circuitry is installed to allow the operator to precisely control the output signals, the display is effectively mechanically limited to operate at 238 Hz.

2.3.3 StreSS

At the same time as the work described in this thesis was being carried out, Vincent Hayward's group at McGill was pursuing an alternative strategy. Hayward reasoned that since some of the mechanoreceptors are particularly sensitive to skin deformations, high quality sensations could be induced by locally stretching and compressing the skin in a lateral manner as shown in figure 2.13.

As a result of this, the Virtual Braille Display (VBD) was constructed [94]. This device (shown in figure 2.14) consists of a stack of piezoelectric bimorph elements, presented so that the subject's finger touches their edges only in much the same way as van Doren's linear display.

The results from this device were very encouraging - it provides a very realistic sensation similar to Braille dots or square edges - leading the team to attempt to

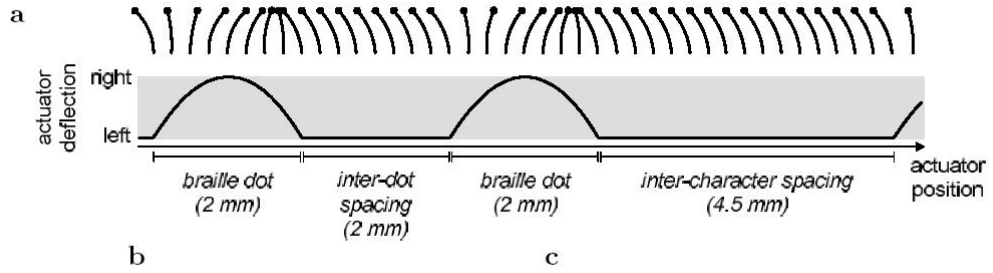

Figure 2.13: Motion of the actuators in the VBD. (*image source: McGill University*)

Figure 2.14: The McGill VBD. (*image source: McGill University*)

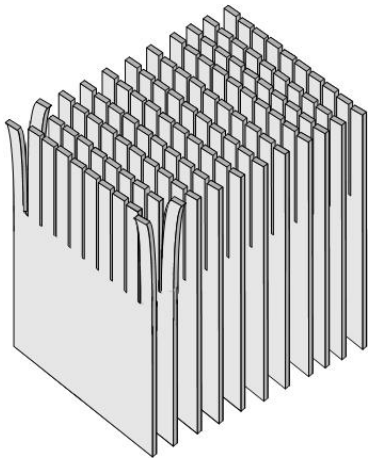

Figure 2.15: Concept of the StreSS actuators. (*image source: McGill University*)

make a 2 dimensional version. The StreSS 2D array was made by cutting bimorphs into a comb as shown in figure 2.15. This first device demonstrated that principle worked, but was far too weak to be a useful display. Subsequent devices have proved much better and the devices are now capable of delivering an excellent sensation [95]. One version used a curved contact plate in an attempt to improve finger contact, although this feature was subsequently dropped as overly complex. The device has recently been integrated into 2D Force-Feedback workspace. Whilst the overall experience is very good, it unfortunately exposes a flaw in the design - its directionality. The performance is noticably different between the left-right and top-bottom directions. Stimuli moving along the plane of the combs are not (in the author's opinion) very good; they are also tricky to model and to code for. Overall though this is a very impressive device. The modular design seen in StreSS2 probably hints at the way future tactile displays will be made. The small actuators allow MEMS drivers to be used, vastly simplifying the drive electronics, and an on-board Field Programmable Gate Array (FPGA) handles much of the signal processing. This has the double advantage of reducing the computing overhead in the controlling device, and greatly simplifies the cabling.

Figure 2.16: The StreSS 2 Device. (*image source: McGill University*)

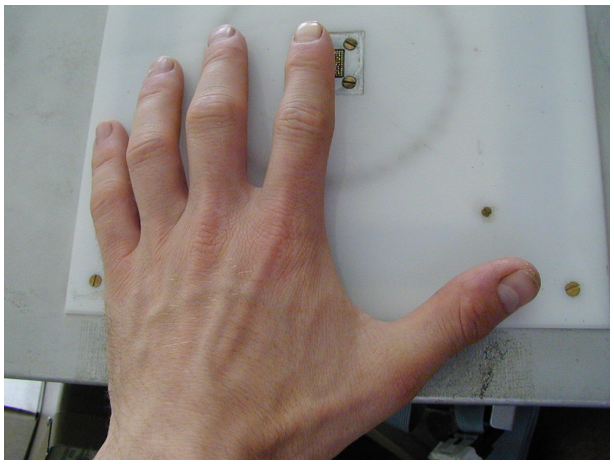

Figure 2.17: The Exeter Tactile Array

2.4 The Exeter Tactile Array

The purpose of the Exeter Tactile Array project was to develop the Optacon-like display concept into a more versatile broadband display, capable of (for example) exploring and utilising the Bolanowski 4-channel model of tactile perception via stimulation at different frequencies. The device was built by Craig Chanter as part of his PhD work [96] and consists of a 10 by 10 grid of driven pins, spaced 1 mm apart as shown in figure 2.18.

The pins are driven by 100 piezoelectric bimorph elements, arranged in a stack

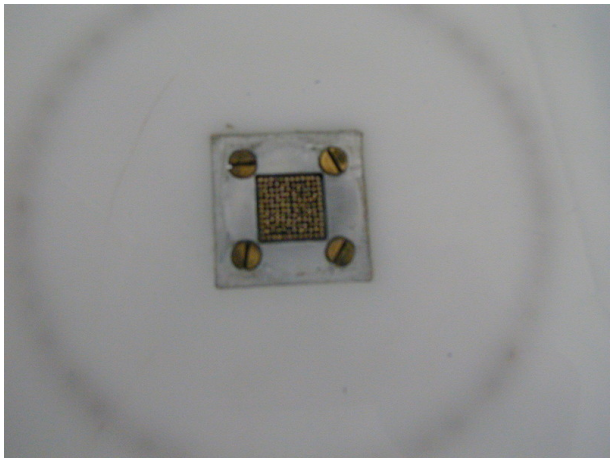

Figure 2.18: The contactor surface of the Exeter Tactile Array, constructed by Chanter

of rings underneath the working surface of the array (figure 2.19).

Each channel is driven by a high voltage amplifier and each amplifier is connected to an 8 bit digital to analogue converter (DAC) so that arbitrary waveforms can be independently generated on every pin. The device is only really limited by its large size and the computing technology available when it was built - waveforms have to be laboriously transferred into external memory chips before they can be displayed, and the maximum duration of an individual stimulus is approximately 2 seconds. However, it is a truly successful broadband device; its output sensitivity is (to a first approximation at least) flat across the tactile sensitivity range. In normal operation it is used with two frequencies (40 Hz and 320 Hz) in accordance with the suggestion of Bernstein [97]. It delivers very realistic (and truly 2 dimensional) sensations, and the results obtained by Chanter successfully demonstrate the existence of two independent channels in tactile perception. [9]

Chanter's Tactile Array is an excellent device. It has high resolution, broad bandwidth (20 – 500 Hz), and perhaps most importantly in use it provides a "realistic"sensation - it genuinely feels as though an object is moving across one's finger.

It is however limited by its relatively weak output - a comfortable sensation can

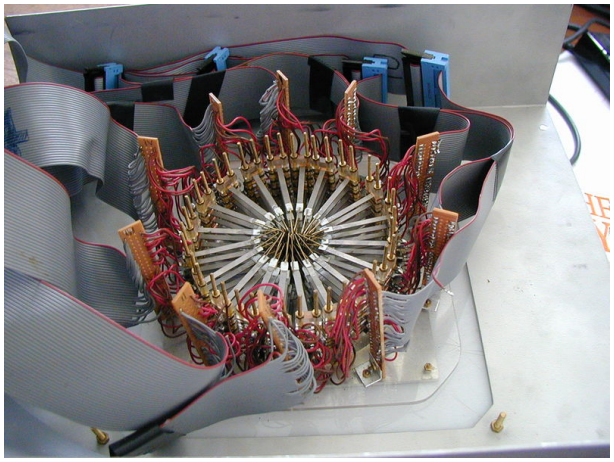

Figure 2.19: The workings of the Exeter Tactile Array

only be achieved by running the amplifiers at full power. Furthermore it is a very complex construction - it is large, fragile, and difficult to maintain. Its large size also means that it can only ever be used as a desktop device for one finger only.

The control hardware is limited presenting short (up to 2 seconds), pre-written stimuli with a long (up to 20 second) gap between stimuli. The software written by Chanter was constrained to 2 fixed frequencies (40Hz and 320Hz), presented in 0.1 second time frames (this was modified by the author and Jon Whybrow to 0.025 second frames).

The devices described in the following chapters seek to improve where possible, and to add additional capabilities.

2.5 Summary

Touch is a complex process that involves several distinct perceptual channels, each with its own specific temporal and spatial characteristics. The design of multi-contactor tactile stimulators to provide effective stimulation via these channels is not easy. The next chapter provides further discussion of design considerations and how the design process is informed by information about the sense of touch.

Chapter 3

Design Considerations for Tactile Arrays

In this chapter we will consider the general form and the actuation technology suitable for the construction of vibrotactile displays, and will develop models to tune the parameters of these actuators.

3.1 Stimulation method

Section 2.3 described a number of approaches towards presenting information to the sense of touch. These approaches fall into two main classes, according to whether the device should attempt to create real shapes, topologies and textures, or whether it should try to create illusions by attempting to mimic the activation patterns within the sensory afferents and in effect "tricking" the perceptual processes. The former approach, whilst intuitively appealing, will always be limited by its geometry at both large and small length scales; that is to say there will always be large step changes or curvatures which are beyond the range of the device, and mechanical considerations mean that there is a very real lower limit on the size of features that can be displayed. Furthermore, by presenting a "real" object, the corresponding "real" perception may be best obtained if the subject has to actively move their fingers over the display. Whilst this is a very natural way to

experience a tactile sensation, it means that the device has to be large enough to present a useful workspace, and there is little or no control over how the subject interacts with the the display. Consequently it is the latter approach (tactile "illusions" created through afferent stimulation) which is followed in this thesis. Of all of the stimulation methods described in the previous chapter, the vibrotactile approach is the most mature and best understood; this is the technique underlying the devices described in the following chapters. The first task to address is "how to deliver discrete vibratory stimuli to points across the surface of the skin?"

3.2 Contactor spacing

Up until this point, the discussion has been deliberately broad about tactile perception across the skin as a whole. However, when building a display it is necessary to design the device to match the part of the body being addressed. Tactile displays have been made to fit the hand [14], the forearm [98], parts of the face [73] (including even the tongue [99]) and the torso [16], but the most logical place to site a display for texture is on the fingertips. The fingertips are amongst the most sensitive parts of the body having a very high density of touch receptors. Perhaps just as importantly they are the part of the body that is generally the most acquainted, i.e. the best trained, to perform tactile discrimination tasks as that is how they are used throughout everyday life.

Having decided to address the fingertips with vibrating contactors, we are now faced with the question, "How many contactors are required, and how should they be spaced?" The goal is to produce an appropriate excitation pattern over the various populations of mechanoreceptors in the skin. The spatial resolution required for the contactor array is thus related to the density of these receptors which is of the order of 1 per mm^2 on the fingertip, or to the spatial acuity on the fingertip, which is around 1 mm [29]. This would imply that the contactor spacing should be 1 mm or less. Is this reasonable? The psychology literature also stress the importance of the size of receptive fields of individual receptors. However, if

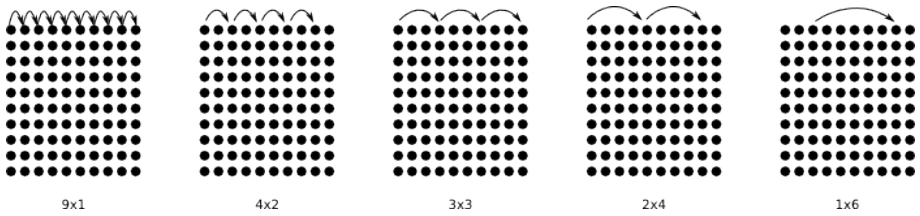

Figure 3.1: Intervals presented as a function of time

we believe van Doren's model, this relates to mechanical transmission across the skin and is largely irrelevant to stimulation via an array.

3.2.1 Experimental study - Pin spacing

As previously noted, the mean spacing of the Merkel touch receptors in the fingertips is of the order of 1 mm, suggesting that tactile actuators need to be arranged to have a similar spacing. However since these are believed to provide a minor role in relation to vibratory stimuli (see section 2.2.2), might a larger actuator spacing be sufficient?

An experiment was designed to investigate this point. Chanter's 100 pin 1mm resolution array was used to present subjects with "moving bar" stimuli[1] with varying step sizes (see figure 3.1). They were then asked to identify the step interval best represented by pictures on a reference card.

All four primary movement directions (left to right, right to left, top to bottom and bottom to top) were presented using drive waveforms at both 40 Hz and 320 Hz. The stimuli were presented in a random order, and the subjects' hearing was muffled using noise masking to remove the possibility of audio cues. A training sequence was provided before the test in an attempt to remove any learning effects.

[1]In a moving bar stimulus, a complete row or column of pins is activated at one edge of the array. This line is deactivated as another parallel set is activated. This continues sequentially across the array until the other edge is reached. The sensation is comparable to sliding ones finger across a raised or embossed line on a surface. The sensation is particularly realistic for vibratory stimuli around 40 Hz.

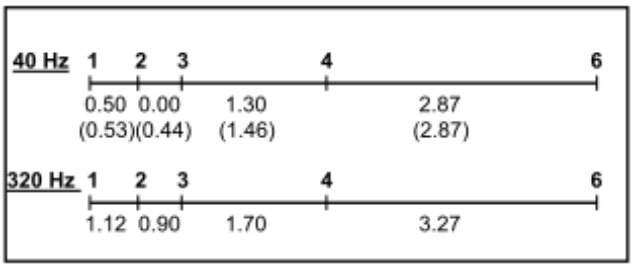

Figure 3.2: Representation (not to scale) of the discrimination index d' between the 5 stimulus presentations.

This kind of experiment generates a huge amount of data. In order to interpret the results, a certain amount of statistical analysis and processing is required, often using a signal technique such as d' analysis[2]. In this case the d' values in figure 3.2 indicate that subjects cannot distinguish between moving targets with 1 mm spacing and 2 mm spacing when the targets are presented at 40 Hz, and the difference is only just noticeable at 320 Hz. This is in agreement with Chanter's observations [9] that spatial acuity is lower at 40 Hz, and with Garcia-Hernandez *et al.* [100] who in a recent study of shape recognition performance of edge-based patterns explored through nonactuated arrays of vertically moving pins found that "a tactile array of 1.8 mm tactor spacing and 1 cm^2 array size transmits the pattern information with a good level of accuracy."

These results suggest that an array with a pin spacing of 2 mm should give equivalent performance to a dense array at 40 Hz, and should have only slightly inferior performance at 320 Hz. This opens the door to devices that are mechanically much simpler than Chanter's array – moving from 1 mm to 2 mm spacing will reduce the number of actuated pins by a factor of four. This will greatly simplify the task of building a compact display.

[2]The discriminability index d' is a statistic used in signal detection theory. In this, we conceive of sensitivity as (broadly) detecting a signal (e.g. against background noise, or compared to another signal), and model how a perceiver decides whether a signal is present. It is calculated as $d' = \frac{\text{separation}}{\text{spread}}$. A higher d' indicates that the signal can be more readily detected.

3.3 Choice of Actuator Technology

The actuator technologies available for vibrotactile transduction have already been described in section 2.3. The key requirements for the actuators are:

- The bandwidth of the actuator must be sufficient to address the RA populations of mechanoreceptors in the skin.
- The actuators must be sufficiently powerful to deliver a strong stimulus.
- The actuators must be capable of dense packing. This does not necessarily mean that the entire actuator must be small, but the form factor must allow for contactors to be tightly grouped without the use of complex linkages.

Linear motors have excellent performance, but the overall size of the device and the complexity of the linkages make them very unattractive as components of a small, lightweight display. Pneumatic and hydraulic systems are also complex, but more importantly are unlikely to have the bandwidth required. Shape Memory Alloy based actuators suffer from the same problem, leaving electromechanical technologies such as voice coils or piezoelectric devices as the logical way to proceed. The decision to use was taken to use piezoelectric bimorph bender elements as they are relatively cheap, simple to use, and have built in mechanical amplification so large amplitudes can easily be achieved. They are described in more detail in the following section.

3.3.1 Piezoelectric bimorphs

A piezoelectric material is one which the internal polarisation density can be modified by an externally applied stress, resulting in the generation of a potential difference across the sample. These materials are typically crystalline or ceramic, but the effect is also exhibited by some polymers. The application to actuators arises from the fact that the piezoelectric effect is reversible. In the reverse piezoelectric effect, a material will undergo a deformation in response to an applied

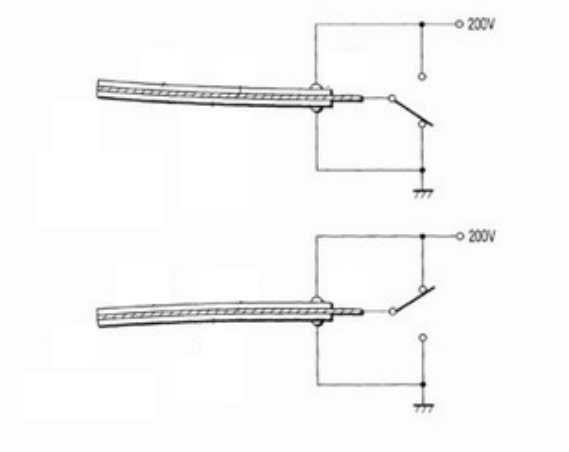

Figure 3.3: Operation of a piezoelectric bimorph.

electric field. For example, lead zirconate titanate (a typical piezoelectric ceramic) will deform by up to about 0.1% of the original dimension. The high field strengths required to produce the maximum range of motion can require relatively high voltages (200–300 V). Care must be taken as too high a field will depolarise the crystal, upsetting the "frozen-in" alignment of the internal electric dipoles in the material and destroying its piezoelectric properties.

Single crystals are not that useful on their own, and are typically used with some kind of amplification mechanism. The simplest of these is a stack. Multiple layers of piezo-ceramic are bonded together, separated by electrodes. These are wired up so that all of the parallel elements distort in the same direction, multiplying both the distance moved and the force generated by the number of stack elements. Piezoelectric stacks are relatively expensive, but can generate quite high forces over short distances (e.g. a $10\times10\times18$ mm stack is capable of generating a blocked force in excess of 3 kN with an applied voltage of 100 V, but the free displacement is less than 15 μm), and are typically used in high precision equipment such as nano-positioning stages.

In order to generate larger movements it is necessary to use a lever. This could be externally attached, but in piezoelectric bimorph bender elements the lever ratio is generated by the geometry of the device.

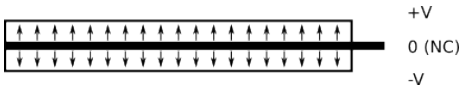

Figure 3.4: Schematic representation of a series poled piezoelectric bimorph.

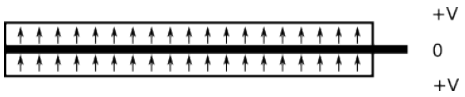

Figure 3.5: Schematic representation of a parallel poled piezoelectric bimorph..

The bimorph is a structure made from two layers of piezo-ceramic. These are wired up so that the applied voltage forces one layer to expand while the other contracts, causing the plate to bend perpendicular to the applied voltage. This effect is proportional to the square of the unsupported (free) length of the bimorph.

Note that there are two ways that the plates could be arranged in such a device. The first and simplest arrangement is the one in which the polarisation of the plates are anti-aligned, with electrical connections being made to the outer faces. This is known as a serial bimorph. These only require 2 electrodes, but as a consequence they require high voltages to operate; this same factor makes serial bimorphs excellent force sensors. Conventional parallel bimorphs have the polarisation of their plates aligned in an anti-parallel manner. The plates are separated by a central third electrode which allows the same voltage to be applied to each plate, in opposite senses. This only requires half the voltage to achieve the same displacement as the two-wire serial arrangement, but at the cost of the third connection and the associated wiring.

3.4 Choice of Bimorph

3.4.1 Design Parameters

The purpose of the actuators is to present linear motion at the skin surface. Ideally the output response should be flat across the frequency spectrum so that the ex-

perimenter can have confidence that the stimulus delivered is what was intended. Of course, this is an unrealistic aim even with the best actuator. Choosing a cantilever (a resonant system) means a non-flat frequency response. The biggest decision is where to place the primary resonance. At first glance it is tempting to design the system such that the resonance is above the range of peak tactile sensitivity i.e. above 500 Hz. However, we have already seen in section 2.2.3 that the human tactile frequency response is not flat. The configuration of the cantilevers in Chanter's array was such that the subjective amplitudes in the two frequency channels (40 Hz and 320 Hz) were approximately equal, allowing a narrow dynamic range of drive amplitudes to be used. This is a useful tool for reducing complexity, and so in the following sections we shall examine how to produce devices which can deliver signals in two frequency channels with amplitudes and power appropriate to tactile sensitivity, based on a model for the cantilever and the bio-mechanics of the skin.

3.5 Modelling

3.5.1 Some useful relations[1]

For a parallel wired bimorph with dimensions l,w and t, the free displacement δz induced by voltage V is given by

$$\delta z = \frac{3 d_{31} V L^2}{2t^2} \tag{3.1}$$

where d_{31} is is the strain coefficient (deflection normal to polarisation direction) of the piezoelectric material.

Under a load force F with no applied voltage,

$$\delta z = \frac{4 F L^3}{E w t^3} \tag{3.2}$$

where E is the Young's modulus of the material.

The spring constant k_0 is the gradient of the force-extension curve, i.e. $\frac{F}{\delta z}$, so rearranging 3.2 we see that for a bimorph:

$$k_0 = \frac{F}{\delta z} = \frac{Ewt^3}{4l^3} \tag{3.3}$$

From this we can obtain the resonant frequency, using the standard relation

$$\omega_0 = \sqrt{\frac{k_0}{m_0}}$$

where $m_0 = 0.24\rho wLt$, the effective mass of the cantilever.

Note also that an applied voltage V is equivalent to an applied force

$$F = \frac{Ewt^3}{4L^3}\frac{3d_{31}L^2}{2t^2}V = \frac{3Ewd_{31}t}{8L}V$$

3.5.2 Simple Dynamic Model of a Bimorph

Background

As a first approximation we can model a bimorph cantilever damped by its contact with the skin of a fingertip as a mass on a spring subject to a force

$$F_r^{'} = \frac{3Ewd_{31}Vt}{8L}$$

from equation 3.5.1.

This is governed by the equation

$$(m_{\text{skin}} + m_0)\ddot{x} + (r_{\text{skin}} + r_0)\dot{x} + (k_{\text{skin}} + k_0)x = F_r^{'} \tag{3.4}$$

where m_0, k_0 and r_0 are the effective mass, spring constant and damping resistance of the cantilever, and m_{skin}, k_{skin} and r_{skin} are additional impedance components provided by the skin's mechanical load, i.e. the skin impedance is

$$z_{skin} = \frac{f}{\dot{x}} = j\omega m_{skin} + r_{\text{skin}} + \frac{k_{skin}}{j\omega}$$

giving us

$$m_0\ddot{x} + r_0\dot{x} + k_0x + z_{skin}\dot{x} = F_r^{'} \tag{3.5}$$

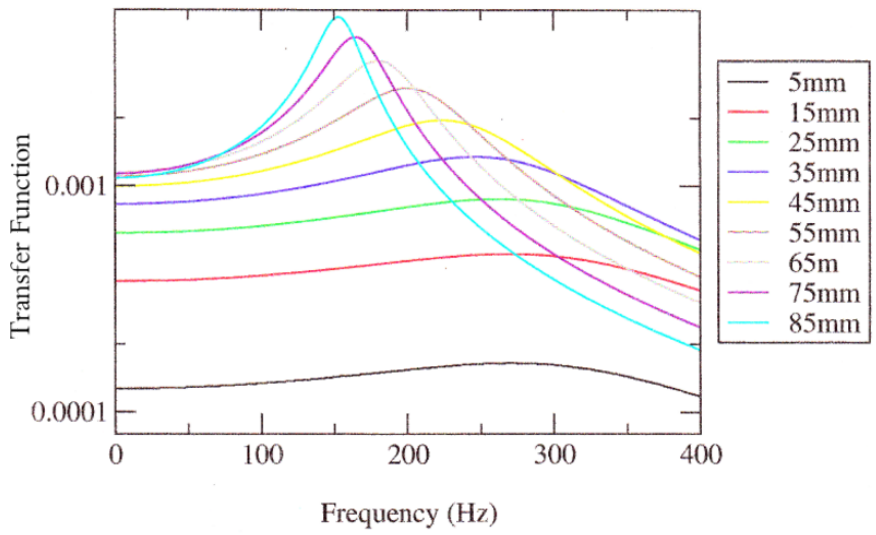

Figure 3.6: Modelling of system frequency response for different lengths of piezoelectric drive element.

By combining equations 3.4 and 3.5, and assuming a periodic solution such that $x = e^{j\omega t}$, we can obtain an expression for the transfer function $\frac{\dot{x}}{V}$

$$\frac{\dot{x}}{V} = \frac{\frac{3Ewd_{31}t}{4L}}{j\omega m_0 + r_0 + \frac{k_0}{j\omega} + z_{skin}} \tag{3.6}$$

Note that below the resonance the response is primarily due to the compliance whilst above resonance it is mass dominated.

Numerical modelling

We can solve equation 3.6 numerically, as in the following examples.

In this way we can "place" the resonance between our low frequency and high frequency channels so that differences in skin sensitivity at the two frequency are balanced by differences in the system response.

Limitations of the model

This model assumes that the tip of the cantilever undergoes simple harmonic motion. It does not account for any higher order modes.

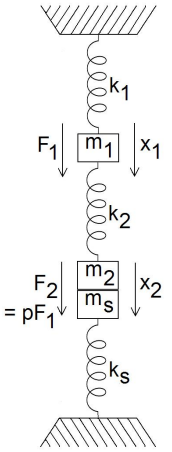

Figure 3.7: Two spring model of a cantilever

Whilst the higher order resonances would seem to be beyond the range of tactile perception, we have not considered the fact that the fingertip can act as node and introduce a set of beam modes. At the tip of the cantilever these appear as "anti-resonances" i.e. major dips in the transfer function.

We are attempting to place high frequency channel above ω_0 - we must take care that this is not too close to the first "anti-resonance". This requires a refinement in the model.

3.5.3 An improved model

We can take account of higher order modes by modelling the cantilever not as a single mass on a spring, but as a chain of masses on springs. Each additional mass and spring will add an extra resonant mode to the model.

We are only interested in the first two modes, so our model is:

$$F_1 = m_1\ddot{x}_1 + r_1\dot{x}_1 + k_1x_1 - k_2(x_2 - x_1) \tag{3.7}$$

$$F_2 = m_2\ddot{x}_2 + r_2\dot{x}_2 + k_2(x_2 - x_1) \tag{3.8}$$

as in section 3.5.2, the mechanical load from the skin (assumed to be in contact with mass m_2 can be represented by increases to the parameters m_2, r_2 and k_2,

and so is not shown explicitly in the analysis.

Substituting $x = e^{j\omega t}$ and rearranging in terms of x_1 gives

$$x_1 = \frac{F_1 + k_2 x_2}{-\omega^2 m_1 + j\omega r_1 + k_1 + k_2} \tag{3.9}$$

$$x_1 = \frac{x_2(-\omega^2 m_2 + j\omega r_2 - k_2)}{k_2} \tag{3.10}$$

Solving for x_2 gives

$$x_2 = \frac{k_2 F_1 + (-\omega^2 m_1 + j\omega r_1 + k_1 + k_2)F_2}{(-\omega^2 m_1 + j\omega r_1 + k_1 + k_2)(-\omega^2 m_2 + j\omega r_2 - k_2) - k_2^2} \tag{3.11}$$

If we assume $F_1 = pF_2$ (where p is a constant),

$$\frac{x_2}{F_1} = \frac{p}{m_2} \frac{-\omega^2 + \frac{j\omega r_1}{m_1} + \frac{k_1 + k_2(1+\frac{1}{p})}{m_1}}{(-\omega^2 + \frac{j\omega r_1}{m_1} + \frac{k_1+k_2}{m_1})(-\omega^2 + \frac{j\omega r_2}{m_2} + \frac{k_2}{m_2}) - \frac{k_2^2}{m_1 m_2}} \tag{3.12}$$

Note that the denominator is quadratic in ω^2, i.e. the denominator is gives a double resonance at frequencies given by

$$(-\omega^2 + \frac{k_1 + k_2}{m_1})(-\omega^2 + \frac{k_2}{m_2}) - \frac{k_2^2}{m_1 m_2} = 0 \tag{3.13}$$

If the roots of this are $\omega^2 = \omega_1^2$ and $\omega^2 = \omega_2^2$ we can rewrite the denominator of equation 3.12 to give

$$\frac{x_2}{F_1} = \frac{p}{m_2} \frac{-\omega^2 + \frac{j\omega r_1}{m_1} + \omega_0^2}{(-\omega^2 + \frac{j\omega r_1'}{m_1} + \omega_1^2)(-\omega^2 + \frac{j\omega r_2'}{m_2} + \omega_2^2)} \tag{3.14}$$

where r_1' and r_2' are chosen to give the same damping, and

$$\omega_0^2 = \frac{k_1 + k_2(1 + \frac{1}{p})}{m_1}$$

$$\omega_1^2 = \frac{1}{2}((\frac{k_2}{m_2} + \frac{k_1 + k_2}{m_1}) - (\sqrt{(\frac{k_2}{m_2} + \frac{k_1 + k_2}{m_1})^2 - \frac{4k_1 k_2}{m_1 m_2}}))$$

$$\omega_2^2 = \frac{1}{2}((\frac{k_2}{m_2} + \frac{k_1 + k_2}{m_1}) + (\sqrt{(\frac{k_2}{m_2} + \frac{k_1 + k_2}{m_1})^2 - \frac{4k_1 k_2}{m_1 m_2}}))$$

Equation 3.14 shows that the response can be modelled with three terms, each with a modulus of form

$$\left(\omega^4 - (2 - \frac{1}{Q_i^2})\omega_i^2\omega^2 + \omega_i^4\right)^{\frac{1}{2}}$$

where Q is the Q-factor of the resonance or anti-resonance.

We can consider a particular case $k_1 = k_2 = k$, $m_1 = m$ and $m_2 = \frac{m}{2a}$, where a is a constant, the first resonance occurs at

$$\omega_1^2 = \frac{k}{m}((1+a) - \sqrt{1+a^2}) \tag{3.15}$$

the second resonance occurs at

$$\omega_2^2 = \frac{k}{m}((1+a) + \sqrt{1+a^2}) \tag{3.16}$$

and the anti-resonance at

$$\omega_0^2 = \frac{k}{m}(2 + \frac{1}{p}) \tag{3.17}$$

Note that

$$\omega_1^2\omega_2^2 = \frac{k^2}{m^2}((1+a)^2 - (1+a^2)) = \frac{2ak^2}{m^2}$$

So

$$\omega_0^2 = \frac{\omega_1\omega_2}{\sqrt{2a}}(2 + \frac{1}{p})$$

Now for a cantilever the expressions for ω_1 and ω_2 are identical except for their constnts, so we require $\frac{\omega_2}{\omega_1} \simeq 6.3$. Using a value $a = 20$ gives $\frac{\omega_2}{\omega_1} = 6.49$ - close enough for the sake of this model. With this value for a, we can derive the relations

$$\frac{\omega_0}{\omega_1} = \sqrt{\frac{2 + \frac{1}{p}}{(1-a) - (1+a^2)^{\frac{1}{2}}}} \simeq \sqrt{2 + \frac{1}{p}}$$

and

$$\frac{\omega_0}{\omega_2} \simeq \frac{1}{6.3}\sqrt{2 + \frac{1}{p}}$$

Some examples of the frequency response given by this model are shown in figure 3.8 which shows how the relation between the anti-resonance frequency ω_0 and the resonant frequencies ω_1 and ω_2 depends on p.

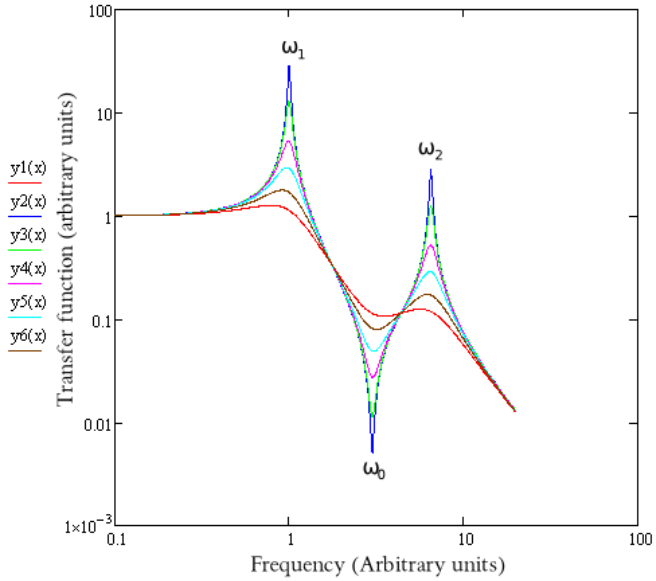

Figure 3.8: Relationship between the anti-resonance frequency ω_0, the resonant frequencies ω_1 and ω_2, and p

It should be noted that this model is still very very basic. It only works for cantilevers with a high aspect ratio and it takes no account of strain or out of plane shear deformations.

3.6 Other design considerations

3.6.1 MRI compatibility

One of the first research tasks the Tactile Array was pressed into was to provide repeatable tactile stimuli as part of a functional Magnetic-Resonance-Imaging (fMRI) study. Although it performed satisfactorily, the experience raised a number of issues. It worked, but as we shall see there are a number of reasons to have predicted otherwise.

A detailed description of MRI (and fMRI) is beyond the scope of this thesis but the following thumbnail sketch highlights the key points. Nuclei with a magnetic moment (unpaired protons and/or neutrons) - typically hydrogen nuclei in water and body tissues - are aligned by a strong static magnetic field. An rf pulse is

applied to push the alignment perpendicular to the static field. As their alignment decays back to the quiescent state, the nuclei emit an rf signal which is detected by receiver coils. The nature of the signal emitted is dependent on the chemical and physical environment of the nucleus. Spatial localisation for 3D imaging can be imposed by varying the precessional frequency of the nuclei across the sample. This is achieved by imposing rapidly switching magnetic field gradients onto the static field.

From this we can see that:

- Any device used in the MR environment has to be non-magnetic because of the very strong static magnetic field (typically 1.5 or 3T).
- Metallic (or other conductive) components can interact with the gradient fields and rf excitation pulses leading to signal artifacts and possibly to heating and vibration.
- The sensitive rf detection equipment requires a screened room - emissions within the room must be strictly controlled. This is an issue because many electronic devices (particularly PCs) generate rf noise. This can find its way onto communicating cables via the earth lines, and these can act as antennae which radiate unwanted interference.

Chanter's array is built on a large aluminium chassis. Such a large piece of paramagnetic material has the potential to harm the imaging by locally distorting the static field; in practice the array should be far enough from the imaging volume for this not to be an issue. More serious is its interaction with time-varying gradient fields which can induce eddy currents within the conductor, exerting a force on it. As the fields switch at audio frequencies, the effect is the generation of acoustic vibration which could potentially mask the tactile stimuli[3]. In practice

[3]Eddy currents should also damp the motion of the piezoelectric bimorphs within the static field. The magnitude of this damping depends on the aspect ratio of the bender element since the drive force is proportional to its width while the damping is proportional to its area. In practice this effect is (surprisingly) not noticeable.

this effect can be minimised by positioning the stimulator outside the region of maximum gradient switching. Although the signal generation and amplification was all performed by custom made electronic hardware, there is a continuous ground between the piezoelectric actuators and the PC. Fortunately the presence of rf noise in the wiring did not seem to affect the image quality.

If these points are considered at the design stage, it should be possible to ensure through material choice and properly isolated electronics that future devices should be MRI compatible.

3.6.2 Complexity and form

The size and weight of the device will be a key factor if it is to be used as for an active application, be it hand-held or even fingertip mounted. The number of parts and complexity suggest that modularity of design will greatly aid assembly and maintenance. Similarly, simplifying the cabling should be a key aim since even a simple device could have 50 or more signal connections.

3.7 Summary

In this chapter, the use of piezoelectric bimorphs as simple, relatively compact and low cost actuaors for vibrotactile displays has been discussed. We have also seen how modelling can be used to tune geometric parameters of the actuators and so to optimise the device's performance at key frequencies.

Chanter's work in Exeter provides a very useful starting point for the development of array stimulators based on a piezoelectric drive mechanism. Mathematical modelling of the piezoelectric bimorph allows the principal resonant frequency to be positioned between the low-frequency and high-frequency drive signals (e.g. at 40 Hz and 320 Hz) and the first anti-resonance to be positioned above the range of the drive signals. The next chapter describes a 25-contactor array along these lines, designed for active exploration of a virtual tactile environment.

Chapter 4

A 25 Contactor Array for Active Exploration

The objective of the work described in this chapter was to produce a rugged, powerful array design that would be flexible enough to adapt to new experimental circumstances and still deliver high quality stimuli.

A new modular design of tactile display is described, along with an simple yet flexible real-time controller which allows "active" experiments to be performed directly with a tactile array.

4.1 Design

Chanter's 10×10 design was based on 20 stacks of 5 bimorph elements arranged in a circle.

Switching to a 25 pin (5×5) design allows 2 mm spacing between contactors on the fingertip, and the design can be greatly simplified. The simpler contactor linkages and larger spacing achieved by making this concession greatly reduce the risk of neighbouring pins interfering and jamming. Furthermore, the reduction in wiring simplifies and potentially streamlines the connection to the device.

The solution decided upon was a linear design. In this design, the actuators are arranged in 4 stacks of 6, with the 25^{th} pin addressed from an individual actuator

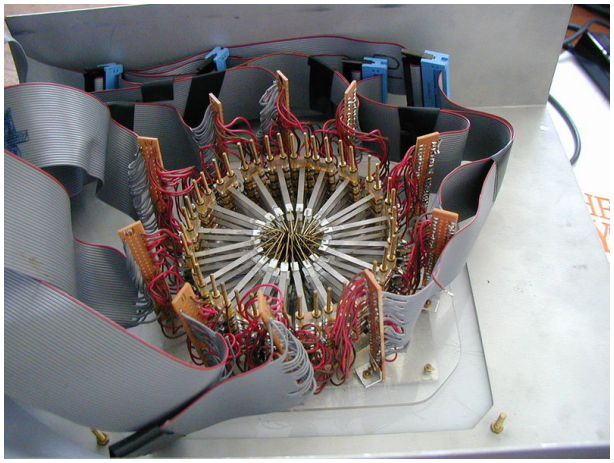

Figure 4.1: The underside of Chanter's Tactile Array showing the circular arrangement of stacks of piezoelectric bimorph elements

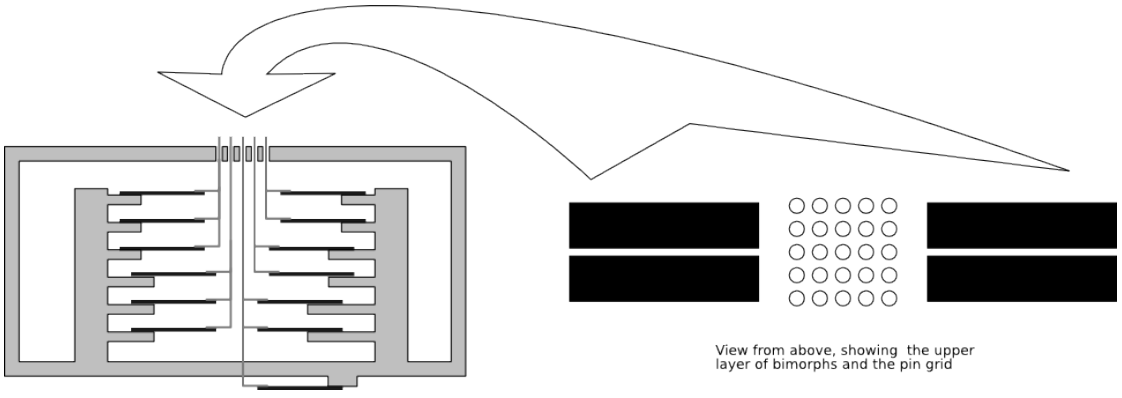

Figure 4.2: Plan and elevation schematic of the 25 pin array design.

mounted under the chassis of the device. Figure 4.2 shows the location of the actuator elements and how the pins are addressed. Note the stepped arrangement of the piezo mounts, corresponding to the row in which the addressed pin is located.

The open-frame linear design facilitates easy assembly and maintenance, making production of more than one device a much less daunting prospect. In addition, the shape allows for side-by-side stacking of the devices, opening the door to multi-finger experiments.

4.2 Hardware Implementation

Actuator selection was driven by two main goals:

- Increased output (compared to the Chanter device, which typically delivered amplitudes of $\simeq 45$ μm at 40 Hz)
- Lower drive voltage

It is immediately apparent that these are conflicting constraints. In order to achieve both, it would be necessary to greatly increase the performance of the actuator. Chanter used bimorph actuators made from PZT-5H (supplied by Morgan Matroc). During background research it was discovered that Stripe™ Actuators from APC[1] International, Ltd. give more deflection and higher blocked force than equivalent size PZT bimorphs. Additionally they come lacquered (i.e. there is less chance of electrocution or of damaging the amplifiers by short circuit), and are significantly cheaper.

Beyond changing the actuator material, improvements can be achieved by modifying the dimensions of the actuators. The blocked force is proportional to the width. The amplitude can be increased by increasing the length, but there are trade offs to be made as this also decreases the blocked force (as l^{-1}), and the resonant frequency drops as l^{-2}. It is easier to vary the length and the width (cut from a standard-thickness sheet) than to vary the thickness; this may involve

[1] American Piezo Company

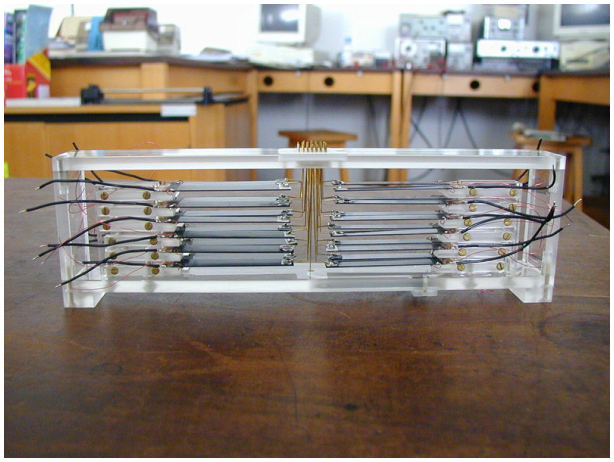

Figure 4.3: The 25 pin Tactile Array

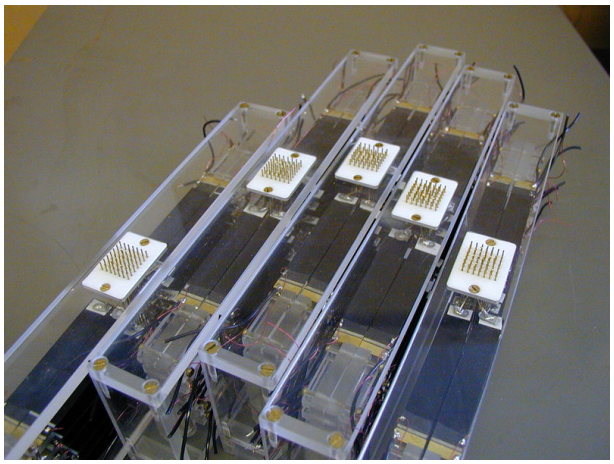

Figure 4.4: 5 actuators arranged for 5 digit stimulation

expensive custom firing. The piezoelectric bimorphs chosen are 10 × 60 mm – unfortunately these appear no longer to be stocked as an off-the-shelf item.

According to the documentation, with an applied voltage of 150 V and a free length of 53 mm, these give a deflection 2.5 mm, and a blocked force of >0.12 N (whilst this level of force might still sound low, it should be remembered that this force will be applied through a contactor with an area of less than 1 mm^2).

Figure 4.3 shows the realised device, and figure 4.4 shows five arranged for stimulating all of the digits on a subject's hand simultaneously.

4.2.1 Performance

The new array certainly delivers more output than Chanter's array. The older device gives what might be described as a "pleasant" level of sensation when a row of its pins is driven with 40Hz sine waves with amplitude 80 V_{pp}. A single pin of the new device becomes uncomfortable (i.e. the sensation is sufficiently strong that it causes discomfort) when the drive is increased much above about 30 V_{pp}.

Figure 4.2.1 shows the frequency response of the 25 pin array driven with 12 V_{pp} sinusoidal drive. The details of the measurements are described in Appendix C. As predicted by the modelling work described in chapter 3, there is a strong resonance at 65 Hz which moves up to approximately 100 Hz when loaded, and an "anti-resonance" at just below 400 Hz. The aim of the design was to achieve a factor of 10 between the output amplitude at 40 Hz and that at 320 Hz, for constant input amplitude (to match the increased tactile sensitivity at 320 Hz compared to 40 Hz as discussed in section 3.4.1). The proximity of the anti-resonance means that performance is poorer than was hoped at 320 Hz, and significant energy couples into the support frame rather than driving the finger load. (The non-ideal frequency of the anti-resonance results from a poor understanding of the phenomenon in the early stages of the project.) However, the device is excellent at 40 Hz making it an effective tool for shape and motion experiments. It does not perform so well at 320 Hz which means it is difficult to make direct comparisons with Chanter's results, but it does work well in the range 200–250 Hz, so there is still adequate headroom for a high frequency channel with a reasonable dynamic range.

In summary, this design of array provides a simple, relatively robust device which can provide a strong stimulus from a low voltage supply. It has sufficient bandwidth to be used for two-channel experiments, and whilst still reasonably large, can be stacked side by side for multi-digit stimulation.

As an important aside, it was noted during the testing in Appendix C that the loading of a bimorph in the array by the skin of a subject's fingertip is largely due

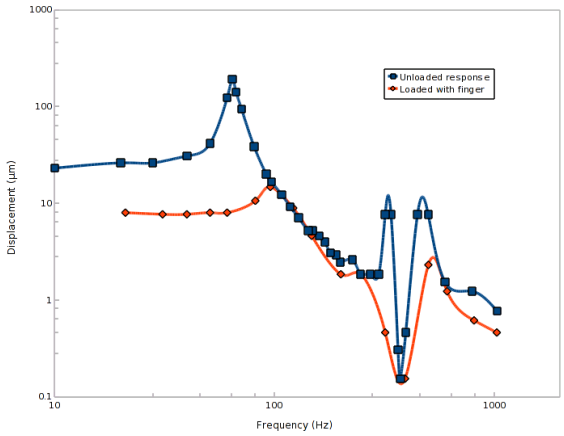

Figure 4.5: Loaded and unloaded frequency dependent output of one pin of the 25 pin Tactile Array

to its compliance - there is negligible effect from the mass of the skin.

Appendix D decribes the sensations one experiences when presented with a sinusoidal vibratory stimulus using this system.

4.3 A simple controller

During the development of the real-time controller described in the next chapter, an opportunity arose to present a demonstration at the World Haptics Conference (Pisa, 2005). What was required was a simple and portable device which could show the possibilities of a modern tactile array. As a demonstration, it would need to be able to run unattended for long periods, and ideally it would have real time control.

Simplicity was achieved by abandoning the option of different drive waveforms in each of the 25 stimulator channels in favour of a single "master" drive waveform – a sinewave of preset amplitude and frequency. In order to create spatio-temporal patterns on the array, all that is needed is to simply switch this master signal on and off for each pin[2].

[2]The drive electronics described here were based on experience developing the tactile stimulator system for the ROSANA project described in appendix B

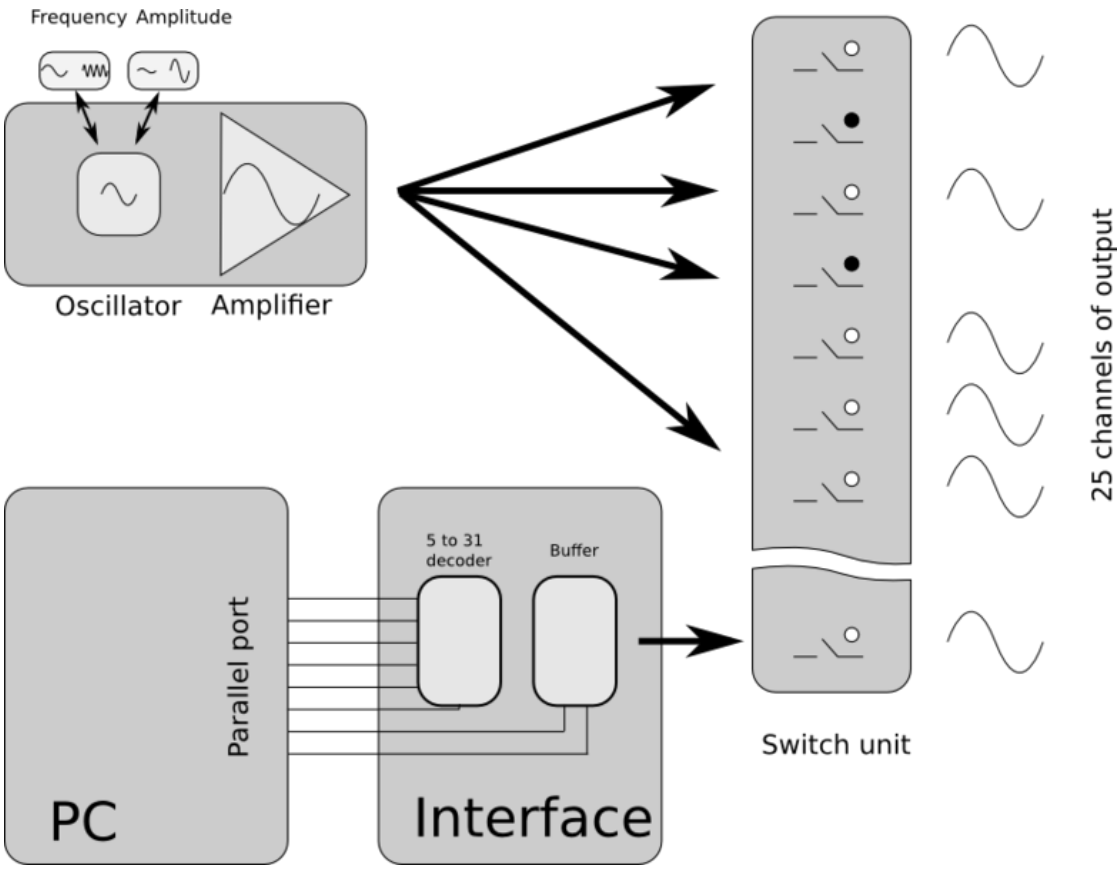

Figure 4.6: Schematic of the operation of the simplified control system.

The master waveform is provided by a programmable oscillator chip (ICL8038). On-board trimming is used to produce a sinewave with minimal distortion , so the only external controls are the frequency and output amplitude. This output waveform is then passed through an OPA551 high-voltage rail-to-rail amplifier[3] before being multiplexed into 25 high-power optically activated switches(PVA2352) as shown in figure 4.6.

The switches are controlled via a custom-made interface card (a schematic of the circuit is shown in figure 4.8) connected to the parallel port of a PC.

Data transfer is performed via the following steps:

- An all-clear pulse is sent to empty the input buffer.
- Each channel number to be activated is then added to the buffer in turn – 5bits of the data are used to code the address. The remaining three bits are control lines used for "reset", "data present" and "activate latch".
- When the activate signal is sent, the data in the input buffer is moved to the output buffer, so that the lines selected are set to logic 1 while all of the other output lines are pulled to logic 0.

A simple program was written in C to create stimuli from a text file using this interface. The format of the text file is straightforward - each time step is represented by a line of 25 numbers, with every number representing one of the pins of the array. If the number corresponding to a pin is 1, the pin is active during that time step. If it is zero, the pin is inactive. Run-time arguments for the code specify the time interval between steps (in milliseconds) and whether the program should continuously loop back to the start of the file once it has reached the end. A description of the data files used to specify experimental conditions is given in appendix F.

This code was used to demonstrate continuously moving bars, dot patterns and a circling dot, and was very well received at the conference. After the event we were

[3]actually 3 amplifiers are used in parallel to spread the capacitive load

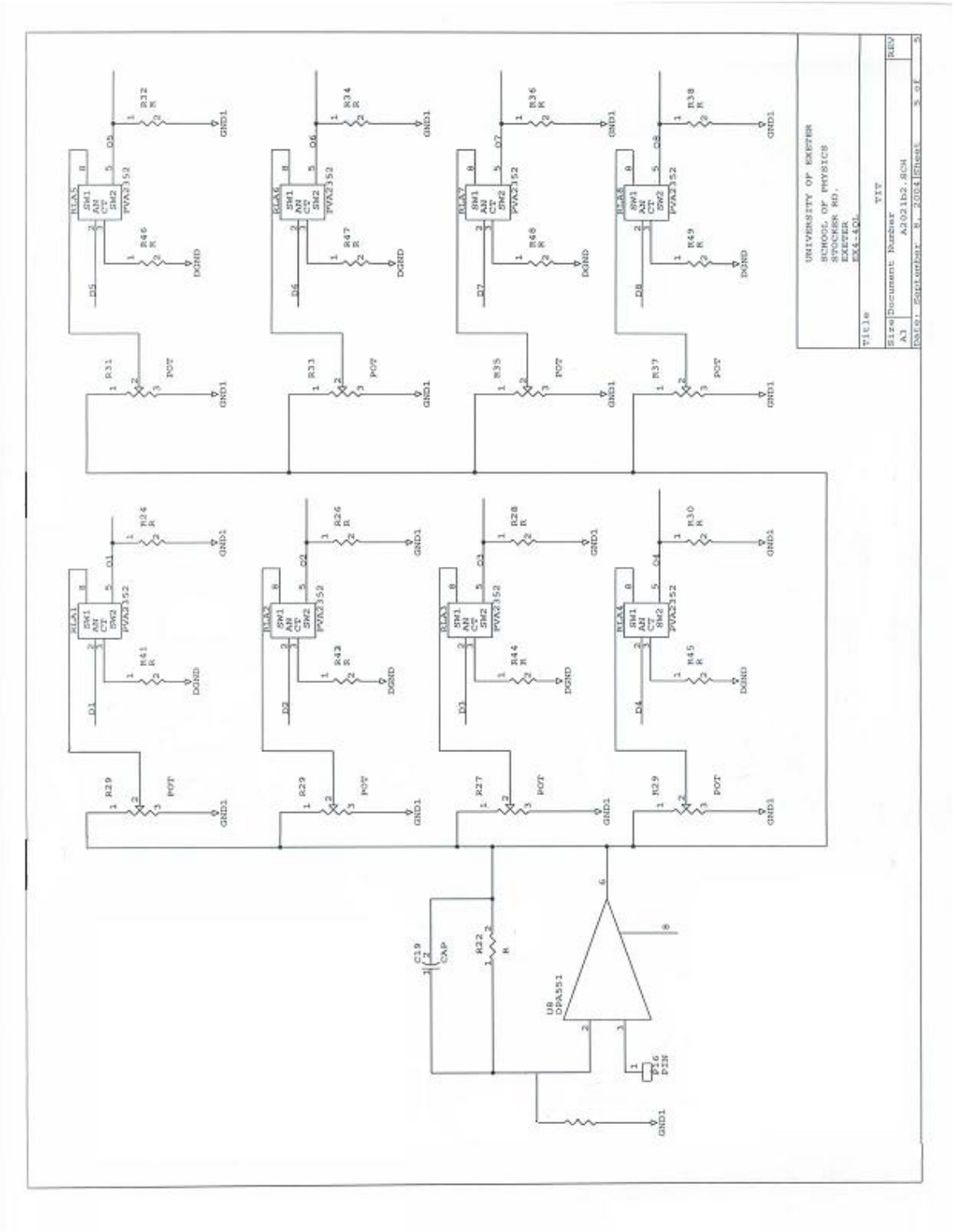

Figure 4.7: Amplifier and switching circuit diagram for the simplified tactile array.

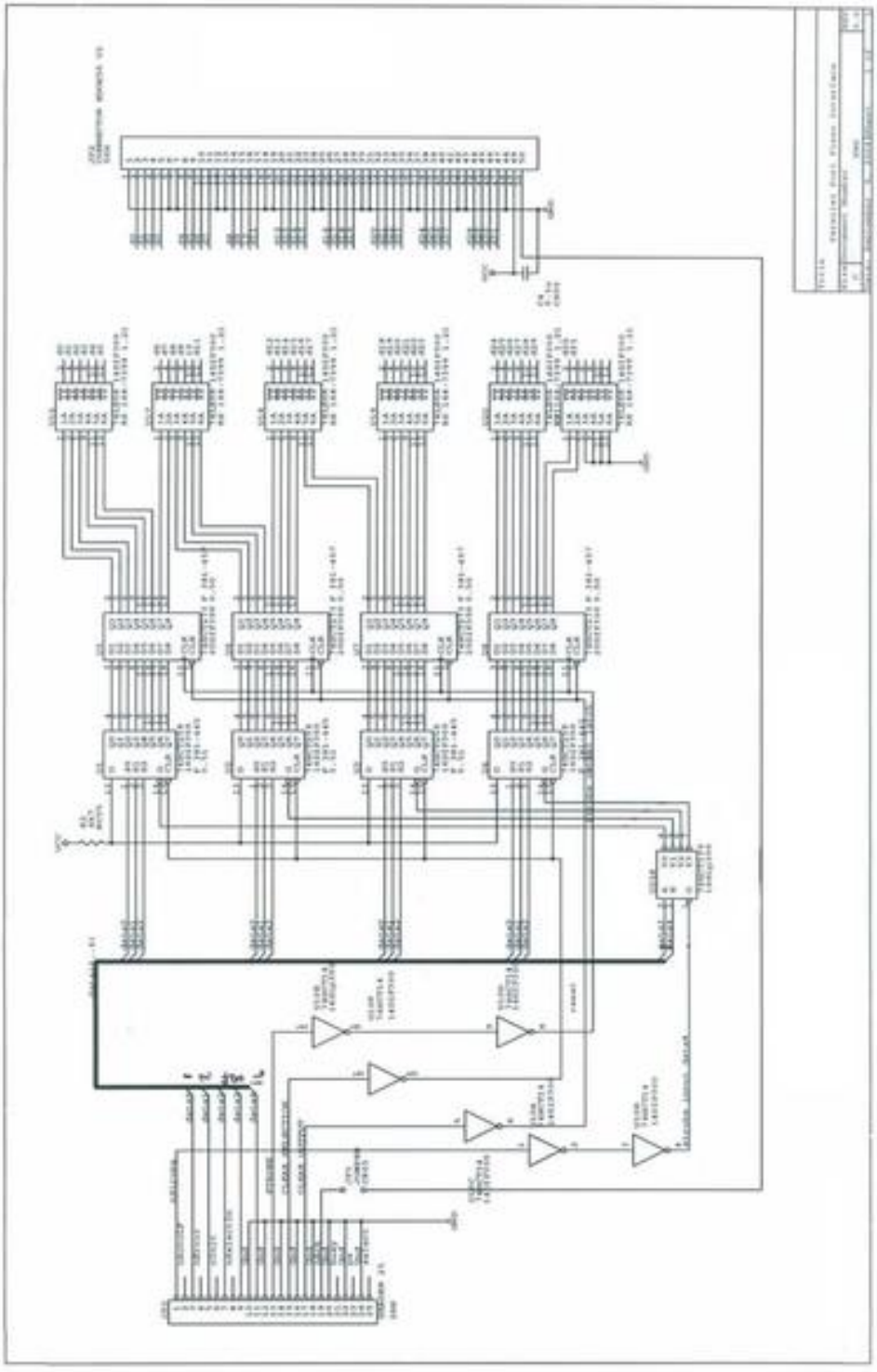

Figure 4.8: Schematic of data transfer to the simplified tactile array.

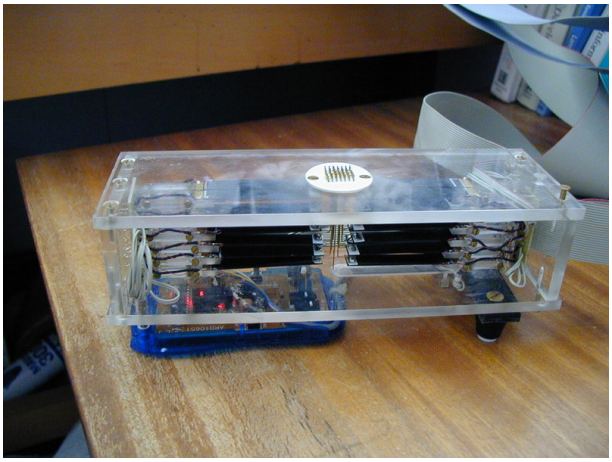

Figure 4.9: The 25 pin Tactile Mouse

left with a very useful tool which could be used to very rapidly perform single-frequency experiments similar to Chanter's moving bars. Some examples of the studies performed using the device in this form are described in sections 4.5 and E. This system is currently under development to provide time-varying tactile stimuli in an fMRI context.

4.4 A Tactile Mouse

The ultimate aim of the work described herein was to develop tactile displays capable of conveying rich textural information in 2D and 3D work-spaces. Mounting a tactile array on a standard optical PC mouse immediately takes what had been a display in which the user is passive and gives it the potential to be an interactive tool with which the user can explore a virtual surface. Whilst a mouse has many disadvantages such as having no absolute position capabilities (see Chapter 5 for a discussion of this), these devices are well known and relatively easy to program. With the control interface described previously, the mouse-mounted array has become a rapid way of testing concepts and performing simple experiments.

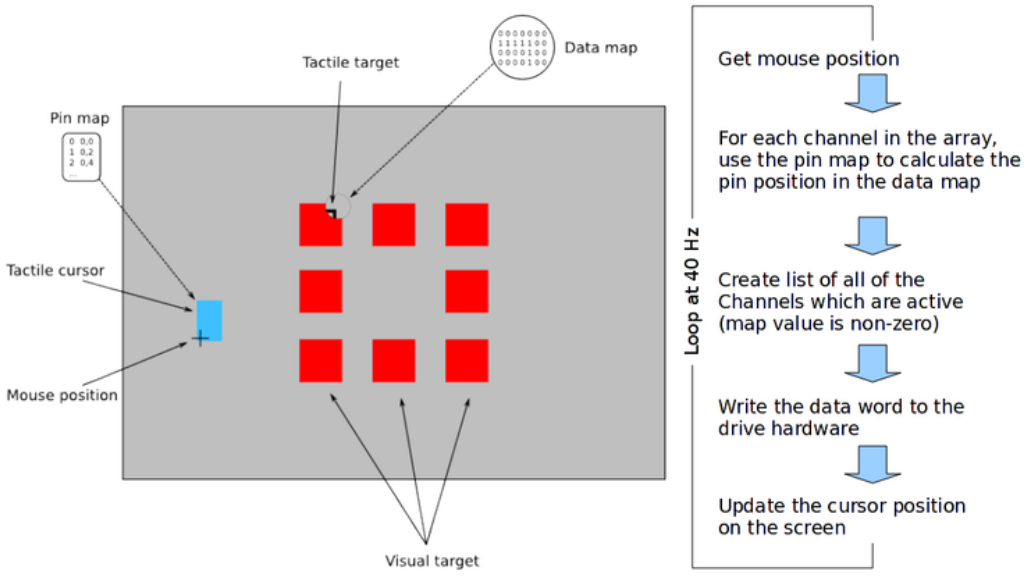

Figure 4.10: Schematic of software design

4.4.1 Software

The mouse interface software was developed on the Linux platform (see chapter 5 for a full discussion of the reasoning behind this), and was written in C using the GTK+ toolkit for graphics[4]. The array mouse was kept separate from the X windows user interface by running a gpm driver process separate from X. This had the side effect that there is no direct link between graphical display and what is being output from the array - in fact the device works perfectly well with no graphical display. A schematic representation of the software is shown in figure 4.10.

Notice that the same software can be used in both an active mode (inferring its position from the movement read from the mouse), or in a playback mode similar to that described in section E. The input file describes a 1mm grid of the entire workspace, or of each time-step with a 0 for off and a 1 for on as before. Mapping

[4]This was later replaced by the cross-platform C++/QT code described in chapter 5

these data into control signals to drive the array output is carried out by a mapping module in the software. This calculates a reference point in the data file at the start of each time-step, and then uses a position translation table to read the value for each pin in the array. In playback mode the "position" is simply the next line in the data file, and the translation algorithm merely reads each character in the line and assigns it to the channel number corresponding to its position in the line. For active use, the position is created by taking the previous recorded position (originally starting with a predefined origin point) modified by the sum of the movement event values recorded in the mouse buffer. These coordinates are combined with Cartesian coordinates from a look-up table which maps the channel number of a pin to its relative position in the array.

The output is written to the parallel port using a routine derived from that described previously. In the active mode the position (and hence the output) is refreshed every $1/40^{\text{th}}$ second. Note that as the pin spacing is 2 mm but the map grid is set to 1 mm[5], all features in the map should have a width of at least 2 mm to prevent them getting lost in between rows.

This device, although intended as test-bed, has proved to be an excellent experimental tool in its own right. The following section describes some of the experiments that have been performed using it.

4.5 Experiments with active virtual touch

In the experiments described in the following sections, the pins were driven with 40 Hz sinusoidal signal. This was to obtain the optimum output from the device and to provide high quality, "realistic" sensations. Furthermore the use of 40 Hz allows a direct comparison with Chanter's results. In the first three cases described below, the subject was sat in front of a screen displaying 8 red target squares arranged around the perimeter of a larger imaginary square (see figure 4.11). The position of the tactile array in this virtual space was represented by a turquoise

[5]The 1 mm spacing was chosen to allow the software to be used todrive Chanter's array.

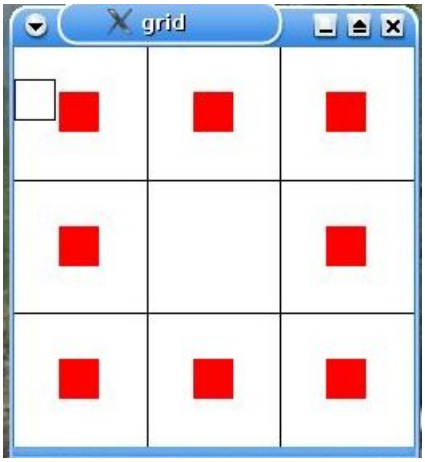

Figure 4.11: The screen display used for the tactile mouse experiments.

rectangle scaled to represent the actual size of the grid of active pins in the virtual space. Exploration of the space - moving the turquoise rectangle around the screen - was achieved by moving the tactile mouse. The subject did this by gripping the sides of the device between their thumb and third and fourth fingers whilst resting their index finger on the display pins.

4.5.1 Orientation of lines

This usage trial was performed as part of the EU-funded ENACTIVE project on multi-modal interfaces in which the author participated over the period 2003–2007. The stimuli presented were all simple lines, one line positioned within each of the target squares – either all but one horizontal, or all but one vertical. Subjects were given the task of identifying the odd-man-out. The orientation task would be trivial if a moving bar was presented to the finger of a passive subject - this experiment sought to test whether subjects could successfully navigate the virtual environment and come up with a strategy to identify and discriminate the targets. Subjects were presented with 16 sets of stimuli, and the time taken to answer, along with their identification of the orientation of the odd-man-out were recorded. General notes were also made about strategies and anecdotal comments made by the subject during and after the test. The experiment was further divided into

two sections. In one, the experiment was as described above, with noise masking provided to block out any potential audio cues. In the second, the noise masking was replaced with an audio feed taken from the centre pin of the array so that when the pin was active, the subject could hear a 40 Hz tone. It had been suggested that audio cues to localisation could significantly assist such a task, perhaps even replacing the tactile information. Half of the subjects did the audio-enhanced version of the test before the audio-masked version and half did the converse. Familiarisation time and a training sequence preceded each test in an attempt to minimise learning effects.

Results

Detailed results are given in in Table 4.1 and Figure 4.12. See Discussion below. The difference between the mean completion times in the T and T+A conditions is not significant (student t-test on paired data, $t = 2.075$, $df = 5$, $p = 0.09$).

	S1	**S2**	**S3**	**S4**	**S5**	**S6**	**Mean**	**±s.e.**
T	36.5	23.3	19.1	19.9	13.1	21.9	22.6	3.5
T & A	29.1	15.6	10.8	22.4	15.1	15.6	18.1	2.7
Difference	9.4	7.7	8.3	-2.5	-2.0	6.3	4.53	2.18

Table 4.1: Task completion times by subject for tactile only (T) and tactile plus audio (T & A) conditions.

User comments and general observations

Some subjects found the "tactile mouse" concept very natural, and were able to use the screen to guide the motion of the tactile cursor, while others found the visual display very distracting, to the point of having to look at their hands while a tactile sensation was being presented. It was generally easier to find vertical lines – the ergonomics of the experiment favour horizontal sweeps (it is easier to move ones hand from side to side whilst using the mouse); hence the preferred strategy for most of the subjects was to use such movements to look for the strong, narrow

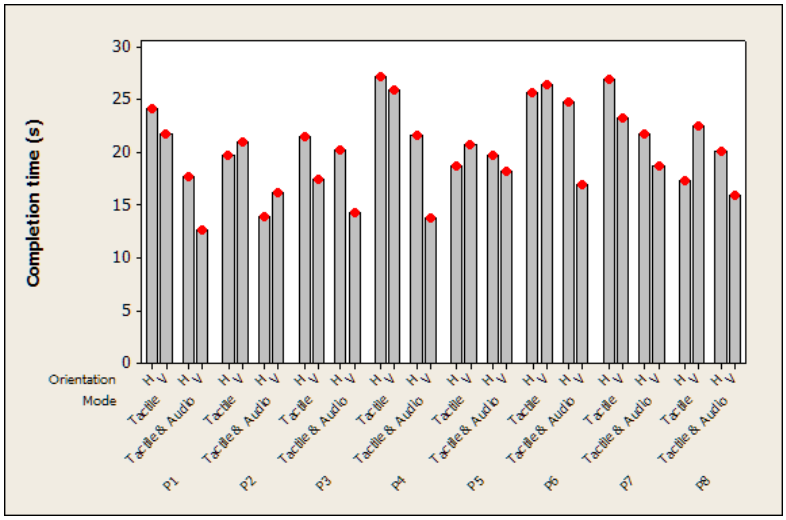

Figure 4.12: Detection time for all subjects by target position (P) – H = horizontal, V = vertical.

vertical lines. Most subjects reported that the additional input of the audio channel required more concentration because it was more sensitive to the alignment of the cursor. Because of this, some subjects simply ignored it all together! One subject did report that the audio signal encouraged a line-following strategy. This subject was slightly slower overall using sound, probably due to the complexity of the task.

Discussion

The first observation to be made is that the task was not only possible, but that all of the subjects could do it relatively quickly and without errors. In fact only one mistake was made throughout the whole study. This was in the middle of a test being performed by an experienced subject, and the answer was given in a time right in the middle of the subject's range, suggesting that this was not a desperate guess but a simple mistake.

Side to side motion is much easier and more intuitive, almost certainly due to ergonomic factors as already mentioned. This is borne out by the result that the audio made the task noticeably quicker for a vertical line odd-man-out – a practised subject could track the cursor from side to side whilst deliberately keeping the centre (audio) pin clear of the level of the horizontal bars. In this way, an "audio-

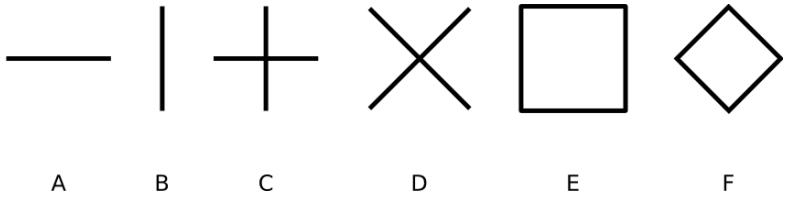

Figure 4.13: Tactile forms used in the shape identification pilot study.

hit" could be very quickly made and the tactile information could effectively be ignored. Interestingly most subjects preferred to use the tactile information to locate horizontal bars.

The comment about line following (i.e. attempting to keep the audio signal active whilst moving the cursor along a line as opposed to receiving a brief audio cue as the cursor crosses the line) is very interesting. This is intrinsically a much more error-prone strategy, but shows that subjects tend to be distracted or at least drawn to more attention grabbing sensations. It is also interesting that the subject who reported this also did not like looking at screen during tactile sensations. This suggests that, for this subject at least, the tactile sense comes low down the attention priority list.

4.5.2 Shape identification

As a follow up to the study described in the previous section, a simple shape-recognition exercise (tactile only) was arranged in which subjects were asked to differentiate between the tactile figures shown in figure 4.13. Two variations of the test were piloted. In the first, subjects were asked to identify which figure on a key card they thought best matched each tactile target. The second test was an odd-man-out test similar to that in section 4.5.1, but with the pairs CD and EF as well as simple horizontal and vertical lines.

These studies proved to be much more difficult than the simple straight-line experiment. Subjects struggled to differentiate between the shapes, even in the odd-man-out task. This should have been easier as the subjects were free to adopt exploration strategies which could have focused on just one aspect of one of the

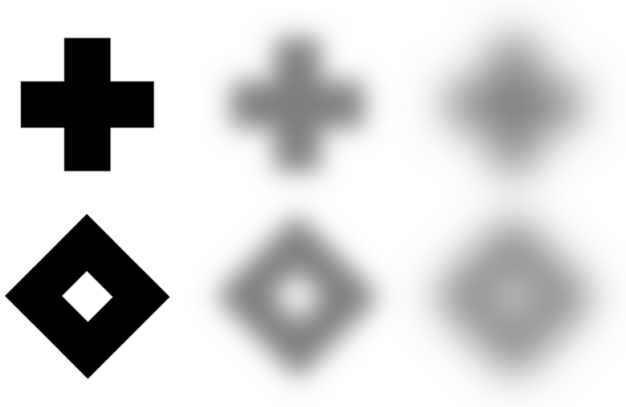

Figure 4.14: Reduced spatial localisation can mask image detail.

pair of targets; however this did not seem to help many of the subjects who seemed to be baffled by what they were feeling

It should be stressed that this was an informal pilot, with much less control over the test conditions, only informal training for the subjects and a much reduced number of test items. However, the difficulty seems to be a real effect. There are a number of reasons why this might be the case. The shapes are relatively complex, particularly when compared to the resolution at which they were displayed. This factor coupled with the fact that spatial localisation at 40 Hz appears inferior to that obtained at higher frequencies (200–300 Hz) almost certainly served to mask the differences between the shapes. (Also as the targets were small – each target approximately the same area as the array – it was difficult to properly explore the detail of the patterns.)

There are also some positional and orientation issues. As mentioned above, the notional position of the array within the virtual tactile landscape is shown by a rectangle whose position is represented by a single point. As this is obtained from a conventional mouse, there is the very real possibility that the absolute position can be lost, leading to uncertainty on the part of the subject. In addition, the tactile cursor is shown to always be aligned squarely with the underlying positioning grid, so there is a very real possibility of confusion if the subject attempts to twist the

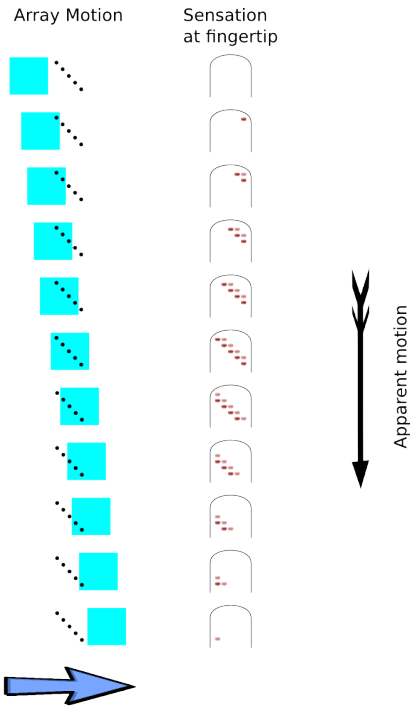

Figure 4.15: A diagonal line can be interpreted as horizontal bar moving vertically, depending on the direction of motion.

array. The natural way to explore slanting lines is to orient the finger so that the feature is approximately aligned to or perpendicular to the finger-pad. This behaviour is not supported with this device; furthermore, additional confusion can arise as diagonal lines presented on the array can feel like horizontal or vertical moving objects.

There is considerable scope for further work in shape recognition with tactile arrays, investigating virtual analogues of raised line drawing studies (e.g. [101]). However this pilot study suggests that a more sophisticated display will probably be required.

4.5.3 Line following

Imagine running your finger around the edge of a wine-glass or tracing the letter shapes in an engraved plaque. These are just two examples of an apparently simple

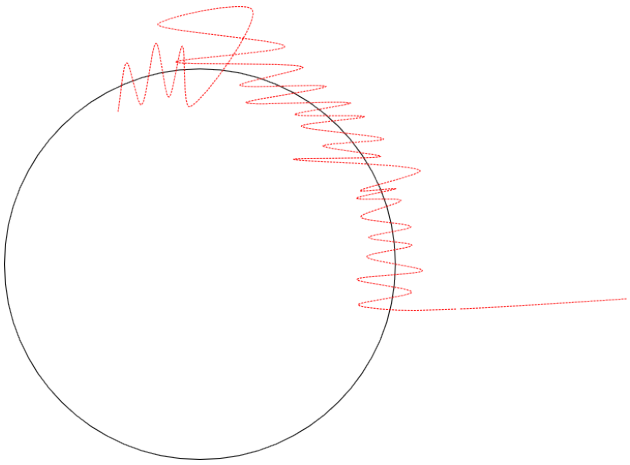

Figure 4.16: Representation of the cursor motion during a line-following task using the tactile mouse.

tactile feature following task; a little thought about the complexity of the fine motor control required highlights the huge volume of information being gathered at the fingertips. Can a simple tactile array provide enough detail to replicate such a task? The subject feedback from the study previously described suggested that it might be possible to use the simple array to accomplish this; a pilot study was conducted to investigate the matter. Two tactile landscapes were used - a large square joining the centres of targets used in the previous studies and a circle with a diameter the same as the width of the square. Both were presented at 40 Hz. For training, the pre-existing target squares were used for the square path while a simple black circle was drawn on the screen as a guide for the circle. The subjects used the visual aids to familiarise themselves with the positioning and to formulate their strategies, and were then asked to attempt to follow the line with the screen turned away. All of the subjects could follow the lines, but nowhere near as quickly or accurately as they could follow a real edge. Tracking the line required a side-to-side motion which invariably became exaggerated into a pronounced zig-zag. This was a slow process, and there was a tendency to lose the line occasionally and to have to hunt to find it again.

More formal testing is required to better quantify and understand this task. How-

ever, certain observations can be made and conclusions drawn from this simple pilot. This test suffered from poor spatial resolution due to both the granularity of the display (as discussed previously in section 4.4.1) and because of the intrinsic lack of localisation at 40 Hz. Better spatial resolution might be achieved by using a higher frequency (or high frequency component), and by using a virtual grid with finer spacing. This could have amplitude-graduated edges (requiring intensity control) in order to better present narrow features. More accurate position acquisition, and perhaps more importantly absolute positioning would also improve matters – this could be achieved through the use of a graphics tablet[6], as described in chapter 5. This task perhaps also pushes at the limitations of a purely vibrotactile display.

The localised change of curvature of the skin is probably one of the primary cues when following a real raised edge; it is possible that the perceptual channels associated with skin curvature are not adequately addressed by vibratory stimuli. Furthermore, there may be a frictional component in the way in which the task is performed, experienced via the vestibular receptors in the finger joints.

Line following tasks are worthy of further investigation, but will require an improved display, perhaps a lightweight device mounted on the fingertip to better associate the fingertip motion with the task. Force-feedback may be useful to simulate the frictional component.

A further experiment performed using this equipment is described in Appendix E.

4.6 Discussion

This chapter has described the construction and testing of a novel tactile array. Although simple in its implementation, as an active multi-contactor vibrotactile display which is capable of being moved with the finger coupled with software capable of controlling the delivered stimuli according to the position or movement of the device is a significant development in the field.

[6]These report the position of their pen nib on their work-surface with sub-millimetre accuracy.

The array has proved to be excellent for passive presentations and is capable of being used (with certain limitations) for interactive, user-driven display tasks. It has shown itself capable of reproducing some of the work reported by Chanter (using a far more complex device); the sensation is excellent, and very "real" if the frequency is chosen correctly. It has clearly been shown that basic line orientation tasks can be performed with such a device. The device in its final form was demonstrated at a public exhibition called "Touch the future", held as part of the Enactive '07 conference at Grenoble.

Nevertheless the device described here has its limitations. Some of the poor performance could be attributed to the inferior spatial acuity of the human tactile sense at 40 Hz, but there are improvements that could be made to the device.

The relatively poor spatial localisation and lack of absolute positioning of a computer mouse introduce an obstacle into the usability of the device. Representation of fine shapes and texture are likely to require combinations of frequency and intensity, meaning that a more complex driver for the array will be necessary. The array itself is limited by its bandwidth, so a device capable of operating up to 400 Hz or higher would be advantageous. The construction of such a system is described in the following chapter.

Chapter 5

Real-time Representation of Texture

HH

5.1 Introduction

This chapter describes a series of experiments designed to investigate the representation of texture through a tactile array. These were performed using a system consisting of a 24 channel actuator with improved bandwidth, control electronics designed to transmit arbitrary waveforms to each channel, and software capable of representing spatially varying tactile "landscapes" constructed from multiple frequencies.

Extending the capabilities of the tactile array system to have broadband performance with individual drive signals, generated "on-the-fly" in real time, required a new level of development of the drive electronics and the control software. Rather than attempt to create a new system from scratch, a modular approach was taken so that elements of the existing software and Chanter's drive hardware could be used until their replacements were available.

The HAPTEX project (described further in chapter 6) required a pair of tactile arrays which were very compact and with actuators located behind the finger-

tip rather than in front of the fingertip as in previous designs. It was clear that this would be a very complex task, so a prototype with the "conventional" layout was constructed to verify the performance of the actuators, to perform some preliminary psychophysics studies, and to inform the equally complex software development process. The development of this prototype is described in the following sections.

5.2 An improved tactile array

Chanter's 100 channel device has an excellent frequency response and spatial resolution, but at the same time the output force is too weak for some purpose and it is a complex, bulky and basically immobile piece of equipment. By contrast, the arrays described in chapter 4 were easy to build and maintain, are robust and powerful in use, and are small enough to move around on a desktop. However, frequency response was disappointing; (the likely reason why this is the case has been previously discussed in chapter 3). They were excellent tools for the development of the interface electronics and software, but not really suitable for any experimental studies requiring higher stimulation frequencies (for example extensions of Chanter's studies, or the HAPTEX project described in the following chapter.) What was required was a compact, easy-to-build device with a working bandwidth comparable to Chanter's array but with increased output force.

5.3 Actuators

Reducing the size of the actuators (see figure 5.1) to make the device more compact should also help to improve its frequency response, but could seriously impact upon the amount of power it would be capable of delivering (the theoretical blocked force would be reduced by a factor of approximately 3.8). A shorter cantilever would have a higher resonant frequency, but tip displacement for a given drive voltage would be reduced. Furthermore, the blocked force would fall off with any

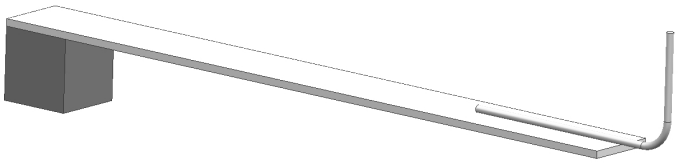

Figure 5.1: A piezoelectric bimorph transducer with contactor pin.

reduction in width. A modelling exercise was performed (using the model described in chapter 3 to try to optimise the geometry; this suggested that a 4.5 mm wide bimorph with a free length l of 40 mm would perform in the manner desired. Chanter's experience showed that developing custom bimorphs is an expensive process. The decision was taken to build the device using off-the-shelf components, arranged in a way to most closely match the ideal. A complete validation of this approach is described in appendix C.

The outcome of this modelling and testing was an actuator design comprising two 2.1 mm wide piezoelectric bimorphs (APC, product code 40-1025) fastened side-by-side and clamped at a free length of 40 mm. The frequency response of this combination is shown in figure 5.2; this is is quite reasonable agreement with the simple model described in chapter 3.

The side-by-side bimorph design provides an actuator unit with the desired frequency response and power delivery. The next problem to be addressed is how these are assembled into a tactile array.

5.3.1 Construction

As in the earlier design described in section 4.1 the piezoelectric bimorphs were arranged in stacks of 6, hanging off support pillars at each end of their array

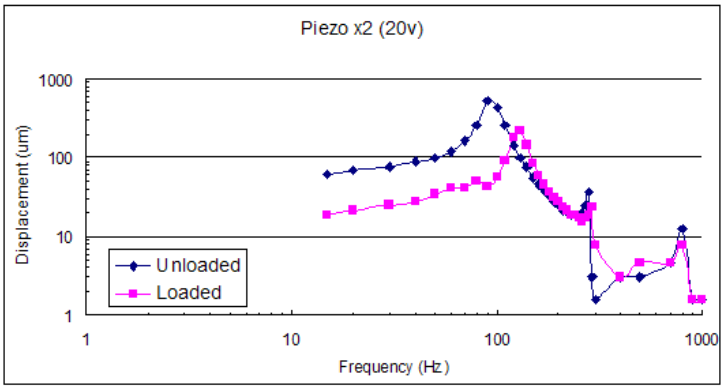

Figure 5.2: Frequency response of the 2 bimorph actuator with and without finger load.

(see figure 5.3). The frame was once again made from clear acrylic and all of the fasteners were brass so as to make the device as MRI compatible as possible. In the first prototype 4 pillars were located outside of the bimorph supports so as to provide a stiff cage-like superstructure. However, this proved to be very tricky to assemble and to maintain, so a design utilising a central support rib was substituted. The contactor pins were once again made from 0.6 mm brass wire bent through 90° at a point just beyond the tip of the bimorphs. As before, the pins were glued onto a rectangle of thin polystyrene sheet. As well as providing insulation and a large area for the glue joint, this also served to join the ends of the parallel bimorphs together to form a single actuator.

Chanter's array and the arrays described in the previous chapter had square contactor areas pins (10 × 10 contactors or 5 × 5). During the development of the Haptex tactile system (described in the following chapter), it was realised that this layout would be impractical and so a 6 × 4 rectangular arrangement of pins was chosen for both the Haptex system and the prototype array described in this chapter (see figure 5.4). Non-moving intermediate pins ("static pins") were incorporated in an attempt to make the surface array feel smoother (less prickly)

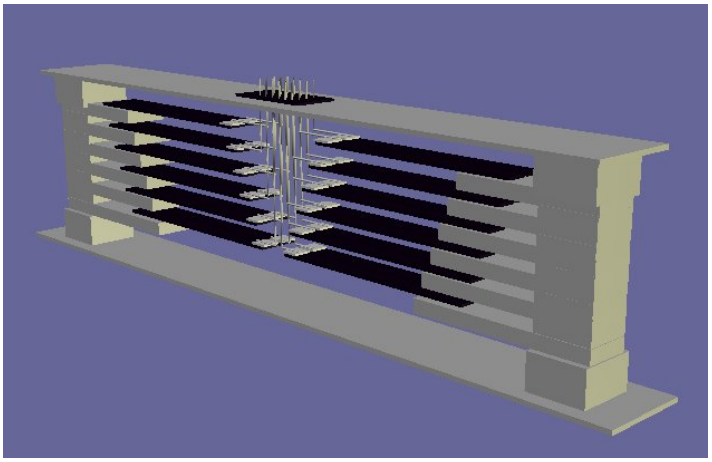

Figure 5.3: Modified array design

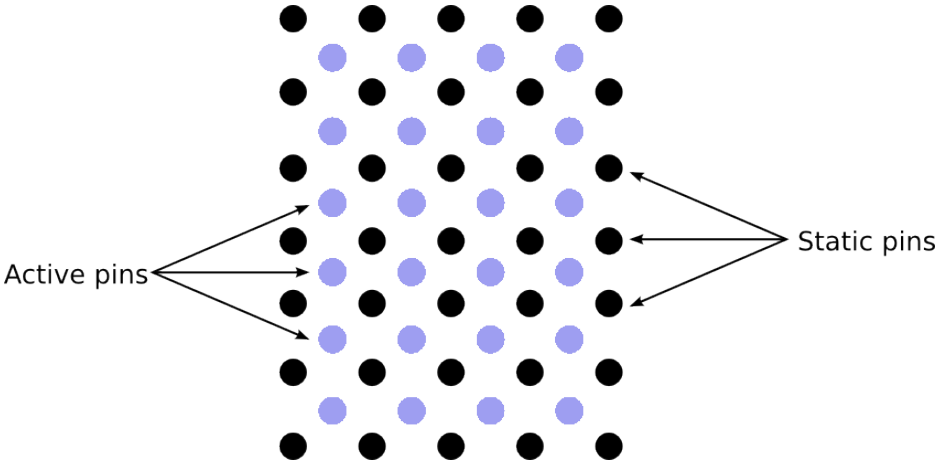

Figure 5.4: Pin layout of new array

and to provide a stiffer surface, able to provide gross mechanical forces (as required for the HAPTEX system). As in the earlier 25-channel design, the spacing between active pins was set to be 2 mm.

The 25 channel arrays described in chapter 4 are driven via a ribbon cable connected to a pair of boards located behind the bimorph stacks. This solution is simple but bulky and proved difficult to maintain. The relatively stiff wire used placed excessive strain on the fragile connections; this factor alone caused a huge number of faults. To overcome these issues, in the new design the ribbon cable was terminated at a single board fixed to the base of the array. From this, each bimorph was connected using very fine gauge wire. This simplifies assembly

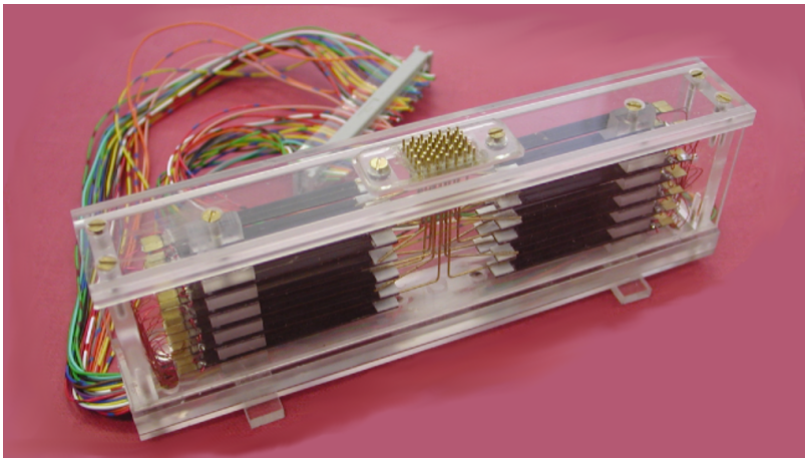

Figure 5.5: The 6×4 Tactile Array

and maintenance, and improves reliability by moving any stiff and bulky wires away from the fragile bimorphs and glue joints. The bimorphs were wired up as described previously, except that now each actuator comprises two piezoelectric elements wired in parallel.

This then (figure 5.5) is a compact, truly broadband tactile array which can be used for active, real-time operation. In order to be used in this way, it requires a drive hardware and software capable of generating continuous, real-time drive signals.

5.4 Position input

As described previously, mounting a tactile array on a standard PC mouse opened up a whole new realm of possibilities for applications and experiments, moving the device from a static display to being a component in a multi-modal interactive experience. However, the mouse has a number of fundamental flaws as described in the previous chapter. To overcome these problems, the mouse was replaced with a Wacom Intuos3 A3 graphics tablet. Whilst the use of a tablet with its restricted workspace would seem to be limiting, in practise the 304.8 × 487.7 mm working area combined with the high resolution of absolute position (0.25 mm accuracy and 200 Hz refresh rate) is more than adequate for the majority of scenarios. In

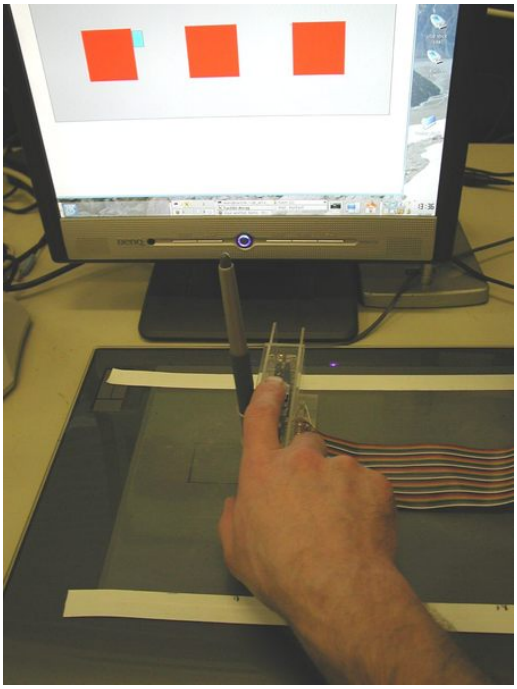

Figure 5.6: The tactile array in use, with Wacom "pen" attached

the working prototype described here, the tablet's unmodified pen controller was mounted to the side of the array (see figure 5.6). It is envisaged that future devices based on such a tablet could extract the position sensing elements from the tablet's controllers so that a more compact device could be constructed.

The one down-side of the tablet-based positioning as implemented is that any angulation of the array away from the axes of the work area can lead to confusion of the subject and slight positional errors because the offset single-point sensor cannot account for any rotational component in the position. Some more advanced tablets (e.g. the Wacom Intuos 4) are fitted with two position sensors which could address this issue.

5.5 Drive Electronics

The key advance in the system described in this chapter is the capability to stream waveforms to the array, generated in real time in response to the user's exploratory movements, with each channel controlled independently. A schematic overview is

shown in figure 5.7. The system has 128 channels, i.e. it can simultaneously drive five 24-channel or 25-channel arrays. At the downstream end, the system is functionally identical to Chanter's, with each array channel individually driven by an amplifier using a drive signal generated by a latching DAC – indeed, the DAC unit is a direct copy of Chanter's. However, whereas Chanter's PC generated waveforms were limited to short duration playback from an external memory block, the system here described can write directly to the DACs from the simulation software. This means that real time waveform generation can be achieved, potentially varying under user control. In order to achieve this, there were some key features which had to be implemented:

- a high bandwidth interface
- rapid generation of the output waveforms
- an operating system environment which can guarantee that the data will be available when required

5.5.1 Data transfer

The multi-channel approach to tactile displays used in this thesis involves drive signals which are the sum of a small number of sinewave components and hence relies on the ability to produce sinewaves at certain key frequencies. Generating these digitally means producing a sequence of samples at an appropriate rate. The Nyquist theorem states that two samples per period are the minimum required; however, the waveform quality of such signals is poor.

Chanter achieved good results with a sample rate of 2560 Hz (8 samples per cycle for 320 Hz and 64 samples per cycle for 40 Hz sinewaves). To put this in to the context of digital data flow, Chanter's 100 pin array operates at a sample period of 391 microseconds. In that time, each of the 100 channels has to be individually addressed before the whole set is updated simultaneously. Each data word is 15 bits long (8 bits describing the amplitude and 7 bits for the address) so, even neglecting

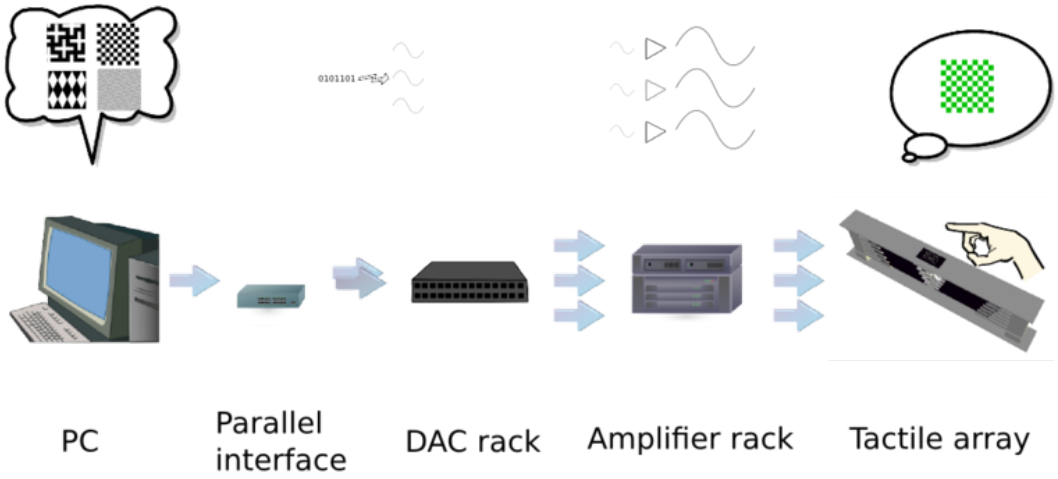

Figure 5.7: Schematic overview of the TA drive electronics

control words, this requires a data rate of at least $2560 \times 100 \times 15 = 3840000$ bits per second.

To allow headroom for expansion, the design specification for the new 128-channel interface allowed for a base frequency of 3200 Hz (this would still be nicely backwards compatible, with 10 samples per period at 320 Hz), giving a required data rate of $3200 \times 128 \times 15 = 6144000$ bits per second.

The standard interfaces fitted to PCs at the time were the RS232 based serial port with a theoretical maximum transfer rate of 115,200 bit/s, and the parallel port. In its basic form the latter was typically capable of transferring data at a rate of 50 to 100 kilobits per second, but later chip-sets (fitted to what were then "modern" – Intel Pentium 4 era – machines) were equipped with the extended EPP and ECP modes, offering the possibility of rates "in excess of 1 megabits per second".

Although the USB standard document had been released in the mid 1990s,

promising a 12 Mbps data rate, at the time this project was launched, hardware was still hard to come by and software support (especially with Linux) was immature [1]. Similarly, whilst it was theoretically possible to achieve transfer rates of 480Mbps using USB 2.0 (the standard was released in 2000) or up to 400 Mbps with IEEE 1394 (Firewire), but hardware simply was not available. Because of this, the PC interface selected was a proprietary high speed parallel card, the PCI7200 from ADLink. This was chosen for both for its 12 Mbps transfer rate and its support of Linux (this later proved to be somewhat of a double-edged sword because of the very limited choice of supported kernels). The 128 channels of 15 bit data were multiplexed onto the 32 output lines of the PCI7200 interface card.

With this hardware in place in the controller PC, it was now possible to stream digital waveforms at a rate sufficient to operate a tactile array in real time. In order to do so, the digital amplitudes would first need to be de-multiplexed and then converted into analogue waveforms.

5.5.2 Interface

It was intended that the DAC controller and its related interfaces should be fully compatible with those in Chanter's system so that components of the old system and the new could be interchanged if required, and so that established and tested units could be used during the development process, allowing elements of the hardware and software to be tested before the system was completed. To do this, an interface was required to convert the 32 line PCI7200 output and its associated control lines into the 27-line input of the DAC unit (3 nine-way D connectors) on the DAC unit.

Additionally, optical isolation was fitted across all of the PC outputs so as to

[1] As explained previously, in this thesis related project elements have been grouped together in a manner that fits logically into the development of a given device rather than in strict chronological order. The development of a real-time interface compatible with Chanter's array hardware was one of the earliest projects launched; it later became subsumed into the complete system described in this chapter.

Port	Maximum data rate	Protocol	Comments
Serial port	100 kbps	Serial	Too slow
Parallel port	100 kbps	Parallel	Too slow
Parallel port (ECP)	1 Mbps	Parallel	Too slow
USB	12 Mbps	Serial	External hardware required. Linux implementation unstable at start of project.
Firewire	400 Mbps	Serial	External hardware required. PC support very limited at start of project.
USB 2.0	480 Mbps	Serial	External hardware required – extremely rare at start of project.
ADLink PCI7200	12 Mbps	Parallel	Simple interface, Windows and Linux drivers available

Table 5.1: Comparison of PC interfaces for data output.

remove any noise generated by the PC from the signal paths. This feature caused a few headaches during development due to the small oversight during the design of the PCB that the chosen opto-isolators are inverting. As a consequence, the data words were inverted in software and hardware inverters were added to the key control lines. A hardware clock was fitted to exactly control the timing of the system (of which more later), and a programmable logic chip was used to facilitate handshaking with the DAC chips.

5.5.3 Digital to Analogue Conversion

As mentioned above, the DAC unit was intended to be compatible with Chanter's system; in fact the circuitry and connectors are entirely identical. The operation

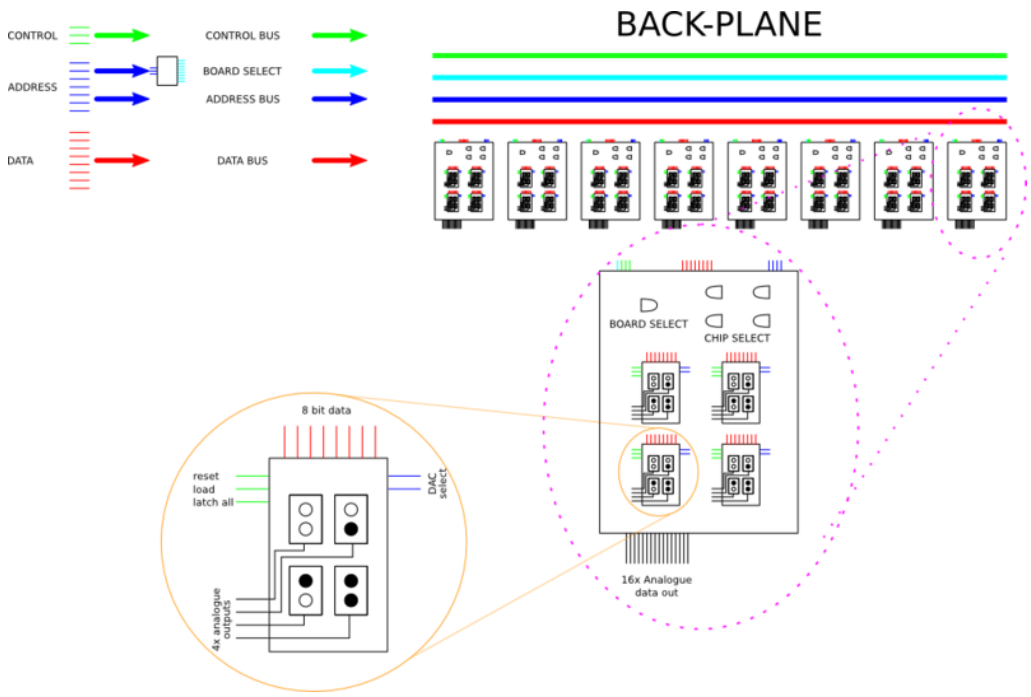

Figure 5.8: Schematic of DAC unit

of the DAC rack is described in detail by Chanter [96], so only a brief overview is included here for completeness. An outline of the operation of the unit is shown in figure 5.8.

The input connectors are three nine-pin RS232-type connectors, providing the data bus, the address bus and some key control lines respectively. These connectors feed into the back-plane of the rack which distributes all of the signals to the 8 daughter boards. These are identical apart from their (8 bit) address jumper. On the daughter boards, the three Most Significant Bits of the address pass through a 3 to 8 decoder, the output of which runs into the address jumper; as only one of the boards will have a bridge in that position, this acts as the board selector. The next 2 bits of the address are used to select one of the four quad DAC chips, and the two Least Significant Bits select the DAC on the chip.

The chips used are MAX 505 quad multiplying DACs which are unusual in that they have 2 reference voltages and latched buffers. Having two reference voltages means that the DAC can produce waveforms which are negative as well as positive with respect to earth, and so can easily drive an amplifier referenced to earth.

The latch means that the individual amplitudes for the next time interval can be loaded to each DAC in a serial manner, but none will switch to the new value until the global latch signal is received. In this way the timing is synchronised across all of the channels. Some modifications were made compared to the original unit, including increasing the number of channels to 128 so that the newer system can drive up to five 25 pin arrays if required. The design of the front panel was modified to improve the insertion and removal of DAC modules.

5.5.4 Drive Amplifiers

One of the drawbacks of piezoelectric bimorph actuators is that to obtain reasonable displacement amplitude requires relatively high drive voltages; as outlined in chapter 3, this could be up to 200 V_{pp}. The drive amplifiers provide gain to increase the DAC output, which is only a few volts. Chanter's equipment uses bridge amplifiers to produce a dynamic range of $\sim$90 V_{pp} from a $\pm$24 V power supply. As part of the development of the new system, a low-distortion amplifier design based on surface-mounted componentry was developed to increase this dynamic range, as well as to make the design smaller and more modular.

The design uses a pair of high power transistors – one for the positive part of the signal and one for the negative part – with an op-amp to handle the crossover region. This new amplifier has a dynamic range of 150 V from a $\pm$70 V supply.

The amplifier board carries five amplifiers (there are 25 boards in all) and was designed with edge connectors carrying both the power supply and all of the signal lines for easy assembly and maintenance. The overall 125-channel output is carried by five 50-way DIL connectors.

Unfortunately the board did not take into account a suitable housing. The case eventually selected was not suitable for use with a back-plane so the edge connectors were not fitted to the amplifier boards. An additional board handles the distribution of the input signals (delivered from the DACs via eight 34 way ribbon connectors). Overall, the amplifier unit contains a huge amount of cabling which

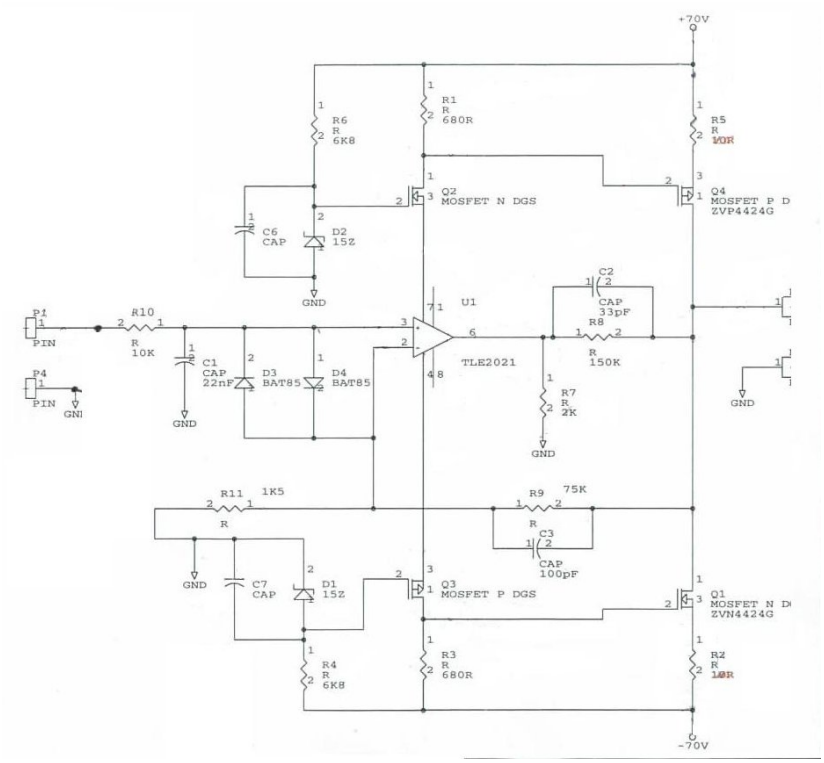

Figure 5.9: Circuit diagram of the type of amplifier use to drive the new tactile array.

is both fragile and very hard to maintain. Furthermore, the power supply connections are vulnerable so it is very easy to damage entire boards or even banks of boards at a time. The amplifiers give excellent performance on the bench, but have proven to be unreliable in use because of the cabling. However, the amplifier unit is capable of providing high-voltage amplification for up to 125 channels in parallel. For the HAPTEX system (described in the next chapter) a more compact and reliable design was developed, based on the bridge-amplifier configuration used by Chanter.

5.6 Computer control

5.6.1 PC hardware

The development of computer hardware moves on very fast. Whilst still modest by today's standards, the PC used to develop the array described here had a massively increased processor speed and significantly faster bus speed compared to that used by Chanter. Whereas previously both the calculation rate and data transfer had been a bottleneck, there was now a possibility of passing signals to the array on demand, in real time.

"Real Time"

It is worth pausing for a moment to consider what is meant by *"real time"*. In the strictest sense, a real-time process is one that is *guaranteed* to occur precisely at a given moment or within a time window. This does not necessarily mean that the time intervals are short. In fact they are often quite long; such *"Hard real-time"* behaviour is normally associated with critical control systems and is typically hard-coded. A good example of this is the controller for the anti-lock brakes on a car – not an instance where the scheduler's hourglass would be appreciated! More often, particularly when streams of data are being processed, it is not really important that every event is processed, but rather that the rate of handling is maintained.

A missing frame of video is unlikely to be noticed, but variable timing almost certainly would. This introduces the concept of *"soft real-time"*; in this, there is still a deadline to be met, but it is assumed that this will not always be achieved. A soft-real time system will usually be programmed with a predetermined strategy for handling a missed deadline – this will typically be to discard the data from the missed frame and proceed with processing the data for the next time event.

At this stage it is worth briefly discussing the choice of operating system. The early development work described in the previous chapter was done using Linux and Open Source development tools. This had more to do with the author's experience than to any technical merits or ideological leanings. Windows is heavily optimised for the user experience; although it might sometimes be difficult to believe, its internal scheduling is biased towards user interaction at the expense of background processes - even when employing low level drivers it is a struggle to achieve timely behaviour. The Win32 API does allow for real-time scheduling, but anecdotal evidence suggested that this was complex and not always reliable[2]. By contrast, the Linux kernel scheduler had been tuned so that (at the time the decision was made) the maximum scheduler latency was of the order of 1.5 ms, compared to about ten times that with Windows. Additionally, by following the Linux route, there was also the possibility of moving to a full real-time enabled kernel if required.

5.6.2 Evolution of the Software

During the early development stages of the project, the programming was coded in C, and the graphics were handled using the GTK+ libraries. However, the burgeoning size and complexity of the code made the encapsulation of Object

[2]In addition to a large number of technical papers on the subject, one of the key decision making points came when a software engineer friend related to the author the difficulties faced at the company she was working for at the time. The company's main business was developing test equipment for GPS systems, and it ran into major timing problems when it switched from a VMS platform to Windows.

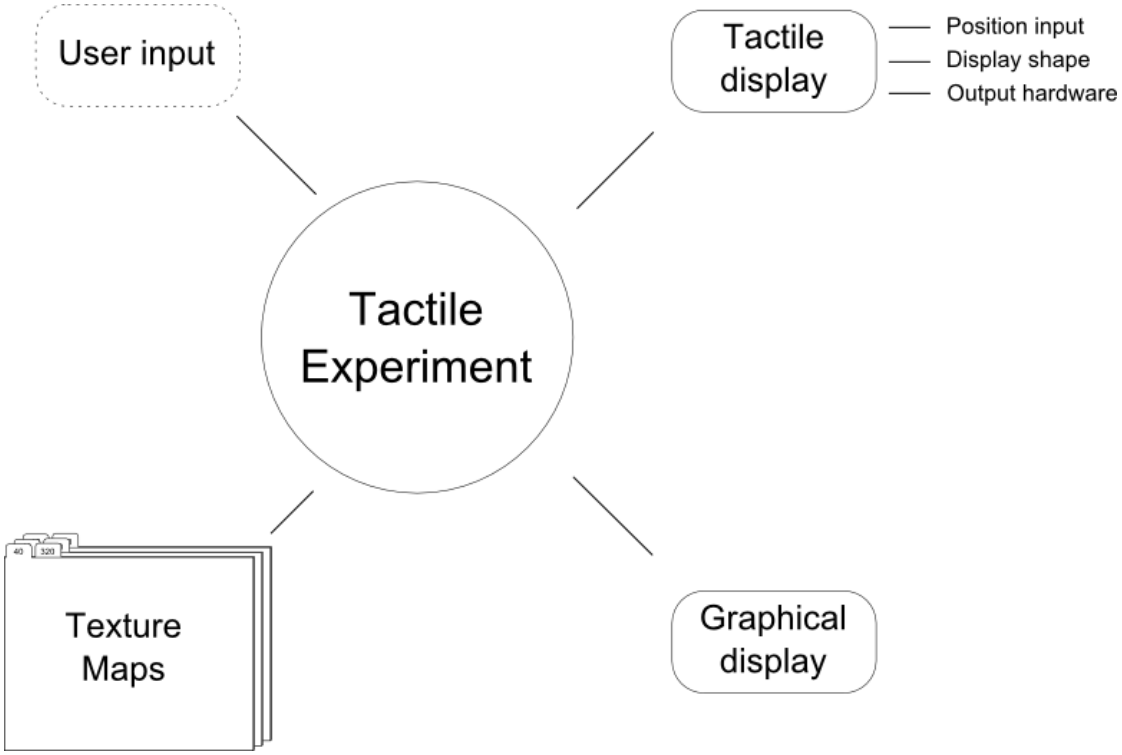

Figure 5.10: Operation of the tactile array software.

Oriented (OO) language look more and more appealing. With the advent of the Haptex project (see chapter 6), a switch to C++ became the logical choice[3].

5.6.3 Software design

The code is completely modular and uses abstraction layers to provide clean interfaces between the interacting components as shown in figure 5.10. This aids debugging (dummy devices are trivial to code), and means that adding a new device or porting the code to a new platform only requires peripheral changes.

Software model

The drive signal for each contactor in the array is composed of a small number of sinusoidal components at predetermined base frequencies (e.g. two components at 40 Hz and 320 Hz), and is specified by the amplitudes of these components.

[3]The switch to C++ also allowed the project to move from GTK+ to QT, a free, fully featured and highly evolved graphical toolkit.

Hence the drive signal for the whole array is specified for each base frequency by an amplitude distribution over the array channels. These amplitude distributions are extracted from the tactile "landscape", for each base frequency, in terms of amplitude over the workspace at 1 mm $\times$ 1 mm resolution. Position within the workspace is relayed through a position device (mouse, tablet etc); alternatively, the traversal can be entirely under software control. In both cases, a key is required to relate the nominal position of the array to the positions of the individual contactors which determine the drive signals in the individual hardware channels.

Whichever method of position input and mapping is used, at the start of a new time frame (the system refreshes at 40 Hz) a list of amplitudes at each frequency is obtained for each channel from the amplitude maps.

Within each 25 ms time frame, data is generated at the drive-signal sample rate of 3200 Hz, i.e. each time frame may be divided into 80 "sub-slices", each of duration 0.3 ms. For every sub-slice, an instantaneous overall amplitude for each channel is obtained from a look-up table (actually a multidimensional array). These are used to build a data word which is sent to the output hardware in time for the next "tick" of the 3200 Hz clock. In this way, no calculation steps are required in the main loop. This whole process is summarised in figure 5.11.

Input files

With the increasing complexity of the software and the desire to have modularity and flexibility in the setup of the hardware, a major rethink was required of the way that the devices and their input/output was described in software. This description would be required to handle multiple ways of describing the positional input (i.e. it should have the facility to use a mouse, a graphics tablet, a controller file, a haptic device etc.), different configurations of output hardware and be able to load sequence of files to run psychophysics experiments The decision was taken to implement this using XML (Extensible Markup Language). XML has similarities to HTML (Hyper-Text Markup Language) inasmuch that the code is written as a

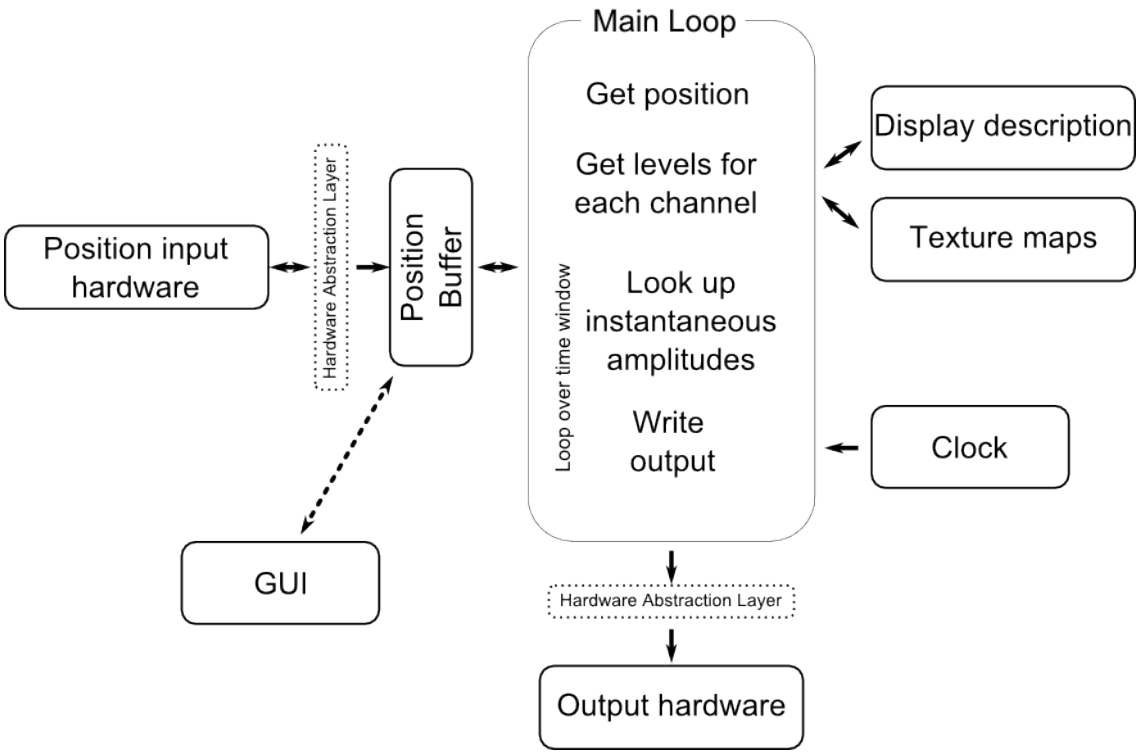

Figure 5.11: Schematic reprenstation of the interaction of the main loop of the tactile array software with its external interfaces.

text file delimited by tags. In HTML these tags are used to indicate formatting information within the document; in XML they can be used to describe arbitrary data objects.

In an HTML web page text can emphasised (usually italicised) using the tag thus:

```
<em>This text will be emphasised.</em>
```

and an image can be inserted using a piece of code such as:

```
<img src="MyPicture" alt="A description of my picture"/>
```

In a similar way, we can define XML tags to handle all of the objects that are used to make up the system. Hence in the tactile array setup files we have sections such as the following:

```
<tactile_experiment title="Tactile Array Experiment">
    <tactile_display>
<device  type="pin_array" label="Digit 1" def_file="array24_1.def.xml">
...
</device>

...

<graphics~mm_scale="3.55"><!-- This is for the laptop screen  -->
<background >
<rectangle x="50" y="40" width="200" height="130" outline="black"
                         colour="grey" label="b1"></rectangle>
</background>
<foreground>

...

<map_data model="simple_map">
<input_file  filename="A1.xml" data_type="ascii" label="file1">
                </input_file>
</map_data>

...

</experiment>
</tactile_experiment>
```

Such XML code is relatively easy for the untrained reader – it only requires a basic understanding of the underlying mapping as described in the previous section to follow what is happening. There are many other advantages to this approach. Files are very easy to create and copy (any text editor will do), and more importantly they are not ultra-sensitive to formatting in the way that the majority of simple text readers are. Existing libraries are used to handle the bulk of the parsing, meaning that the functionality is straightforward to expand. For example, the example above shows how the xml parser can load sub-files so that detailed descriptions of hardware and experiment sets can be stored logically.

The array hardware, input device(s), the graphical display, the output hardware and the amplitude maps can all be described in this way. Appendix F contains some more complete examples.

Amplitudes

As is the case for vision and audition, subjective intensity for the sense of touch corresponds approximately to a logarithmic scale of stimulus amplitude [102]. Because of this it is convenient to specify stimulus amplitudes in 1 dB steps within the range available (which is 0–127, since the data is 8-bit). For example the top four steps in our scale will correspond to peak amplitudes of (in descending order) 127, 113, 101 and 90.

Following the initial pilot study described in section 5.8.1 it was realised that 1 dB steps were too coarse, so intermediate 0.5 dB steps were included. This scale and its translation into its corresponding 0 to 127 values is built into the code; amplitude maps are expressed using this reduced palette in a manner which is very intuitive. The complete list of amplitudes and their corresponding dB values is given in appendix G.

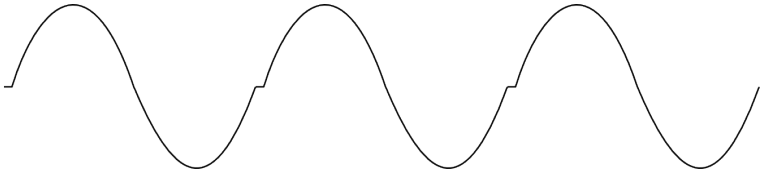

Figure 5.12: An example of a waveform generated by a slow running loop

5.7 Timing issues

Ensuring that correct timing could be achieved was perhaps the trickiest problem to overcome in the realisation of the real-time array. During initial testing, it was noted that the output of the array did not feel and particularly did not sound as expected. Connecting an oscilloscope across one of the piezoelectric actuators showed the waveform depicted in figure 5.12.

Why was this?

Each time-slice at 3200 Hz (data clock frequency) is 312.5μs long. In this time the data buffer has to be filled with the full set of updated amplitude data for each channel, and this buffer has to be moved into a Direct Memory Access (DMA) portion of the PC's memory[4]. From here it is loaded into the First In – First Out (FIFO) buffer on the PCI7200 which streams the data out. The data handling is relatively fast. (In tests, time delays placed into the relevant programme blocks did not affect the waveform). The transfer is slower (still within the time window, but see below). The data is handled using the DOContWritePort() function; the time signal is waited for using the DIContReadPort() function (ideally this would generate an interrupt, but this does not seem to be possible within the PCI7200 API). Each of these functions spawns a background process (this typically has an overhead of 100 μs, although it can be longer), and this introduces context switching issues. As a consequence, placing both the read and write processes within the main loop leaves very little of the time window. The loop often overruns its time-frame. The clock pulse is missed and the waveform is stretched.

[4]DMA is a feature which allows certain hardware subsystems within the computer to access system memory for reading and/or writing independently of the central processing unit.

In an attempt to overcome this, the hardware handshake was disabled and replaced with a dedicated timer thread in the software. The Linux clock is able to count the number of clock pulses since boot – this information is available through the `gettimeofday()` function to microsecond resolution. Using this it is possible to implement a software delay which will wait for at least a stated time period. In practise, this is very accurate and reliable. In the initial realisation of the interface unit, the DACs were latched using a hardware clock on the interface board. With the improved timeliness of the main loop, the mismatch between the hardware clock and the software delay was seen as a beat phenomenon. This was overcome by bypassing the hardware clock and using a spare data line as the latch. This produced waveforms which were much better, but the implementation was CPU intensive and occasionally missed a time-frame when other high priority and bus intensive processes such as graphics conflicted with it. It appears that any graphical changes are dealt with by high priority processes. This seems to cause a bandwidth problem on the PCI bus – any graphical update seems to interrupt the data throughput to the PCI7200. A workaround was to disable to cursor until the system could be moved onto a client-server architecture via an ethernet link. One pilot was run with no graphics at all – visual direction came from a drawing on a piece of acetate taped to the graphics tablet.

A more complete working solution was found which used a slave PC running only two processes – a system clock interval counting thread and a parser which converted data words received via ethernet[5] into a data string for the PCI7200.

The client-server implementation worked well, but there were still occasional glitches. Continually interrogating the system clock requires significant system resource. On the low-specification machine used as the array driver client, this meant that the scheduled CPU load was often near (or occasionally even above) 100% – once again, the scheduler was struggling to cope. What was needed was a lighter weight solution, as follows: PC motherboards have a Real Time clock chip

[5]The ethernet protocol used is User Datagram Protocol (UDP). This is fast and transparent, and uses small packets with no ordering and no error checking.

which is programmable to power-of-2 frequencies (i.e. 1, 2, 4, 8, 16, 32, 64, 128, 256, 512, 1024, 2048, 4096, 8192 Hz) – indeed some have a completely tunable clock chip, accessible via the interrupt line IRQ 8. In this way, the software could be set to block until woken by the interrupt signal. In contrast to the software delay, this implementation is barely noticeable on the CPU load monitor. Although not ideal for compatibility with earlier work [6], running the clock at 2048 Hz was found to be stable and reliable.

This system proved to be completely robust under test conditions with frame rates of up to 100 Hz while running 128 channels at 2 base frequencies, and was used for the following experiments.

5.8 Virtual Texture Experiments

We have already seen in Chanter's work and chapter 4 that a tactile array can produce a realistic sensation of an edge or linear object, and can be used for shape discrimination and line following tasks. What else can we usefully represent with an active broadband array? Along with edge detection, the primary sources of information imparted by the sense of touch relate to local curvature and fine texture; tactile cues also provide information about contact pressure (particularly of soft objects) and grip. From this list we can put aside grip dynamics, contact pressure and surface curvature as these also depend upon information from the kinaesthetic sense (primarily from the finger joints) about the direction and magnitude of the contact forces. It could be argued that there is also a kinaesthetic component at work in detecting changes of friction associated with surface texture (this is discussed further in chapter 6). However, the magnitudes of these forces are very small, so it seems reasonable to assume that texture perception is primarily a tactile task.

[6] The closest available frame length at this base frequency is 26.9 ms. This means that a "40 Hz" sinewave will actually be rendered at 40.16 Hz, and "320 Hz" will be delivered as 321.25 Hz. For simplicity, these will still be referred to as 40 Hz and 320 Hz in the text.

Can the tactile array create the sensation of a textured surface?

Approach

It takes only a moment's consideration to appreciate that this is a potentially massive field for exploration.

Clearly some assumptions and approximations are required. The approach used was to represent the surface texture as local variations in the amplitudes of the frequency components within the tactile stimulus. Initially at least, stimulus components would be restricted to the established frequency pair of 40 Hz and 320 Hz. Would subjects be sensitive to the spatial variations; would this be the same in the two frequency channels? Would this simplified representation allow a texture to be distinguished from a uniform sensation, or from another texture?

5.8.1 Texture pilot study

A short study was conducted to look at discrimination of overall intensity for a surface and whether a "textured" surface (i.e. one with amplitude variation over its area) could be distinguished from a uniform one. It also served to establish the optimal output levels for the array hardware.

The experiments described in the previous chapter suffered somewhat from having too many targets and targets that were too small. The large number of targets made the tasks trickier than necessary for the subjects. The size of the targets was restrictive for shape identification (and would make a texture-identification task almost impossible[7]). To allow the use of fewer, larger targets, it was decided that a classic one-out-of-three odd-man-out task would be more appropriate. Targets that are large compared to the tactile cursor allow the subject to move around within the active area so that the texture can be explored away from any edges.

[7]Further details of the random texture experiment are given in section 5.9.

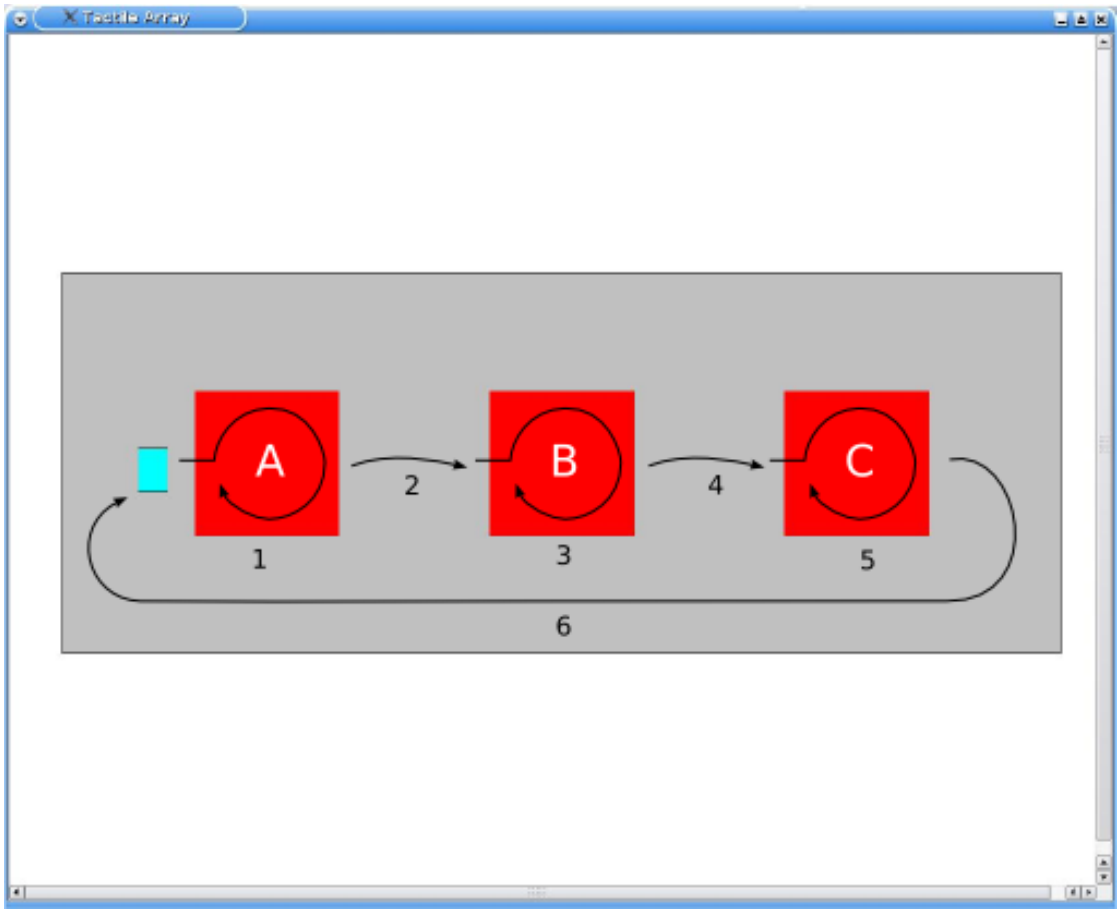

Figure 5.13: The new graphical display. The numbers and arrows indicate the suggested exploration strategy. Each red sqaure is 40 × 40 mm.

Method

Nine young adult subjects (5 male and 4 female, aged between 22 and 35 years) subjects were presented with a set of six stimuli presented at 40 Hz, repeated at three different overall intensity levels (the levels were set using the lowest 3 reference voltages on the DAC controller). In order to standardise the task, as well as to keep the experiment time down, subjects were encouraged to use a standard exploration strategy with a limited number of passes. The graphical display (showing the red active target areas) and the suggested exploration strategy is shown in figure 5.13. The stimulus set consisted of four stimuli which required the discrimination of 1, 2, 3 or 4 dB increments of overall intensity (i.e. two targets with the same intensity and one of a different intensity), and two stimuli which required a texture/no-texture discrimination (i.e. two uniform targets and one with random variation of amplitude [$\pm$2 dB] over the surface).

No formal training was provided – the intention was purely to gauge whether the task was possible.

Results and discussion

All of the subjects scored well above chance (33%) on the 1 dB increment, and near 100% for the 2 dB, 3 dB and 4 dB increments for discriminations of overall intensity. (Following this result, additional 1/2 dB steps were added into the range, as previously mentioned in section 5.6, in an attempt to better map out the psychometric curve.) Subjects with no prior experience of of using tactile arrays had no success identifying the "texture", but experienced subjects could consistently make this discrimination.

The subjective sensation of the textured target with spatially varying amplitudes is difficult to put into words. However, when contrasted to the sensation when moving across a block of uniform amplitude, the variation of intensity with position is discernible and arguably warrants the label "texture". At 40 Hz the feeling as one moves the array across the target is of subtle overall intensity changes. By

contrast, at 320 Hz individual "hot-spots" are quite noticeable, giving the target a "prickly" feeling.

5.9 Formal experiments examining the tactile perception of texture

5.9.1 General comments

The one-from-three design used in the initial pilot study worked well, and was used for all of the subsequent studies described here. However, for the formal experiments described below a forced-choice paradigm was adopted (an answer of "I don't know" was no longer acceptable) allowing standard psychophysics analysis tools to be employed.

The experiments described below were conducted using broad-band noise masking ("pink noise") to eliminate any auditory cues from the vibration of the array.

5.9.2 Random variation as "Texture"

When designing the spatial variation to represent surface texture the decision was taken to deliberately avoid the use of geometric patterns, but instead to specify a random (Gaussian) variation with position. A standard set of texture blocks was generated with varying standard deviation, using the logarithmic scales described previously in section 5.6.3 as the palette. As described previously, stimuli are specified at 1mm resolution within the workspace. However, spatial averaging at a length scale of 2 mm, matching the pin spacing, was performed to ensure that features could not "vanish" between the rows of the array. An example of such a block is shown in figure 5.14.

The standard textures were scaled across the intensity range to produce a set of textures, labelled by the mean amplitude level and the standard deviation about the mean. Note that this scaling required some truncation at lower end of the scale

7	7	10	12	11	14	13	12	12	6
13	13	12	14	12	11	9	7	9	6
14	12	9	11	11	8	6	4	5	7
10	12	7	6	8	12	13	12	12	13
4	10	12	8	8	10	15	16	15	14
9	11	12	8	8	6	12	14	9	10
15	16	10	8	7	6	12	6	4	9
9	15	14	13	10	8	14	9	4	9
4	6	10	7	5	11	14	13	14	9
6	6	9	9	7	11	11	12	16	10

Figure 5.14: An example of a "texture" based on a Gaussian distribution – the colours are a guide to the eye.

(this was not considered problematic because the levels are substantially below the threshold of perception) and also placed an effective upper limit on the maximum amplitude that can be used without clipping.

5.9.3 Discrimination of Vibrotactile Intensity

A detailed pilot experiment was carried using two experienced subjects to look in more detail at amplitude discrimination for uniform (i.e. un-textured) stimuli in active tasks, and to try to establish whether the additional 1/2 dB steps would be sufficient to allow psychometric functions to be mapped. All of the stimuli consisted of mixtures of 40 Hz and 320 Hz. Two types of stimuli were included. In type-1 stimuli, one of the frequency components was held at a constant level while the other one was varied to contrast the targets, by an increment in the range 1/2 to 4 dB (1/2 dB steps within this range). In stimuli of type 2, the intensity balance between the two components was swapped to contrast the targets (e.g. a target with 320 Hz level X dB higher than its 40 Hz level was contrasted to a target with 40 Hz level X dB higher than its 320 Hz level, with X in the range 1–8 dB [1 dB steps in this range]) Each test pair was represented in all six of its possible permutations, giving a total of 144 test items. These were presented in a

random order. Training was not provided as both subjects were very experienced and were heavily involved in the development process.

Results and discussion

The number of correct responses is tabulated below in table 5.2.

LD (dB)	**Subject 1** (/6)			**Subject 2** (/6)			**Combined** (/12)		
type 1/type 2	40 Hz varying	320 Hz varying	Swapped	40 Hz varying	320 Hz varying	Swapped	40 Hz varying	320 Hz varying	Swapped
1/2/1	1	4	3	3	1	5	4	5	8
1/2	3	1	1	4	3	5	7	4	6
1 1/2/3	4	4	6	2	1	6	6	5	12
2/4	4	5	0	4	1	4	8	6	4
2 1/2/5	6	6	4	3	3	6	9	9	10
3/6	5	4	3	6	5	9	11	9	
3 1/2/7	6	6	5	4	2	6	10	8	11
4/8	6	6	5	5	5	5	11	11	10

Table 5.2: Results from the discrimination of vibrotactile intensity pilot study, showing level difference(LD) for each subject and the combined score.

Whilst there are insufficient data here to draw statistically valid conclusions, it is possible to see some trends emerging. Subject 1 can clearly discriminate the type-1 stimuli; the single varying frequency results could be fitted to a classic sigmoidal plot. Subject 1 found the lower contrast type-2 stimuli quite difficult; perhaps this was due to having to first identify the type of stimulus before concentrating on the odd-man-out. Subject 2 appears to be less sensitive overall (the subject is a climber who has very thick skin on the fingertips), but seems to have no difficulty at all with the swapped intensity task (type-2 stimuli). This may be because the subjective intensities of the two frequencies are poorly matched for this subject, so the intended spectral balance is in fact an overall-intensity cue. Whilst these results are informative, this test format was considered to be too complex for a full

study; in particular, mixing stimuli which vary in different ways was an unnecessary complication. A more ordered test structure was needed. Furthermore, although this test involved a large number of test items, none of these contained any spatial variation – the stimulus attribute of virtual texture (arguably the most important attribute that the array can offer) was not addressed.

5.10 Experimental investigation of a perceptual space for virtual texture

Building on Chanter's results for two-component (40 Hz and 320 Hz) stimuli and the pilot experiment described in the previous section (in which the two subjects appear able to detect contrasts in both overall stimulus intensity and in spectral balance), it seems reasonable to posit that there exist two independent perceptual dimensions associated with stimuli produced by a tactile array. Informal tests performed alongside the trial described in section 5.8.1 also suggest that "texture" can accentuate the distinguishability of the spectral balance between frequency components.

Generally we can demonstrate the existence of the two separate perceptual dimensions by looking at the discriminability of 3 points A, B & C and showing that $d_{BC} \neq d_{AB} + d_{AC}$ (see figure 5.15).

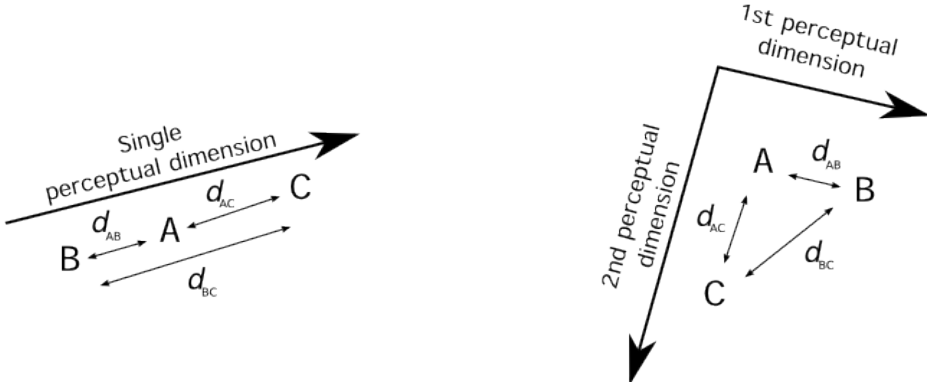

Figure 5.15: Discriminability in 1 and 2 perceptual dimensions

What pairs should be chosen from the massive search space?

Using A_{40} to represent the amplitude of the 40 Hz component and A_{320} to represent the amplitude of the 320 Hz component, in practice the available stimulus space can be explored by investigating all possible (A_{40}, A_{320}) pairs over the available ranges. There are many possible combinations ($(60 + 1) \times (60 + 1) = 3721$ with the amplitude set described in appendix G) within the perceptual space, so a strategy is required in order to design an experiment of a reasonable size.

The strategy selected was to begin with a line of equal subjective intensity. This can be considered as a trajectory through the stimulus space[8]. On the basis of previous experiments at Exeter [103] and informal measurements by the author, (A_{40}, A_{320}) pairs for equal subjective intensity were chosen, as shown in table 5.3. This trajectory is plotted in figure 5.16.

	trajectory 1 equal intensity		trajectory 2 equal intensity		trajectory 3 equal intensity	
	A_{40} (dB)	A_{320} (dB)	A_{40} (dB)	A_{320} (dB)	A_{40} (dB)	A_{320} (dB)
A	–	13.0	–	9.5	–	15.5
B	-5.0	12.0	-8.0	9.0	-3.5	13.5
C	1.0	11.0	-1.5	8.5	1.5	11.5
D	4.0	10.0	2.0	8.0	4.0	10.0
E	6.5	8.5	5.0	7.0	6.0	8.0
F	8.5	6.5	8.0	6.0	7.0	5.0
G	10.0	4.0	10.0	4.0	8.0	2.0
H	11.0	1.0	11.5	1.5	8.5	-1.5
I	12.0	1.0	13.5	-3.5	9.0	-8.0
J	13.0	–	15.5	–	9.5	–

Table 5.3: Amplitude pairs defining the perceptual trajectory.

Note: the reference values for the A_{40} and A_{320} described scales are different – chosen to allow for the difference in tactile sensitivity between 40 Hz and 320 Hz.

[8]Note the distinction here between the "perceptual space", whose dimensions are the perceptual "qualities" and "stimulus space" whose dimensions are A_{40} and A_{320}

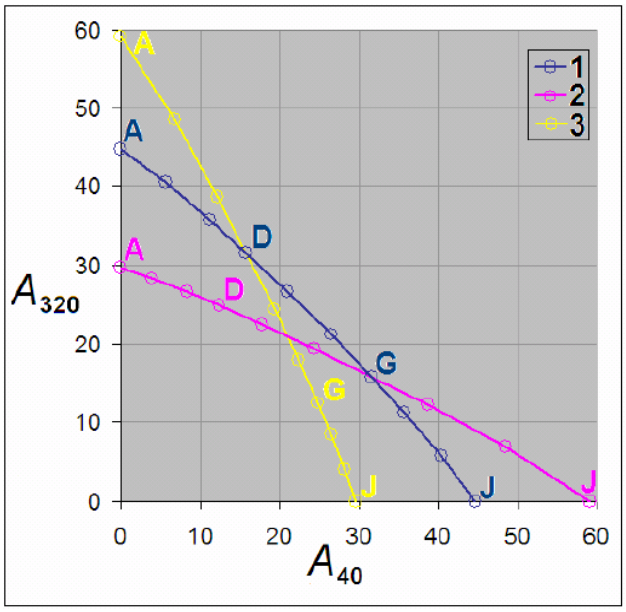

Figure 5.16: "Trajectories" through the perceptual space. The amplitude values shown are the 7-bit output values corresponding to the logarithm steps shown in table 5.4

The intention is that equal dB values on the two scales correspond to equal subjective intensity.

The specified (A_{40}, A_{320}) pairs are not necessarily correct (or for that matter universal across all subjects), so skewed variants (which may be closer to the true equal intensity line) can be included (see additional data in table 5.3 and additional trajectories in figure 5.16). The 10 specified points on each trajectory are separated by steps of spectral balance which are intended to be approximately (subjectively) equal.

Initially the discrimination of 24 test pairs (Table 5.4) were investigated. These points selected were equally spaced along the trajectories and were defined by the intersection points in Figure 5.16.

Since we also wish to compare subjects' performance with "textured" test items to those with uniform test items, this number is doubled. There are 6 permutations for each of the 48 pairs giving a total of 288 test items.

For the test, Gaussian textures were created with a standard deviation of 2 dB

A1/D1	A1/G1	A1/J1	D1/G1	D1/J1	G1/J1
A2/D1	A2/G2	A2/J2	D1/G2	D1/J2	G2/J2
A3/D3	A3/G1	A3/J3	D3/G1	D3/J3	G1/J3
A2/A1	A2/A3	A1/A3	J2/J1	J2/J3	J1/J3

Table 5.4: Test pairs along the perceptual trajectory.

(range ±4 dB). This range was selected as large enough to produce detectable effects but small enough to leave headroom within the overall dynamic range of the system.

This experiment in the form described was abandoned at a very early stage as subjects consistently scored at or near 100%. The logical conclusion was that intermediate points along the trajectories should be used, so as to give less distinguishable contrasts.

5.10.1 The revised experiment

As described previously, figure 5.16 shows 10 points along each trajectory. Once again, this gives potentially a very large number of combinations for investigation of stimulus contrast. A subset was chosen, as shown in figure 5.17.

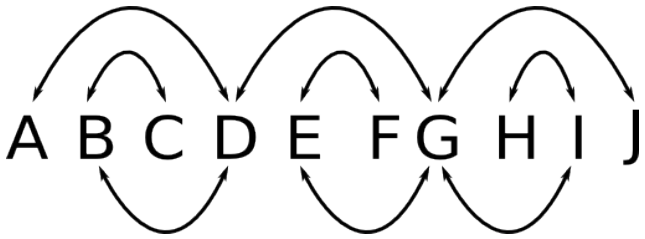

Figure 5.17: Revised pairs on the "trajectory'.

There are 3 "step size 1" pairs (BC, EF, HI), 3 "step size 2" pairs BD EG GI and "3 step size 3" pairs AD DG GJ for each trajectory, each with "uniform" and "Gaussian" versions. With 6 one-from-three alternatives, this gives a total of $3 \times 3 \times 3 \times 2 \times 6 = 324$ split over 6 test blocks.

Notice that the pairs BC, BD, AD have their spectral balance dominated by the

320 Hz component. These are referred to as the "High" range pairs. Similarly the pairs HI, GI, GJ are dominated by the 40 Hz component and are referred to as the "Low" range pairs. The EF, EG, DG pairs have approximately equal 40 Hz and 320 Hz components; they form the "Mid" range.

A comprehensive training sequence was developed to introduce (or refresh) the subjects to the full range of stimuli that they would experience in a logical and progressive way. This was accompanied by a short test set, with feedback about the correct answer.

Results and Discussion

The test was undertaken by eight subjects (3 male and 5 female, aged between 22 and 35). A ninth individual, designated subject 5, was unable to complete the full set of experiments and has been omitted from these results. The experimental variables were step size (1, 2, 3) spectral range, (low, mid, high), trajectory (1, 2, 3) and texture (i.e., spatial variation: uniform, Gaussian). The results are shown in figure 5.18.

Figure 5.19 shows the mean discrimination scores as a function of step size (pooled over all other variables). All of the scores are well above the chance level (33%), even for the smallest step size. As expected, scores rise with increasing step size, and analysis of variance (ANOVA) shows the main effect of step size to be significant ($p<0.001$). Calculated mean values for the discrimination index d' are:

- $d' = 1.22$ for step size 1
- $d' = 2.58$ for step size 2
- $d' = 3.19$ for step size 3

Similarly, the mean discrimination scores as a function of trajectory in figure 5.20 appear to show a increase in favour of the 320 Hz biased data-set, and this is significant ($p < 0.001$).

Trajectory	Spectral range	Step size	Subject 1		Subject 2		Subject 3		Subject 4		Subject 6		Subject 7		Subject 8		Subject 9	
			Texture	Uniform	Texture	Uniform	Texture	Uniform	Texture	Uniform	Texture	Uniform	Texture	Uniform	Texture	Uniform	Texture	Uniform
"Flat" (1)	Mid	1	1	3	3	3	1	2	2	2	2	6	1	4	2	3	4	2
		2	5	5	6	5	1	4	5	5	4	6	4	3	5	3	1	3
		3	6	5	5	6	5	5	6	3	5	6	3	6	6	5	4	4
	Low	1	1	3	2	4	3	2	2	1	3	3	1	3	4	3	2	1
		2	5	5	5	4	3	4	3	5	4	4	2	3	3	5	4	4
		3	4	5	5	4	3	5	3	3	5	6	4	2	5	4	5	2
	High	1	4	6	5	4	2	2	2	4	2	3	3	3	3	2	4	1
		2	3	5	4	5	3	4	3	4	5	6	3	4	4	3	3	4
		3	3	5	6	4	2	2	5	4	5	5	3	5	5	5	4	5
Biased to 40 Hz (2)	Mid	1	4	3	4	3	3	1	2	2	2	4	2	4	2	4	2	3
		2	5	6	5	6	2	1	3	4	6	3	4	5	5	5	3	1
		3	4	5	5	6	6	5	4	6	5	5	4	4	5	4	6	5
	Low	1	3	3	2	1	2	1	1	4	1	1	0	2	2	1	2	3
		2	2	2	5	3	3	2	3	2	0	1	4	1	5	2	4	2
		3	3	4	4	1	1	2	4	3	5	3	4	2	6	4	3	1
	High	1	3	3	5	3	4	1	2	3	1	3	2	3	3	2	6	2
		2	3	4	6	3	6	5	3	2	6	2	5	1	6	6	6	5
		3	6	6	6	6	4	3	6	4	5	5	5	5	6	6	5	6
Biased to 320 Hz (3)	Mid	1	4	4	4	3	4	2	2	0	5	4	3	3	3	4	4	0
		2	5	6	5	6	5	3	6	2	5	6	4	4	5	4	6	5
		3	6	6	6	6	5	3	4	6	6	6	5	5	6	5	6	5
	Low	1	5	3	3	4	1	4	5	6	4	3	0	2	4	3	3	2
		2	6	6	4	5	2	4	5	6	2	6	4	6	2	5	3	6
		3	5	4	4	5	5	4	5	5	3	5	2	4	1	4	5	5
	High	1	6	3	3	2	5	3	3	2	6	5	4	3	5	3	2	2
		2	6	5	6	6	6	4	6	1	6	6	6	3	5	5	6	5
		3	6	6	6	6	5	6	6	5	6	6	6	5	6	6	6	6

Figure 5.18: Scores out of 6 for all experimental conditions, for all subjects

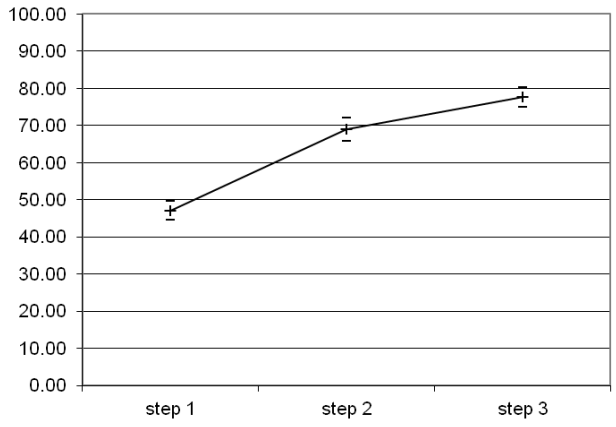

Figure 5.19: Mean discrimination scores (pooled over all conditions) as a function of step size.

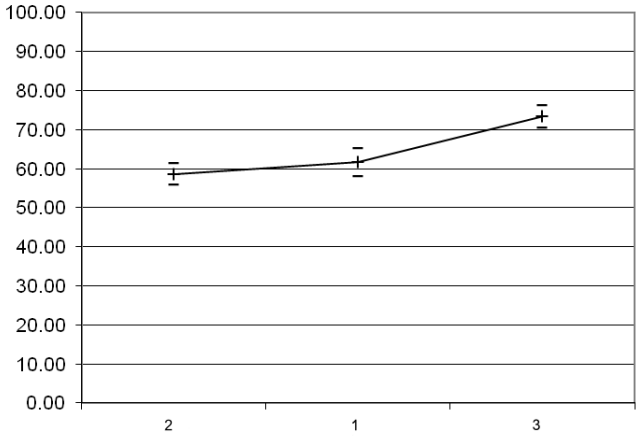

Figure 5.20: Mean discrimination scores (pooled over all conditions) as a function of trajectory.

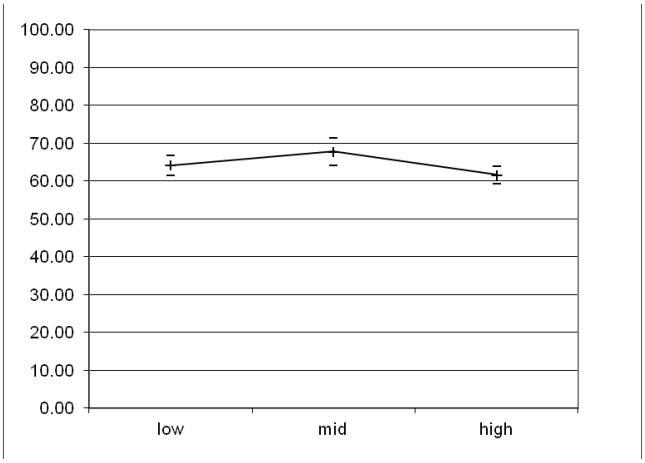

Figure 5.21: Mean discrimination scores (pooled over all conditions) as a function of spectral range.

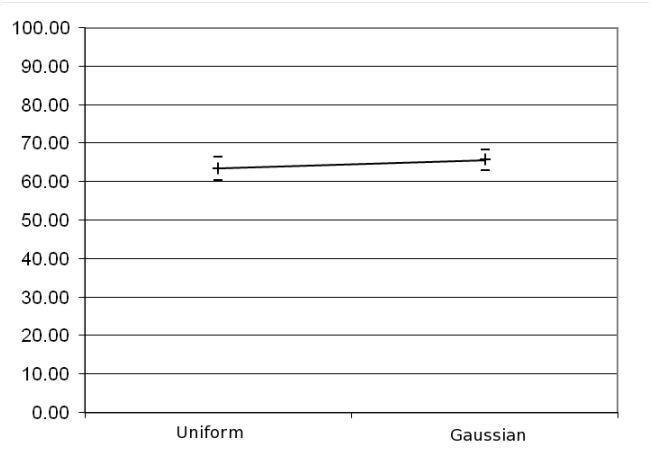

Figure 5.22: Mean discrimination scores (pooled over all conditions) as a function of texture.

The main effect of spectral range (i.e. how the amplitude balance of the two frequency components was balanced) shown in figure 5.21 is (just) significant ($p = 0.048$), although it is not immediately apparent how this should be interpreted.

A more surprising result is shown in figure 5.22. Subjects report that the Gaussian spatial variation is much easier to perceive in surfaces where the 320 Hz component dominates than in surfaces where the 40 Hz component dominates, although the flat graph indicates that this does not affect the results of the present experiment in any obvious way. ANOVA shows that the main effect of texture is not significant ($p = 0.367$). This apparent conflict was deemed worthy of further exploration — see the next section (5.10.2) for more discussion of this point.

The data in figure 5.23 display a complex interaction between the experimental variables. In the case of the interaction of trajectory and spectral range, the scores for the 40 Hz dominated trajectory fall off as the overall spectral balance moves towards 320 Hz whereas the scores for the other two trajectories improve; this effect is significant ($p < 0.001$). Similarly, the the two curves in the plot showing the interaction between texture and trajectory exhibit different behaviour, with the texture curve showing a relative reduction in the score for the balanced trajectory. Once again, this effect is significant ($p = 0.033$). There is a difference between

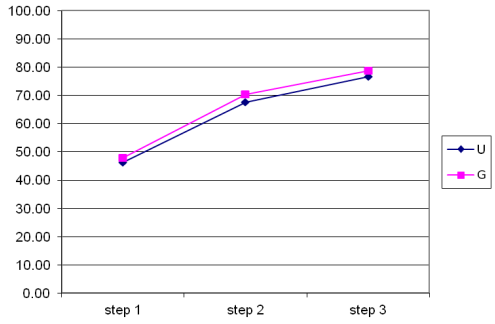

(a) Texture and Step Size. Typical standard error ≃3 percentage points.

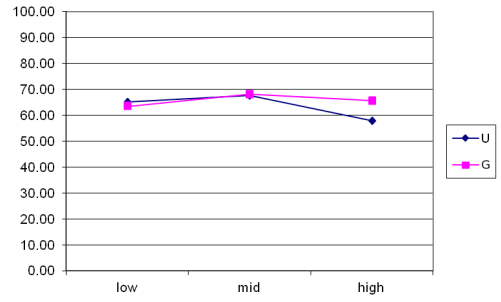

(b) Texture and Spectral Range. Typical standard error ≃3 percentage points.

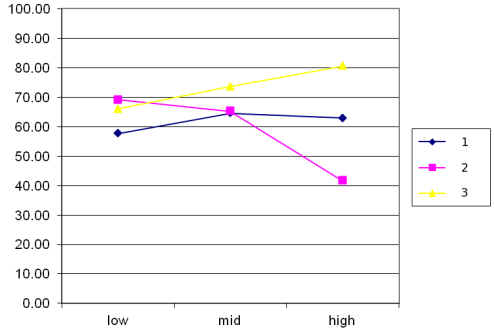

(c) Trajectory and Spectral Range. Typical standard error ≃4 percentage points.

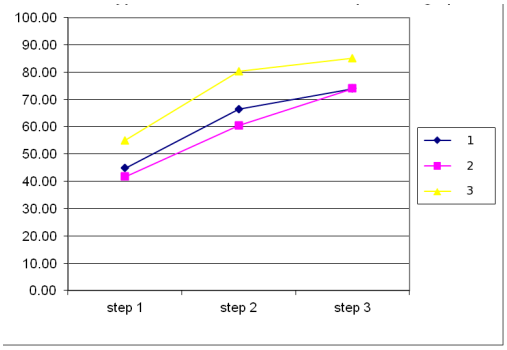

(d) Trajectory and Step Size. Typical standard error ≃4 percentage points.

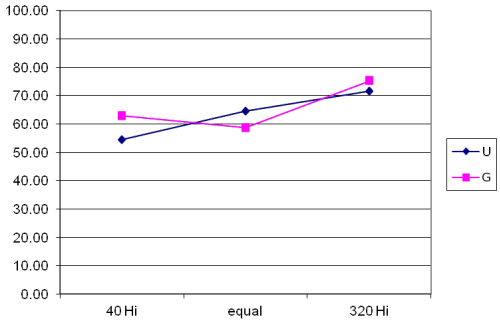

(e) Texture and Trajectory. Typical standard error ≃4 percentage points.

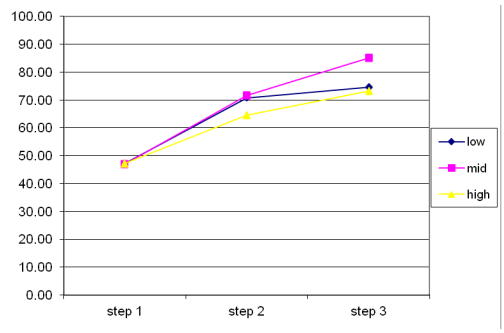

(f) Spectral Range and Step Size.. Typical standard error ≃5 percentage points.

Figure 5.23: Interaction of experimental variables (mean scores from 8 subjects) with other categories pooled. The labels and legends identify data for the different trajectories, as shown in Figure 5.16, the spectral range (low, mid, high) the step size (1,2 or 3) and the texture (U = uniform, G = Gaussian).

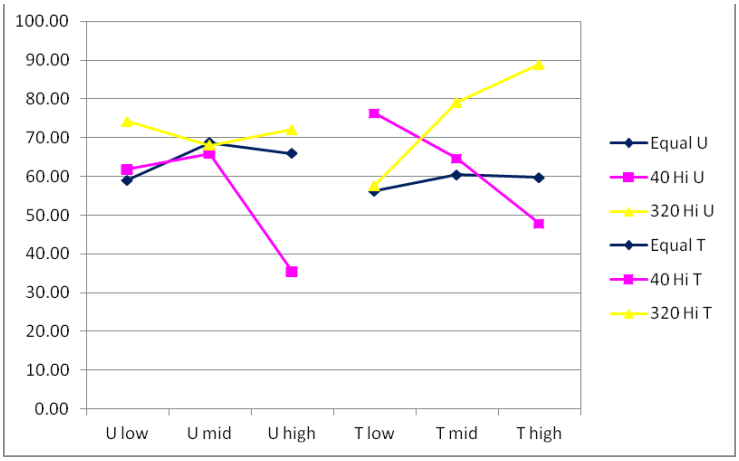

Figure 5.24: The 3-way interaction of trajectory, texture and spectral range. Typical standard error ≃5 percentage points.

the scores for Gaussian test items compared to uniform ones in the high frequency range, and ANOVA indicates that this interaction of texture and spectral range is (just) significant ($p = 0.045$).

The curves for the interactions between step size and the other experimental variables all show similar trends and are not significant: for texture and step size, $p = 0.965$; for trajectory and step size, $p = 0.591$; for spectral range and step size, $p = 0.202$.

The final set of curves in figure 5.24 considers the interaction of trajectory, texture and spectral range with the data pooled over step size. For the case of Gaussian texture (lines to the right of the figure), scores show little variation with spectral range for discrimination along trajectory 1, but fall with spectral range (i.e., from left to right) for discrimination along trajectory 2, and rise with spectral range for discrimination along trajectory 3. A different pattern is observed in the case of uniform spatial variation (lines to the left of the figure). Analysis of variance shows this interaction of trajectory, texture and texture to be significant ($p < 0.001$).

For both the uniform and Gaussian cases, the cumulative discrimination index is ∼11 for trajectory 3 and ∼9.0 for trajectory 1 or 2. This suggests that a substantial number of distinct virtual surfaces is available within the perceptual space offered

by this rendering strategy.

5.10.2 A subsidiary experiment

In the experiment described in the previous section, subjects had reported that the spatial variation (texture) within the target is easier to detect at 320 Hz that at 40 Hz, though this was not reflected in the overall scores. The following experiment was therefore devised to examine the contrast between uniform targets and textured targets.

In common with the earlier experiment, the subjects were presented with sets of three targets and asked to find odd-man-out. There were two test conditions for texture – spatial variation with s.d. 1 dB (±2 dB range) and spatial variation with s.d. 2 dB (±4 dB range). Stimuli fell along the equal intensity line (trajectory 1 in figure 5.16) at positions A1, D1, E1 and J1 (see figure 5.16), i.e. across the full range of spectral balance. All 6 permutations of odd-man-odd configuration were used, making a total of 48 stimulus presentations. As before, "pink"-noise masking delivered through headphones was used to block out audio cues.

Results from six adult subjects (2 male and 4 female, aged 23-35) who had taken part in the previous study are shown in figure 5.25. As expected, the textured targets were easier to discriminate at 2 dB s.d. than at 1 dB s.d. The overall rising trend in the data also suggest that texture is more noticeable at 320 Hz.

In order to apply statistical tools to these results it is necessary to pool the data in some way. The method selected is based on the observation that the straight-line fits in the figure can be completely defined by their end points, i.e. the effective score at 100% 40 Hz and at 100% 320 Hz for both the 1 dB s.d. and 2 dB s.d. cases, to give two data points in the two test conditions. Analysis of variance (ANOVA) based on such straight line fits for the individual subject data shows the effect of textural range to be significant ($p = 0.021$). The effect of spectral balance is also significant ($p = 0.025$).

The finding that spatial variation in the virtual surface is more easily detected at

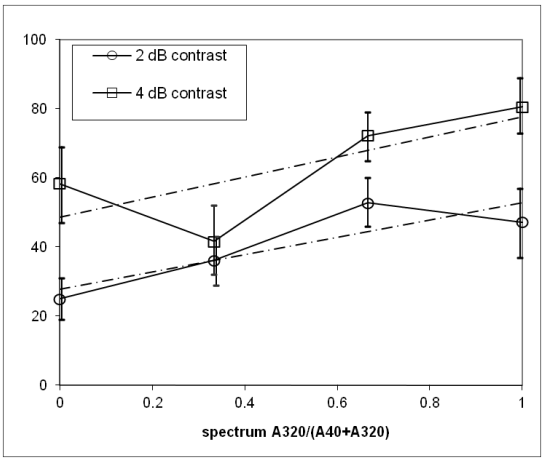

Figure 5.25: Plot of the results of the subsidiary experiment showing subjects' pooled score in each test condition as a function of position along the trajectory.

320 Hz than 40 Hz is particularly interesting because it conflicts with the consensus in the literature that perception in the region of 300 Hz is dominated by the response of pacinian corpuscles which have lower spatial acuity than the non-pacinian receptors which dominate at lower frequencies.

5.11 Conclusion

This chapter has described the development of a new high performance broadband tactile array. It has a bandwidth comparable to and output amplitude greater than Chanter's original device, but is compact enough to be easily moved around on a desktop to perform active tasks. The associated drive electronics and control software are fully capable of real-time, broadband operation. Furthermore, the programming interface developed for it has been designed to facilitate the rapid development of experiments, making this a very powerful tool for psychophysics experiments. It is not unreasonable to suggest that the system described here is at the cutting edge of desktop tactile display technologies.

Experiments have shown that both spatial and temporal (spectral) vibrotactile tactile cues are accessible to subjects; broadband tactile arrays are a logical tool to map out these parameters in a systematic manner.

In summary, the hardware and software described here offer a flexible system to generate surface textures during active exploration of a virtual tactile environment. The potential of this system has been demonstrated by experiments which show that a wide range of virtual textures can be produced, distinguishable from each other and from non-textured (uniform) surfaces. The following chapter describes how strategies for producing virtual textures were developed within the HAPTEX project as part of a multi-modal interface to display virtual textiles, and how the tactile array concept was adapted to be compatible with finger-and-thumb grasping.

Chapter 6

Virtual Textiles

The previous chapter described the construction and evaluation of a truly broadband and real-time tactile array capable of being used in active exploration tasks. The detailed psychophysics studies in section 5.10 has started to explore the possibilities of such devices for pure research. It is this kind of work which will ultimately inform the development of new, better displays; however we can also ask the question, "Using our existing knowledge and technology, what can be done with an array?" For example, could they be used as integral components in a next-generation Virtual Reality system incorporating vision with kinaesthetic and tactile touch sensations. The HAPTEX (Haptic Representation of Textiles) project set out to build just such a system – a visuo-haptic VR System for interacting with virtual textiles.

The work presented in this chapter is a synthesis of work by all of the HAPTEX partners. The tactile stimulator array was designed, built and tested by the author and coworkers at Exeter. The tactile drive electronics were designed and built by the author and coworkers in Exeter and Hanover. The tactile renderer was developed by the Hanover team using concepts developed in discussions with the author and I R Summers; the same partnership was responsible for the final evaluation of the system.

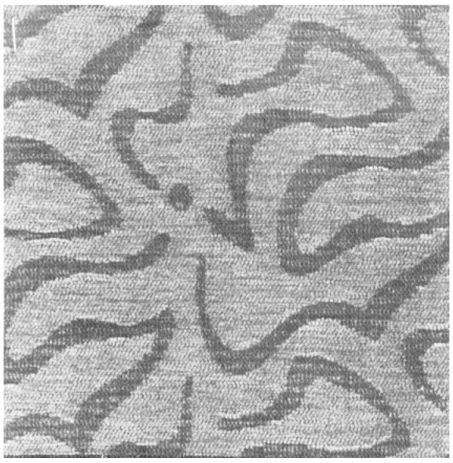

Figure 6.1: Woven-in motifs in Jacquard fabric by using two opposing weaves

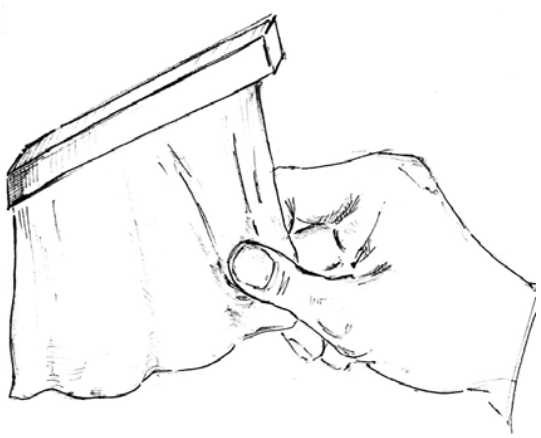

Figure 6.2: The virtual scenario envisaged by the HAPTEX project

6.1 The HAPTEX project

HAPTEX was an EC supported project (IST-6549) funded as part of the Future and Emerging Technologies initiative. Its aim was to produce a working demonstration of a virtual reality system capable of displaying the look and feel of a piece of textile such as that illustrated in figure 6.1. Specifically the goal was to reproduce in real time the scenario indicated in figure 6.2 – a one-handed interaction with a square of fabric hanging on a stand – through both visual and haptic modalities.

As an added feature, the textiles represented were to be based on real fabrics;

the visual pattern, the physical parameters governing their mechanical behaviour and the fine detail of the texture were to be derived from swatches of material. This was clearly an ambitious goal and would require expertise from a number of specialised fields.

6.1.1 Project partners

The HAPTEX consortium was composed of five partner institutions. Exeter[1] provided the tactile expertise (both in terms of display hardware and in rendering strategies) and extensive experience of performing psychophysics studies. Joining us were teams from

- MIRALab at the University of Geneva. specialists in computer graphics and complex computer animation.
- the PERCRO Laboratory at the Scuola Superiore SantAnna (Pisa). This group focuses on developing methodologies and technologies for Virtual Environments; their primary role in the project was to bring their extensive experience in developing haptic interfaces.
- WelfenLab at the University of Hanover. The focus of this group is applying theoretically advanced methods of mathematics in the context of Computational Geometry/Topology and Computer Graphics. They were responsible for developing the integrated software framework which would bind the diverse components of the system together.
- SmartWearLab at Tampere University of Technology. With a background of research into "smart" and functional clothing and textiles, to HAPTEX they brought detailed knowledge of fabrics and the KES-F system for objective assessment of hand properties [2].

[1] The Exeter team comprised of I R Summers, Jianguo Qu and the author; useful contributions were also made by a number of undergraduate project students

[2] Fabric Hand – The quality of a fabric assessed by the reaction obtained from the sense of touch

6.1.2 Overview of the system

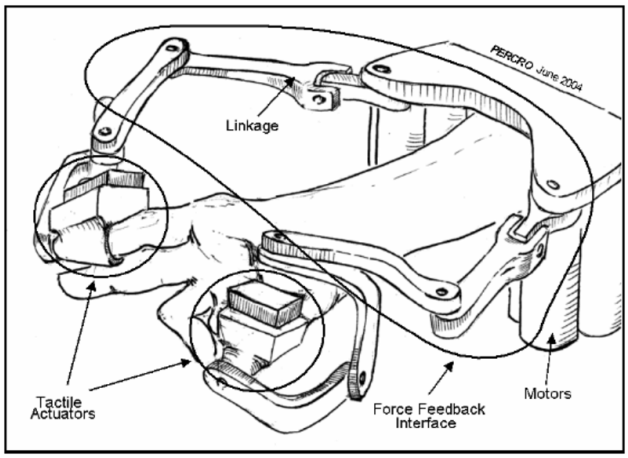

Figure 6.3: Concept of the HAPTEX device (initial proposal).

The core of the project was the development of an integrated tactile array and fingertip force-feedback device along with the real-time control software to drive it. In the scenario shown in figure 6.2, the finger and thumb experience large forces relating to the gross mechanical properties of the fabric (stretching, shearing and compression) and small distributed forces related to the fabric surface (e.g. when the fabric is stroked).

How can this be implemented?

An early concept which illustrates the key mechanical components of the system is shown in figure 6.3. Attached to the wrist-mounted device are two articulated arms which provide force-feedback to the user's thumb and forefinger via a pair of thimbles, and aach thimble is equipped with a distributed tactile display on its inner surface.

Each element of the display (visual, kinaesthetic and tactile) has its own requirements from the underlying software model. While the visual motion of the global cloth object can be computed with frame rates of about 25 Hz for achieving realistic visual feedback, realistic haptic interaction requires at least 1 kHz for rendering properly the mechanical effect of the user interaction and the force feedback. However, this rendering only needs to be carried out locally, around

the haptic contact points. In order to make optimum use of system resources, the simulation is divided into two layers as shown in figure 6.4. The large-scale layer which is responsible for the global motion of the cloth object, and the small-scale layer which features high frequency local mechanical simulation for haptic rendering. The textile simulation method addresses the large-scale simulation, while the small-scale simulation is part of the haptic rendering. The haptic rendering is

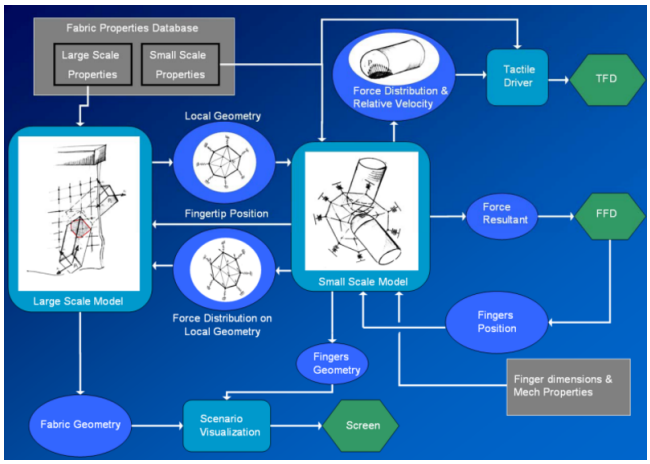

Figure 6.4: A conceptual map of the HAPTEX system architecture.

further sub-divided. At the top level, a contact handler uses the high resolution mesh and a model of the fingertip to generate inputs for a module handling the contact forces and also to the tactile renderer described in section 6.4.1.

6.2 Modelling the Fabric

There are clearly a wide variety of mechanical properties which could be incorporated into the computer model; there are similarly a large number of ways in which such properties could be evaluated or measured. Given this very broad landscape, it would seem sensible to concentrate on the techniques used and properties involved when people actually examine and evaluate cloth. Fortunately this is a well understood area within the textile industry, and there is a long established and well formulated way of characterising textiles using certain key properties and manipulations. These characteristics are collectively referred to as fabric hand, or

simply the hand properties of a garment. Conventionally fabric hand is assessed by subjective evaluation performed by experienced individuals. However, the human element introduces an unavoidable degree of variability, so there has been a great deal of work to develop purpose built machines which can be used to make equivalent objective measurements of hand properties, describing the fabrics in terms of a set of "characteristic values". One of the main standards in this field, and the one chosen for use in the HAPTEX project, is the Kawabata Evaluation System (KES-F) [104]. KES-F is comprised of a set of machines which are used to perform tests on fabric samples in order to extract a set numerical values which are derived directly from the mechanical properties of the fabric but which can be understood in the context of fabric hand. The KES-F system is described in more detail in appendix I.

A broad library of fabric samples was assembled and tested using a set of KES-F equipment by SmartWearLab for the HAPTEX project. All of the fabric models generated used physical property data corresponding to real fabrics in this library. In addition to the standard KES-F tests, the raw surface profile data was recorded (via an ADC onto an external PC) for use by the tactile renderer.

6.3 HAPTEX System Hardware

One of the cornerstones of the HAPTEX project was the development of a hardware interface which would be capable of presenting the senastions to an operator through the sense of touch, simutaneously adressing both the kinaesthetic and cutaneous aspects. In order to do this, elements were required to provide both large scale force feedback interactions and smaller scale distributed tactile displays.

6.3.1 Force feedback elements

The force feedback hardware for the HAPTEX project was developed by the PERCRO laboratory. The development consisted of two phases. In the first, a new

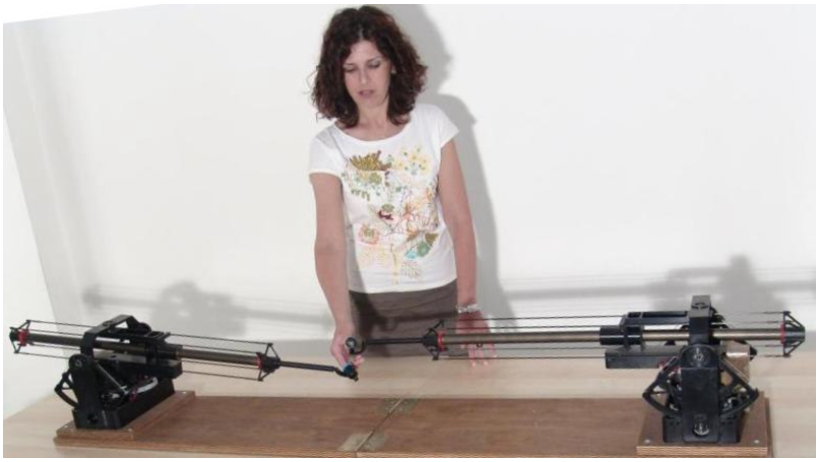

Figure 6.5: The GRAB system from PERCRO

end-effector was developed for their existing GRAB system. The second phase required the development of a completely new device – a hand mounted glove-like machine called the HandExos.

GRAB

The GRAB device is a force feedback device consisting of two identical and independent robotic manipulators (see Figure 6.5), each having the base link fixed to the desktop and the end-effector (contact part) attached to the palmar surface of the user's thumb or index fingertip. Each manipulator measures the absolute position and orientation of the contact part. In the context of the HAPTEX control system, these are used by the haptic renderer to compute an appropriate force, representing the overall force generated when handling the virtual surface. The manipulator is able to generate this force on the contact part within a workspace of 400 mm in width, 300 mm in height and 200 mm in depth. The work-spaces of both manipulators overlap. Force errors are limited in a range of about +/- 10 grams force (0.1 N). The device can exert forces up to 20 N.

Mounting a tactile array on to the end of the GRAB arms required a number of changes to be made to the device:

- The end effector gimbals were fitted with position encoders so as to provide

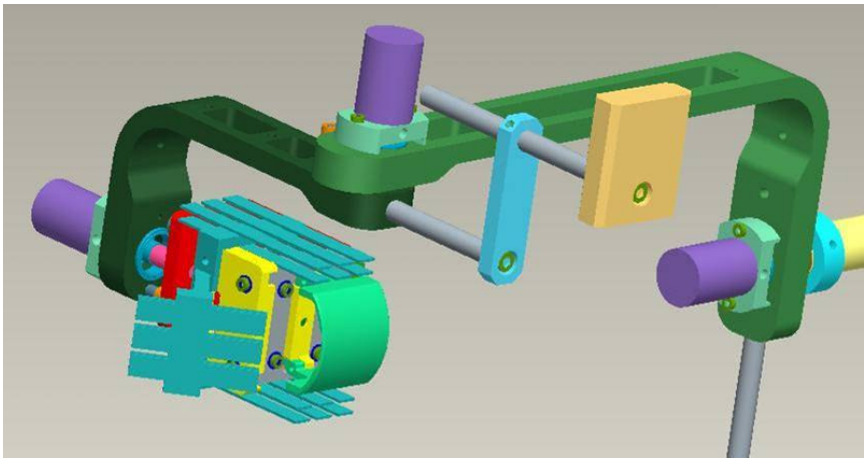

Figure 6.6: CAD model of the GRAB modifications

information about the array orientation to the control software.

- The gimbals were increased in size and counterbalanced to incorporate the array(see figure 6.6).

- A force transducer was incorporated into the end effector to measure the force delivered to the the finger/thumb via the force-plate which represents the contactor surface of the array.

- A revised control loop was implemented to handle the changed inertia of the system and to interface with the new software.

Figure 6.7 shows a prototype of the new gimbal with the new force transducer and force plate attached.

HandExos

The final embodiment of the HAPTEX system was intended to be a compact, wearable device not unlike a glove. Figure 6.8 shows how the concept would have worked.

Although much development work was done and a working prototype demonstrated together with a compatible tactile array, the limited time (and funding)

Figure 6.7: The force transducer (centre) attached to the curved force plate (below), and the gimbal (above, right) which links to the force-feedback device.

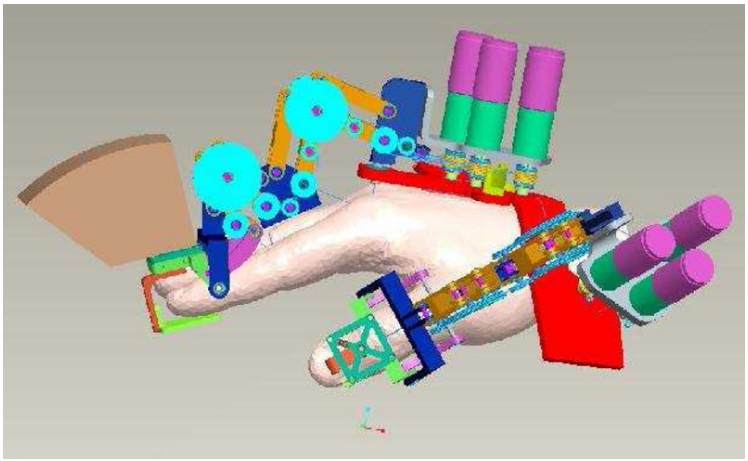

Figure 6.8: CAD model of the HandExos concept, including a tactile array on the index finger.

associated with this multi-centre project unfortunately prevented the final goal of operating the tactile displays on the HandExos from being realised.

Nevertheless, the individual components produced were novel and the level of system integration achieved was groundbreaking, and overall the project was considered a success. In particular, the tactile display element produced a number of innovations; these are the subject of the rest of this chapter.

6.4 The HAPTEX Tactile Display

The tactile display elements within the HAPTEX project presented a a number of challenges at every level of the system. At a high level, a way needed to be developed to process textural information from real objects and encode it in a way that would be recognisable when presented through the medium of a vibrotactile pin array, and the effects of friction and the speed of movement of the fingerip would have to be incorporated. Complex signals would need to be delivered to the arrays in real time in a 3D environment from a controller in which system resources would be at a premium. Finally, and perhaps most significantly, the array hardware would need to be compact, lightweight and would have to be compatible with the complex manipulation tasks envisaged within HAPTEX, including pinch interactions.

6.4.1 Control system

This section describes the control system for the HAPTEX tactile display, covering the software systems responsible for encoding and rendering of textural information from fabric measurements and the electronic hardware developed to translate the outputs from this into drive signals for the indivual tactile actuators.

Texture rendering

The tactile renderer for the HAPTEX project was implemented by Dennis Allerkamp at Hanover, building on discussions with the the author and I R Summers, and is described in Appendix J; the following is a brief overview.

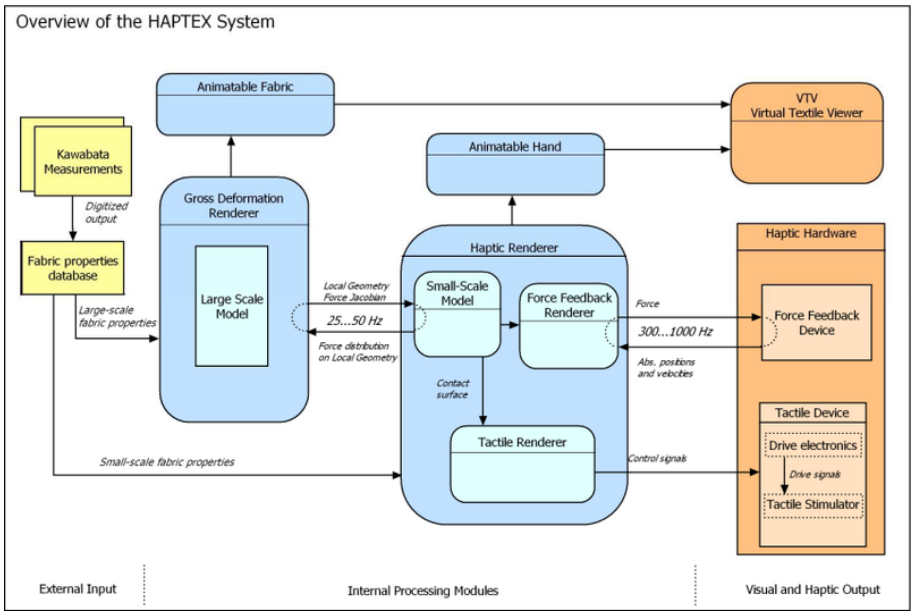

Figure 6.9: Overview of the HAPTEX system

To recap, the tactile element of the HAPTEX system is controlled by the surface model (figure 6.9) which describes small scale surface fluctuations across the fingertip contact area and is derived from the height profile of the fabric. It receives its contact information from the small-scale model. This generates the output to the haptic renderer and derives from a refinement of the large-scale model which in turn gives the geometrical shape interpolation of the contact point. The tactile renderer is called every 25 ms, i.e. it runs in a 40 Hz loop. However, the contact data is computed by the haptic renderer every millisecond and we need to re-sample that data. To avoid aliasing the data is passed through an anti-aliasing filter that suppresses frequency components above 20 Hz.

In the tactile rendering strategies described previously the workspace was assumed to be planar as illustrated in figure 6.10. Furthermore the finger was assumed to always be in contact with the tactile surface. However, in the HAPTEX

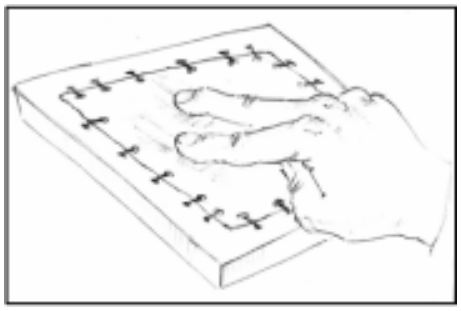

Figure 6.10: A representation of a desktop tactile experiment.

scenario, the object being modelled is a fabric which may have folds and wrinkles; as a result the contact geometry can be far more complex than in the simple planar case. The consequence of this is that instead of the single contact point used in the earlier models, the tactile renderer requires a contact area to decide which contactor pins have to be activated. Note that only the pins of the tactile actuator inside the contact area are activated; it is also possible that at any given moment the contact area may not exist, i.e. the finger is not touching the fabric. The shape of each finger's contact area is provided by the force-feedback renderer. The contact model contains a model of the fingertip and the geometry of the tactile actuator. It uses these to determine the position (in local coordinates of the fabric) and the normal force at each contactor pin. The fingertip model is able to deform due to the contact pressure which also influences the shape of the contact area.

The contact model is also used to scale the amplitude of the sensations according to the contact forces, based on the observation that the intensity of tactile sensations depend on the force with which the finger is pressed against the surface. The amplitudes computed by the tactile renderer are multiplied by $k_F \cdot F$ before they are transmitted to the tactile actuator, where F denotes the force between the finger and the fabric and k_F is a constant relating the force to the intensity. Whilst this is clearly a simplification, e.g. tactile sensations are masked at higher forces, a linear dependency between the force and the sensation for relatively small forces seems a reasonable place to start.

In common with the display system described in chapter 5 the purpose of the tac-

tile component of the HAPTEX software engine is to produce vibrotactile stimuli consisting of a superposition of two sinewaves. However, whereas in the previous embodiment the waveforms were generated on the host computer, for reasons described in section 6.4.1 in the HAPTEX system the host computer is only required to calculate the instantaneous sinewave amplitudes.

A point on the skin moving across the height profile of the fabric experiences a displacement whose temporal profile is dictated by the speed of movement across the surface. It is this time-varying stimulus that is detected by the mechanoreceptors in the skin. Using our knowledge of these receptor channels, it should be possible to create a reduced data set suitable for use with a vibrotactile array (i.e. amplitudes for the frequency components in each channel), working from the surface profile data obtained during the KES-F measurements.

To achieve this, the raw data derived directly from the weave textures were preprocessed to generate the appropriate small scale surface model of the given fabrics in the spatial domain. The renderer combines these 1D models with the rate of traversal of the fingertip across the fabric to generate an effective temporal spectrum for each pin in the array. A pair of filter functions is then used to distribute this spectral content into amplitudes for the two system drive frequencies.

An experiment to evaluate the performance of the renderer is described in Appendix J.

Drive Electronics

In the original proposal for the HAPTEX system it was envisaged that the tactile drive signals would be delivered using a system similar to that described in chapter 4, i.e. the host computer would control a series of switches which would direct the signals from external sinewave generators to active channels on the stimulator array(s) as required. This would either be a simple on/off control as in the earlier system, or would add a very basic level of amplitude control using in-line resistors. It was considered that a more eleborate controller would place an unnecessarily

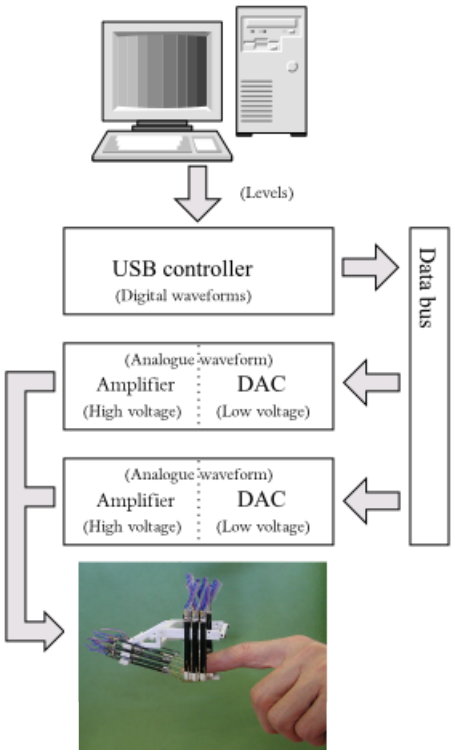

Figure 6.11: Schematic representation of the HAPTEX drive electronics.

high burden on system resources which would already be strained by the complex graphical and force-feedback tasks. However, when the time came to design the tactile system interface, the author realised that the overall architecture used in the system in chapter 5, with its much greater flexibility and dynamic range, could be implemented within HAPTEX with one conceptually simple change – the process could be split so that the high-bandwidth tasks would be performed by a microcontroller.

The chip selected to do this is a CY7C64713 Cypress Semiconductor microcontroller, which contains a 24 MHz Intel 8051 microprocessor, 16 kBytes on-chip RAM and a USB transceiver, and can be programmed via the USB link.

The onboard control software (firmware) running on the microprocessor performs the same task as the bandwidth heavy back-end modules in the previous software, converting the amplitudes into waveforms using on-board look-up tables and in so doing removes a large processing and data output overhead from the controller pc. A number of implementations of the firmware were used, all of which were capable

of running with base clock speeds in excess of 5 kHz. It should be noted that the restriction to only two frequencies is only implemented in the software part of the system – there are no hardware restrictions as to why this could not be increased if required.

Data from the micro-controller is transmitted as a parallel data stream (8 bits of data, 5 bit address) to the back-plane. The digital data is processed into analogue waveforms by a series of quad DACs (in this case the MAX5100). Individual DAC chips are selected by a simple logic circuit programmed by jumpers in the same way as those described in chapter 5. The outputs of each DAC is passed through a first order low pass filter with cut-off $\sim$1 KHz (this removes any digitisation-induced higher harmonics) and fed to the amplifiers. The amplifiers use a bridge design similar to that used by Chanter, except that the amplifier chip used is the OPA 551. This chip can operate from supplies of up to 35 V, greatly increasing the maximum output amplitudes achievable from the system. (In the HAPTEX system, the amplifiers were set with a power supply running off 24 V rails, giving a maximum range of about 90 V peak-to-peak).

Each DAC is housed on its own board with its own set of 4 amplifiers (see figure 6.12). The board layout is quite straightforward – digital data passes from the back-plane to the DAC and the address decoder. The output from the DACs passes down the board to the amplifiers. Note that until this point the only cabling required has been a single USB connection to the control PC and the power connections into the back plane. This is a vast improvement over earlier designs.

The complete system then comprises the host-controller board, a back plane for the distribution of the parallel data and power, and 6 DAC boards The prototype of this is shown without its case in figure 6.12

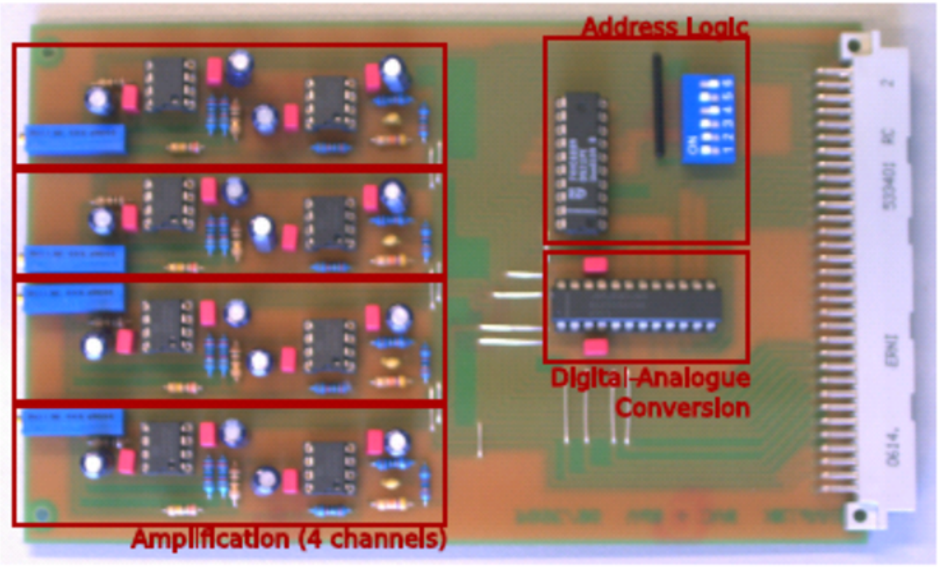

Figure 6.12: Layout of the HAPTEX DAC/amplifier board

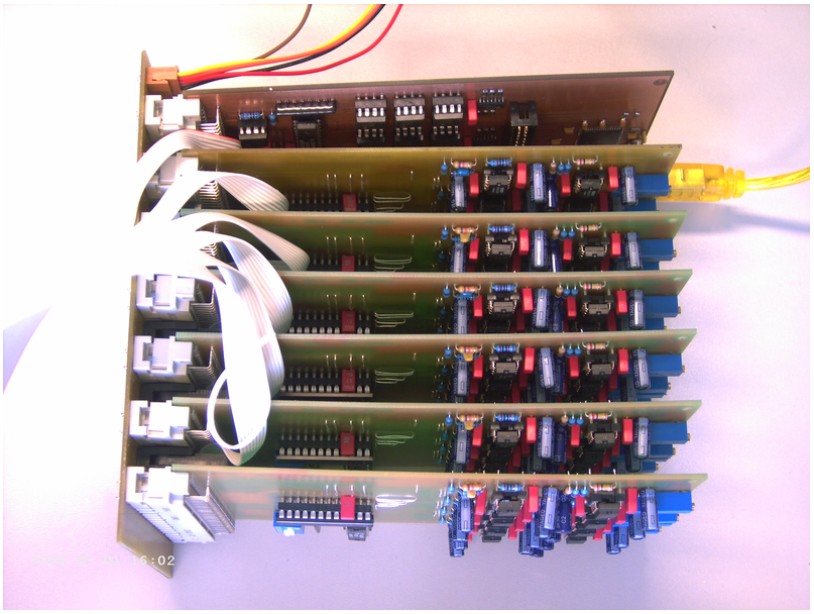

Figure 6.13: The naked HAPTEX drive electronics (24 channels for one finger)

6.4.2 The HAPTEX Tactile Array

The HAPTEX scenario proved a formidable challenge for array design. What was required was a device with the characteristics and performance of the texture array described in the previous chapter, but which could be mounted onto a force-feedback device capable of fingertip grasping manipulations.

Clearly the existing large chassis would have to be pared down to minimise weight and bulk. What was not so clear was how to change a device which in its current design had 24 actuators positioned below the fingertip so as to have very little mechanism below the fingertip, in order that the finger and thumb could be brought together. As an added complication, the geometry of the GRAB gimbal and the new force sensing element placed significant restrictions on the space available for the array mechanism.

Specifications

The technical specification for each of the tactile displays for the HAPTEX system are summarised below:

- Number of channels: 24
- Spatial resolution on the finger: 2 mm
- Working bandwidth: 25 to 400 Hz[3]
- Maximum output amplitude: 100 μm
- Spatial resolution of the virtual workspace: 1 mm
- Input data: Data frames with 32 bits per channel, i.e., around 800 bits per frame for 24 channels
- Input data rate: Frame rate of 40 Hz, i.e., around 30 kbits s^{-1} for 24 channels

This specification is essentially the same as that for the system described in chapter 5. The key difference between that system and the HAPTEX displays is the intended use. Whereas the texture array (figure 6.14) is a table-top device, the HAPTEX displays need to be mountable on independently actuated force-feedback devices (refer to figure 6.3); they must be compact and of minimal mass so as to cause as little degradation to the performance of the haptic device as

[3]As before the device was intended to work at two operating frequencies: 40 and 320 Hz.

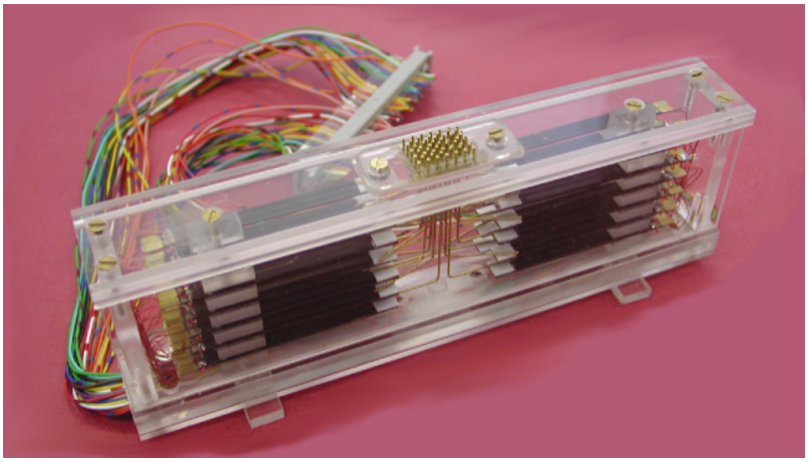

Figure 6.14: The texture array from chapter 5 – this cannot be used for grasping!

possible. Furthermore, the chosen scenario requires that the device be suitable for representing two-fingered grasping manipulations of thin objects. This means that the display mechanism must have minimal thickness below the fingertip, unlike the texture array.

Concept

It is immediately apparent that the geometric constraints enforced by the requirement to allow the finger and thumb to "grasp" add a whole new layer of complexity to the design. Furthermore, interfacing the device with force-feedback hardware introduces an additional raft of requirements.

The first problem to address is the geometric one, i.e. how can the stimuli be delivered, and where will the piezoelectric bimorphs be located? In the first analysis, it would appear that the best available space is above the finger. Figure 6.15 shows an early concept in which the direct actuation by straight rods below the finger has been replaced by hooked shaped wires actuated from behind the finger.

In this scheme, all of the bimorphs are located directly above the finger. This means that rather than the contactors being simple extensions of the cantilever tips, stimuli have to be delivered to the fingertip by more complex paths. This

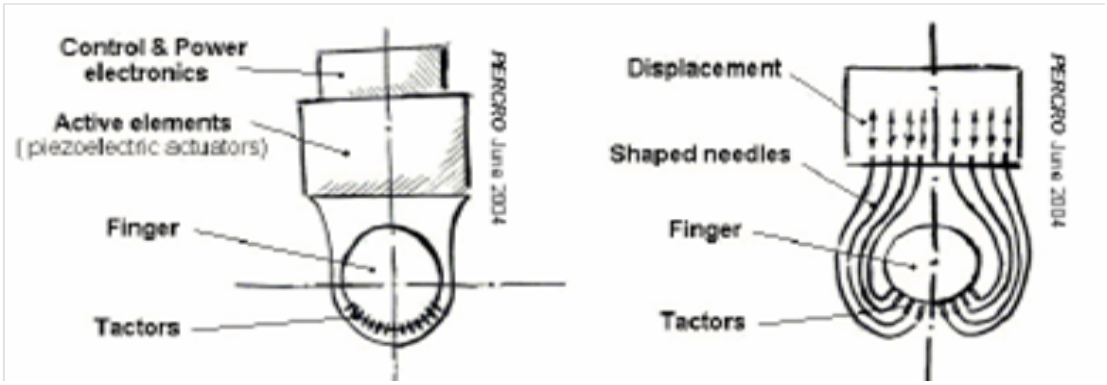

Figure 6.15: Actuation from above the finger (initial proposal).

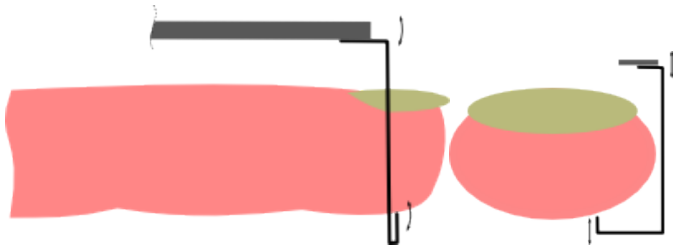

Figure 6.16: Possible implementation of a vibrotactile pin contactor driven by a piezoelectric bimorph mounted behind the finger.

could be achieved using hook like linkages as illustrated in figure 6.16, although it quickly becomes apparent when looking at potential layouts that is not a trivial task to get all of the contactors into place and there is not much room in the available space; the region above the finger is significantly smaller than was used in the construction of earlier devices (e.g. look at the space occupied in figure 6.14).

A way to address this space problem would be to move some of the actuators elsewhere – but where to? In previous designs, the pins were driven in a direction normal to skin surface at the centre of the finger (referred to here as the *vertical* direction). Of course, the fingertip in its free state has a curved surface, so as the contact point moves away from centerline, the skin surface normal vector moves around towards the horizontal. It had not been necessary to consider this in the earlier designs as over the central region addressed by the arrays there is still a significant vertical component to the surface normal. Furthermore, the subject's fingerpad is slightly deformed onto a flat contact surface, effectively pulling the

surface normal across the fingerpad back towards the vertical. However, if the contact surface is curved rather than planar, there may be little difference between a pin vibrating in the vertical or horizontal directions. Figure 6.17 shows how this could be realised; notice that the bimorph sits alongside the finger.

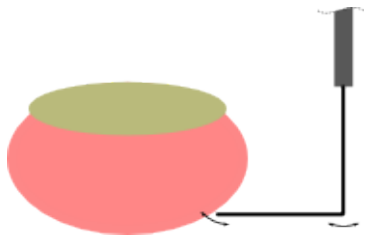

Figure 6.17: Side-actuated pin

The outer rows on each side of the array (fully half of the driven pins) can be driven this way, meaning that only the central two rows require driving vertically.

Fitting two stacks of six bimorphs above the finger is a much more realistic proposition than attempting to fit twenty four actuators into the space – however whilst a this was being developed, a further space issue became apparent.

In order to be able to accurately deliver the fine forces required by the fabric simulation, the force-feedback system had been modified to incorporate a system to measure the contact forces at the user's fingertips as described in section 6.3.1. In figure 6.7 in can be seen that the bulk of the mechanical and electronic components for this force sensor assembly reside in a volume directly behind the finger – exactly the space being contemplated for the tactile array hardware.

Figure 6.18 shows a schematic evaluation of space requirements around the user's finger for the HAPTEX system, taking into account the force-feedback hardware as well as the general requirements of allowing grasping manipulations and multi-digit implementations.

Taking this into consideration, it can be seen that the side-mounted piezos fit nicely into the available space. The vertical acting group could sit above the force sensor, but would need to have very long linkages to drive the contactor pin; this would almost certainly compromise the stiffness of the linkages and would

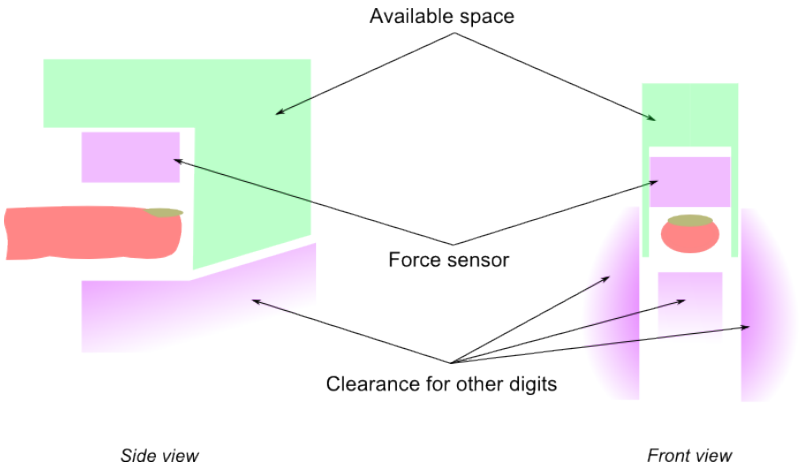

Figure 6.18: The regions of space available for use by the tactile array hardware

also make them a lot more prone to bending and sticking. There is however an alternative space available – in front of finger. Figure 6.19 shows how this might be utilised.

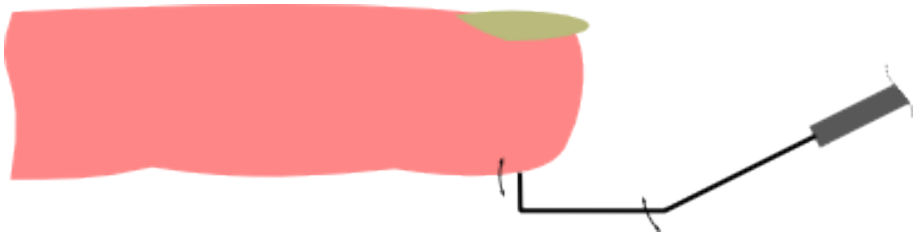

Figure 6.19: End-actuated Centre pin

A scheme to meet all of the requirements, combining the two approaches described previously, is illustrated in figure 6.20.

A Prototype

Many sketches were drawn to develop the concept into a detailed design. However, it is often the case with complex mechanisms that "the Devil is in the detail", especially in sitituations such as this where many of the components are fashioned and assembled by hand.

In order to fully understand the subtleties of the design, and to answer the fundamental question of whether it could it be made to work, it was decidede that

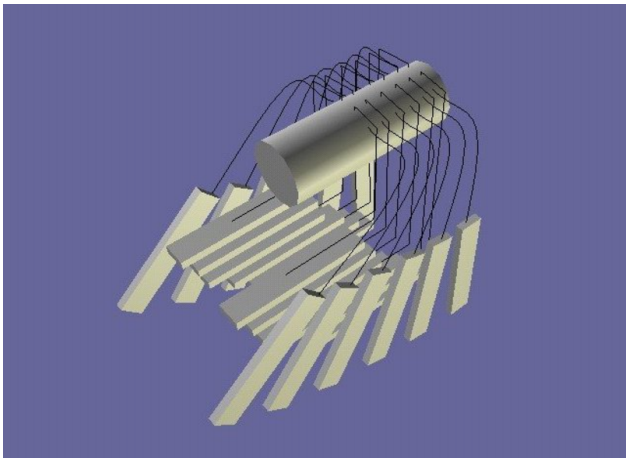

Figure 6.20: A possible implementation of the HAPTEX array, using cross-driven actuators for the outer rows of the array

the best course of action would be to develop a flexible prototype.

The main structure was constructed using 3 mm square cross-section polystyrene bar-stock obatined from a modelling shop. Polystyrene was chosen because it ideally suited the experimental and adaptable nature of a first build, being easy to shape, modify and assemble. Sub-components can be shaped with a scalpel, modelling saw or microdrill and then welded together using dichloromethane. A photograph of the assembled device is shown in figure 6.21. The horizontally-acting piezoelectric bimorphs for the outer rows of contactor pins have been set into two banks to save space. This refinement utilises thin plastic spacers to separate the two banks; the contactor wires of each inner and outer set of bimorph pairs are fixed to on opposite edges of the actuators to allow clearance for the outer wire to pass through to the contact area. The bimorphs driving the central two rows of the array are mounted on angled cantilevered supports extending out beyond the end of the finger. Figure 6.22 shows the routing of the contactor wires.

The finger-plate has to perform two roles within overall system: it is a direct replacement for the GRAB force-plate (shown in figure 6.7), measuring and transmitting the fingertip contact forces as part of the force-feedback hardware; it also has to take the place of the PTFE guide and fixed interstitial pins of the texture

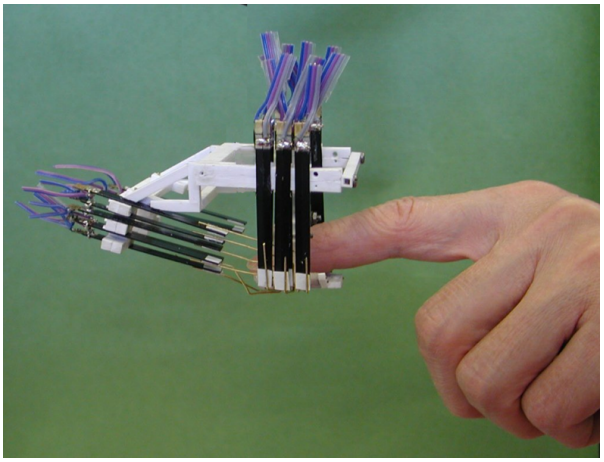

Figure 6.21: The HAPTEX Tactile Array (first prototype in polystyrene). Notice double rows of side-mounted piezos and angled, cantilevered mountings for the piezos driving the central rows of pins. The holes in the frame and frame and the force-plate are for the attachment of an assembly fixture for mounting the array to the GRAB.

array described in chapter 5.

Figure 6.23 shows a CAD model of this critical piece. Note how the outer rows of holes are angled to align with the laterally actuated pins, and how the intermediate pins of the earlier device have replaced by ridges and bosses on the plate. This complex component would be difficult to make using conventional machining techniques, so the prototypes were fabricated (from nylon) using the technique of "Selective Laser Sintering" (SLS)[4].

Whilst the connector pin routings shown in figure 6.22 might seem to be unsatisfactory – some of the linkages are longer than ideal and some have to be bent

[4]In this process, the 3D part is created layer by layer directly from the 3D CAD model. To do this, the CAD model is sliced into layers 0.1 mm thick by software in the host computer. In the machine itself, a compact layer of a powdered polymer is spread on a table; a high-powered laser then raster-scans across the powder bed, fusing together an image of the first layer of the CAD model. This writing operation is typically performed at a working resolution of 0.1 mm. The machine then spreads another layer of powder, and repeats the process, stepping through the model a layer at a time. At the end of the process, a solid workpiece in the shape of the CAD model is left, sat in a container of powder.

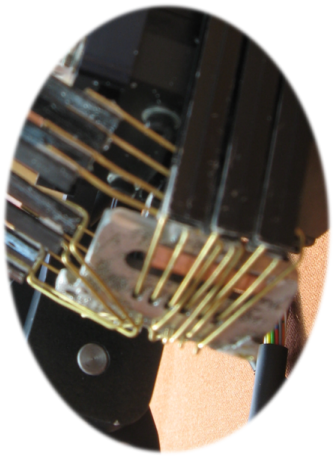

Figure 6.22: Detail of the connector pins for the HAPTEX Tactile Array, showing how they pass through the finger-plate.

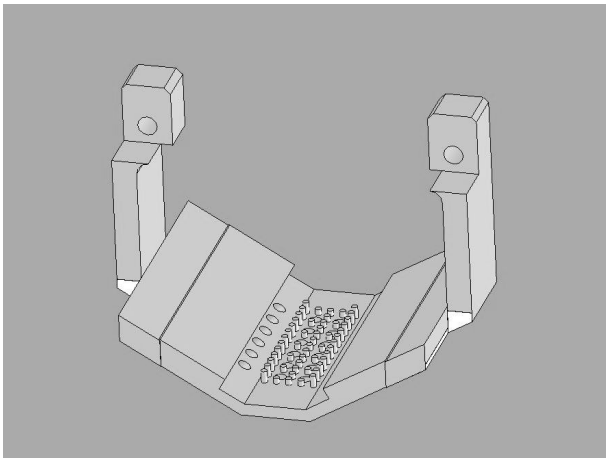

Figure 6.23: CAD model of the force plate for the HAPTEX Tactile Array

into relatively complex shapes) – initial performance tests showed that the device performs remarkably well. There is no noticable difference in the sensation from the outer pins compared to that experienced from "conventionally" driven pins on the earlier table-top arrays. The central rows are also capable of delivering stimuli which are comparable to the benchmark devices if care is taken with the pin paths during assembly.

Fitting the tactile array to the GRAB is a delicate operation and requires a fixture to perform without damaging the This is because the fixation for the finger-plate is carried by the force sensor; in its role as part of the force sensor, the finger-plate has

to be mechanically decoupled from the supporting structure of the array. Ideally, the tactile array would be assembled in situ on the force sensor. However, as the arrays were being built in Exeter while the GRAB components were developed and tested in Italy, this was not practicable. Instead, the a dummy force sensor was used to hold the finger-plate in place while the array was assembled; fixing the array to the GRAB requires that this fixture be removed, leaving the finger-plate unattached with the contactor pins in place. The fixing holes for the external bracing fixture developed for this purpose are visible in figure 6.21.

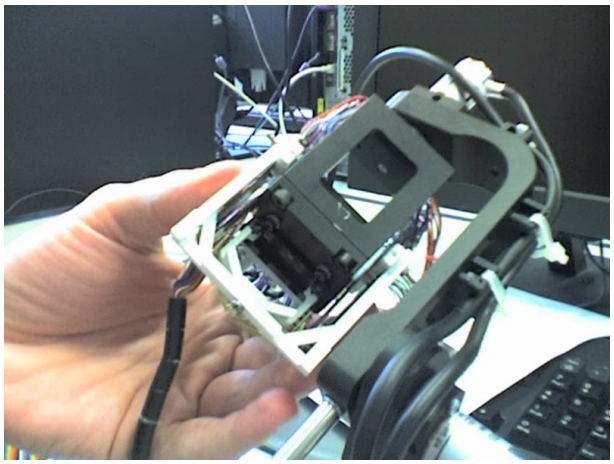

Figure 6.24: The prototype tactile array mounted on a GRAB end-effector. The (prototype) external bracing fixture is still in place.

In light of the good performance (in fact better than expected) of the prototype and a successful integration trial with the GRAB, this design was chosen for the HAPTEX Tactile Array.

Construction of the HAPTEX Tacile Array

The final design of the support structure for the HAPTEX Tactile Array is shown in figure 6.25. The superstructure of the array has been completely removed leaving only the force plate and a frame for attaching the bimorphs – it relies on the casing of the force sensor body for stiffness and support. The main structure is made from acrylic, as with the previous systems described in this thesis. The

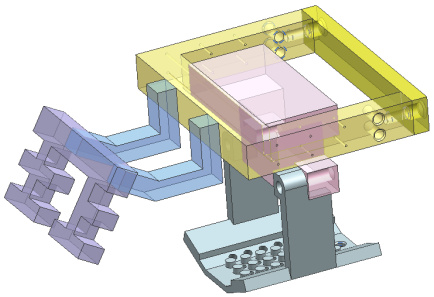

Figure 6.25: The final design of the chassis of the HAPTEX Tactile Array, with dummy force-sensor in place. The pairs of holes along the flanks are used to align the bimorphs.

nylon finger plate used in the prototype was not considered to be strong enough for use with a force-feedback device (SLS parts are particularly weak along the build-plane layers), so Direct Metal Sintering[5] was used to produce the part from stainless steel[6].

Figure 6.26 shows a photograph of unpopulated skeleton of the new arrayand figure 6.27 shows the fully assembled device.

As describe in section 6.4.2, jigging pieces are required to hold the array in shape whilst it is fitted to the haptic device. After the piezoelectric bimorphs (with electrical connections in place) and the contactor wires have been built onto the frame, an external brace is fitted. This forms a rigid link around the outside of the array, holding the finger-plate in place relative to the array chassis (figure 6.28). It also acts as a resisiliant case for the array during transit. In figure 6.29, a tactile array can be seen part way through the mounting procedure. With the external brace in place, the dummy force sensor fixture has been removed and replaced with a mounting adaptor.

[5]In common with other SLS processes, this technique suffers from a relatively rough surface texture; it was, however, a simple matter to clean up the contact faces and holes.

[6]At the time this was a very new process and lighter metals were not available.

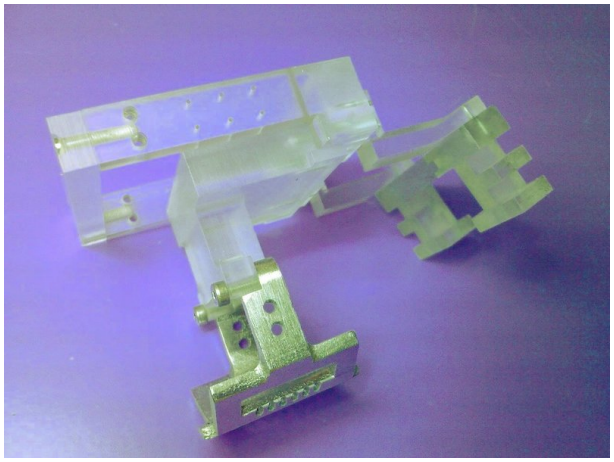

Figure 6.26: Framework for the HAPTEX Tactile Array. The force-plate is held in place by a jigging piece.

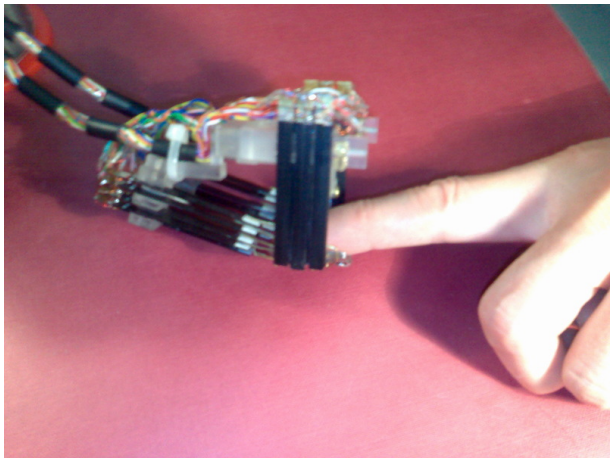

Figure 6.27: The HAPTEX Tactile Array.

The actuator pins are very vulnerable, especially since the device is intended to be used as one of a pair. In figure 6.30 a completed array fitted to a GRAB end effector can be seen, complete with a safety shield fitted over the pins. This is held in place using the same screw holes as the external brace.

The total thickness of the device below the finger-pad is 5 mm including the protective cover. Figure 6.31 shows a pair of devices in place in a pinch configuration. The GRAB end-effectors are passive gimbals; each moving mass has to be counterbalanced to allow free rotation. In figure 6.31 the improvised weights that were used during the initial trials can clearly be seen.

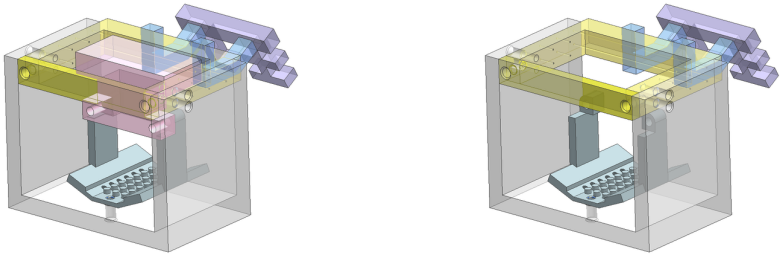

(a) The external fixture secures the finger plate...

(b) ... allowing the assembly piece to be removed.

Figure 6.28: Framework for the HAPTEX Tactile Array. The force-plate is held in place by a jigging piece.

Figure 6.29: Fitting the HAPTEX Tactile Array onto the GRAB

The realisation of the HAPTEX demonstrator with its integration of diverse software components and its combination force-feedback and high resolution tactile displays is a significant achievement – but how well does it perform?

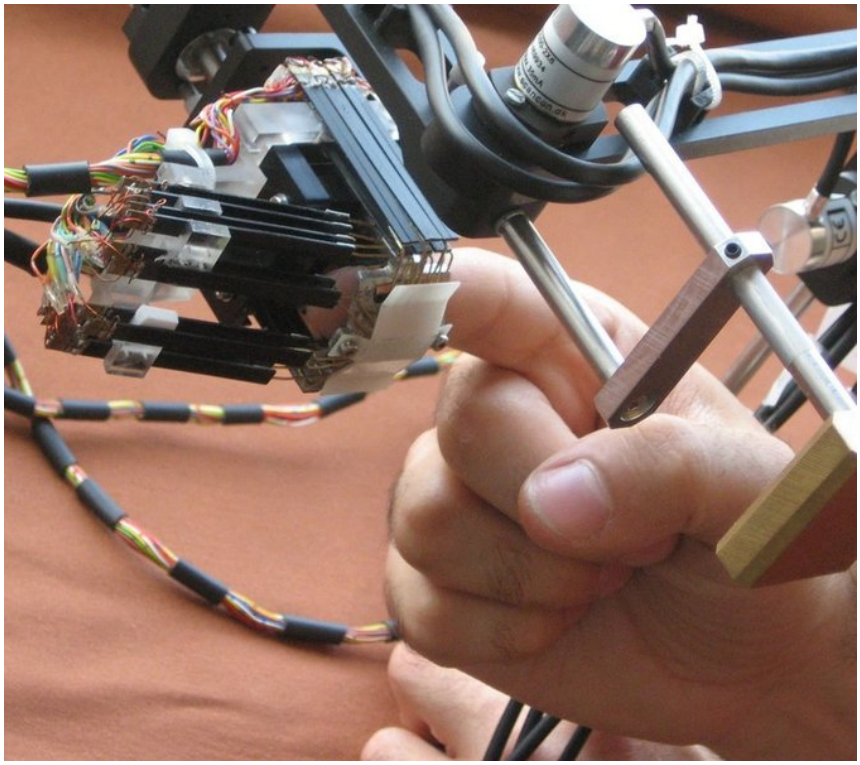

Figure 6.30: The HAPTEX Tactile Array fitted to a modified GRAB end-effector

6.5 Performance of the HAPTEX System

The goal of the HAPTEX project was to build an integrated multi-modal display, so a significant amount of the time available was dedicated to integration activities and ironing out system level problems. As a consequence, there was very little time to perform bench tests to characterise the tactile array in isolation, and so what follows is an evaluation of the tactile components of the overall system.

6.5.1 Subjective performance

The significant result is that the integrated system actually *works* – members of the project team and many of the delegates at the HAPTEX symposium who were able to try the system reported that they experienced a sensation of grasping a deformable, textured object. Similarly, in the formal evaluation of the system (see section 6.5.2, below) users were able to manipulate and explore textiles in the virtual environment using similar strategies to those they employed with real

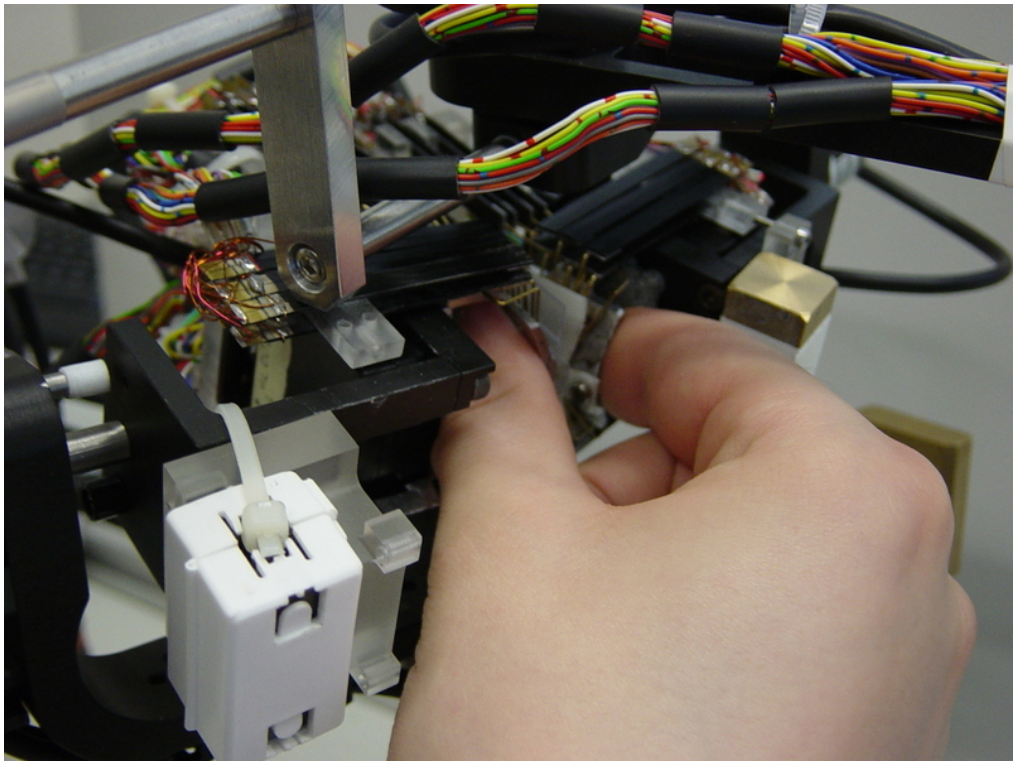

Figure 6.31: Two HAPTEX Tactile Arrays in use with the GRAB. Notice the improvised counterweights.

textiles.

The tactile renderer delivers distinct stimuli (the effectiveness of this is examined in section 6.5.2) for each fabric in the HAPTEX library – figure 6.33 (prepared by Matthew Philpott) shows the mean amplitudes of the two frequency components generated by the renderer (at 40 Hz and 320 Hz), for 29 representative textiles from the HAPTEX database. I t can be seen that the textiles are represented by a wide range of renderer outputs within the available 2D space of figure 6.33. Both amplitudes vary over more than an order of magnitude and, although there is some correlation between the two amplitudes, independent variation of the two frequency components contributes to the separation of the textiles within the 2D space. Similarly figure 6.34 (also prepared by Matthew Philpott) shows the spatial variation of the of the two frequency components over the surface of the virtual textile, for the 29 representative textiles. Again, for this spatial aspect of the virtual textiles, the textiles are represented by a wide range of renderer outputs.

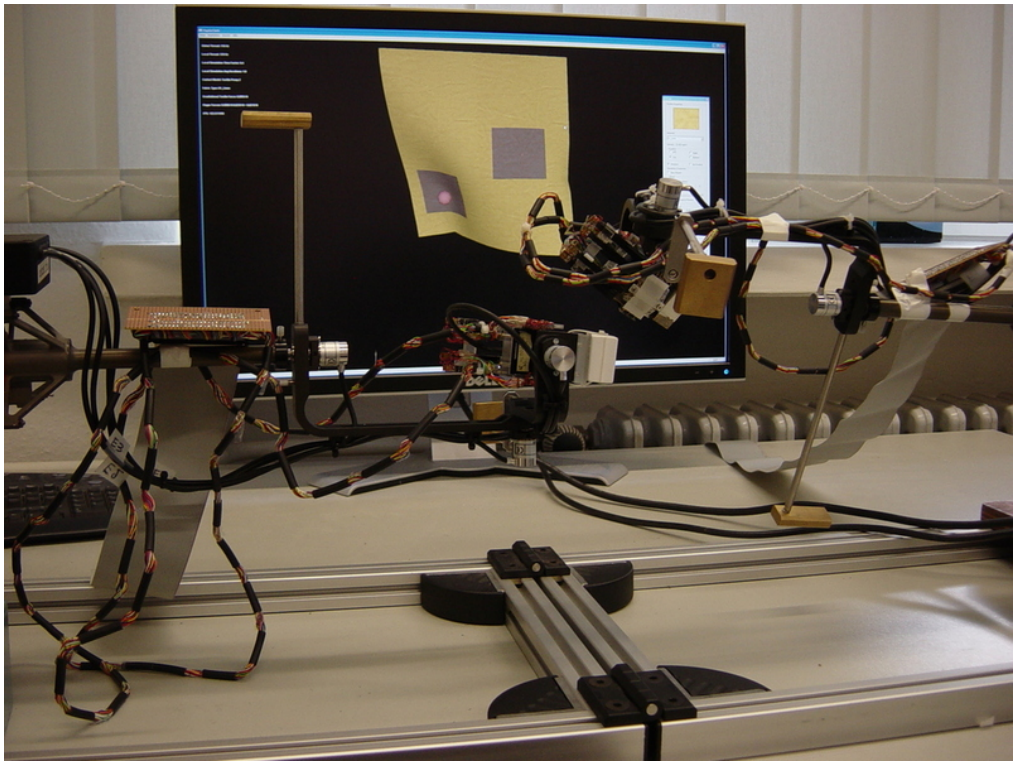

Figure 6.32: The HAPTEX Tactile System

The stimulator arrays, too, perform well[7], providing good, uniform sensations comparable to the texture array (chapter 5) when tested on the bench.

However, it is apparent that the performance of the interface has various non-ideal aspects, some of which result in significant limitations to the user:

- The spacing between the digits caused by the tactile mechanisms is about 10 mm. As the maximum (virtual) stiffness between the finger and thumb is limited because of instabilities in the force control loop, the force-feedback renderer enforces an additional separation of 6 mm in order to avoid collisions between the mechanisms. This means that the virtual fabrics are all forced to be a rather un-realistic 16mm thick.

- In order to avoid collisions between the mechanisms (and allowing some safety margin), the user must not apply normal forces greater than approx-

[7]The rather eccentric path of some of their actuator pins do not seem to affect their performance.

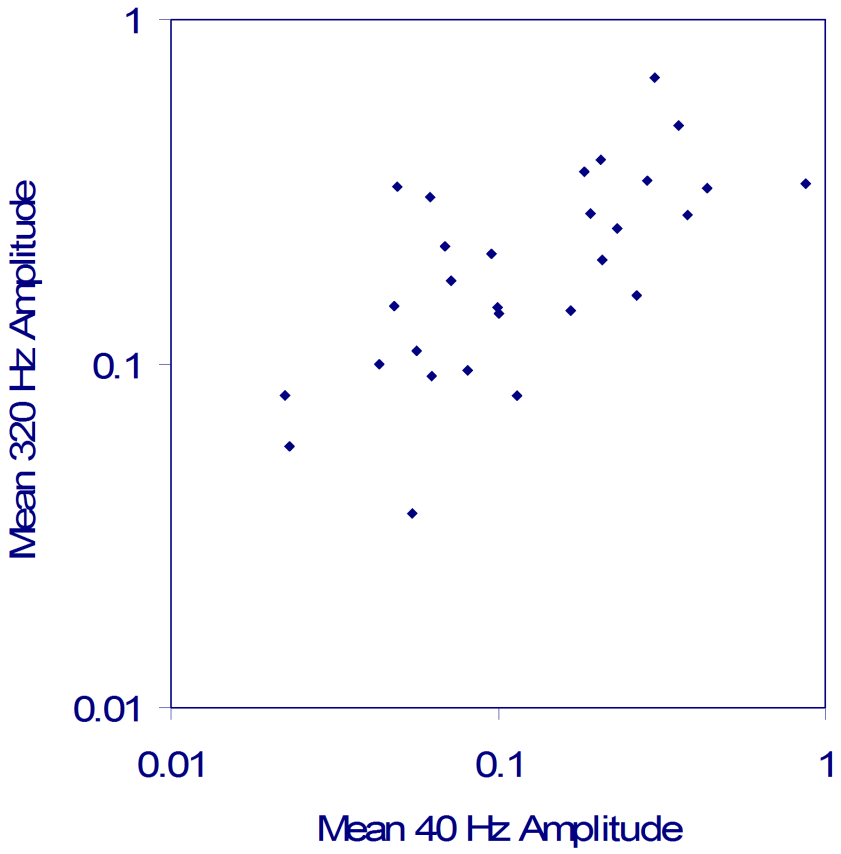

Figure 6.33: Mean amplitudes of the two frequency components generated by the renderer for 29 representative textiles from the HAPTEX database, at an exploration speed of 0.1 ms[1]. Amplitudes are given in normalised units such that 1 represents the upper limit of the available dynamic range of the renderers output.

imately 5 N. This limit prevents the accurate simulation of some textile manipulations, since a normal force of 10 N or more may sometimes be used during manipulation of real textiles. (It is not possible to increase the virtual stiffness between the mechanisms because this creates instability in the force control loop.)

- The GRAB does not provide torques to support rotations of the hand, so the user must provide the torques required to overcome the rotational inertia and rotational resistance of the GRAB gimbal. It is difficult for the user to apply such torques because of the limited mechanical coupling between the user's

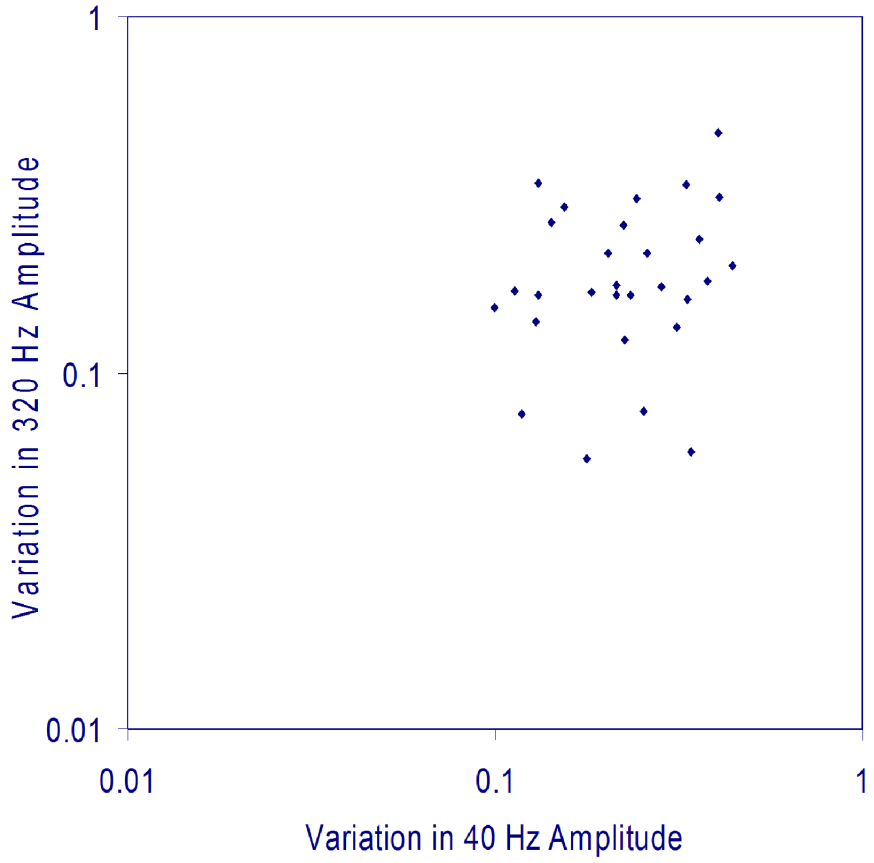

Figure 6.34: Coefficient of variation over the virtual surface of the two frequency components generated by the renderer for 29 representative textiles from the HAPTEX database, at an exploration speed of 0.1 ms[1]

hand and the end effectors of the GRAB. Consequently, the system works best with manipulations that maintain a relatively constant orientation of the fingers.

- The force feedback does not entirely compensate for drag and inertial forces in the GRAB mechanism – the user is often aware of forces associated with movement through the workspace, and in some cases the small forces from the virtual textile are masked.

These points should not detract from the achievements of the device, which provides a novel and more importantly an experimentally useful user experience. Furthermore, most of the issues described here would almost certainly be addressed

by replacing the GRAB with the HandExos as was the intention at the inception of the project.

6.5.2 An Experiment with Virtual Textiles: Comparing real fabric with virtual fabric

Evaluation of the complete HAPTEX system was focused on manipulations within the "single-handed" scenario illustrated in figure 6.2. Each manipulation was carefully specified and intended to provide information about a particular textile property. The approach chosen was to perform a suite of carefully defined manipulations on both the real fabrics and the virtual ones to in an attempt to see whether they would be ranked in the same order. The manipulations selected (shown in figure 6.35) were based on those used for evaluating fabric hand properties, but were modified to accommodate the limitations of the HAPTEX system.

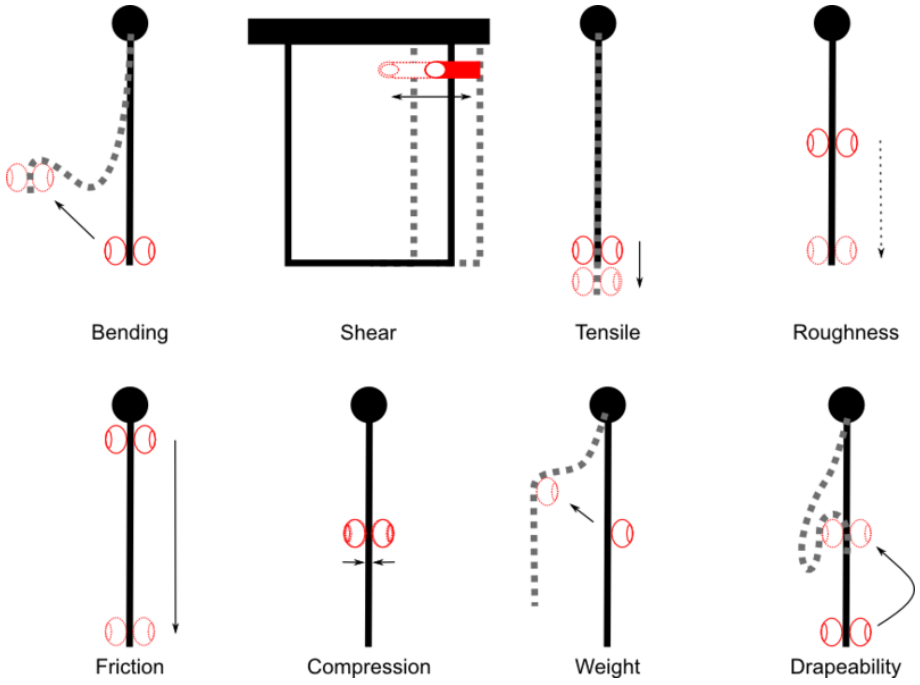

Figure 6.35: The manipulations chosen for the evaluation of the HAPTEX system

In relation to the tactile component of the HAPTEX system, the manipulations to determine roughness and friction are particularly relevant (the latter less so,

because perceived surface friction is presumably largely determined by the drag force presented by the GRAB system, calculated on the basis of Kawabata data for the mean coefficient of friction MIU, with tactile information of secondary importance). The evaluator instructions for these two manipulations (for either real or virtual textiles) are as follows:

- Surface roughness: Grasp halfway up sample with thumb and forefinger and slide your fingers downwards. To slide your fingers upwards fix the free end of the sample with your other hand.

- Friction: Grasp the sample close to the fixation with thumb and forefinger and slide your fingers downwards. To slide your fingers upwards fix the free end of the sample with your other hand.

Prior to the evaluation, five textiles were selected from the HAPTEX library, for which real and virtual samples were available – each set of five was chosen to provide the fullest range and best spread of KES-F values for the parameter under investigation. The virtual textiles were manipulated and their various properties were rated. These ratings were compared to those obtained in an equivalent assessment of the real textiles, and to physical data obtained using the Kawabata measurement system and other techniques. Subjects were asked to rate each test item from 1 to 5, compared to two standard items (representing 1 and 5 on the scale) presented alongside it.

For each property, each textile was presented twice in a sequence of 10 items. Textiles were hung in the warp direction (weft direction for the tensile manipulation only).

Full details of the experiment are described in the Deliverable 5.2 of the HAPTEX project [105]. The results for the tactile properties only are reproduced here.

Data were obtained in Hanover from two users who have some familiarity with the system: S1 from Exeter and S2 from Hanover. As mentioned above, each textile was assessed twice by each user. Figure 6.36 shows the relation between first and second assessments. It can be seen that, for both subjects, repeatability is good for

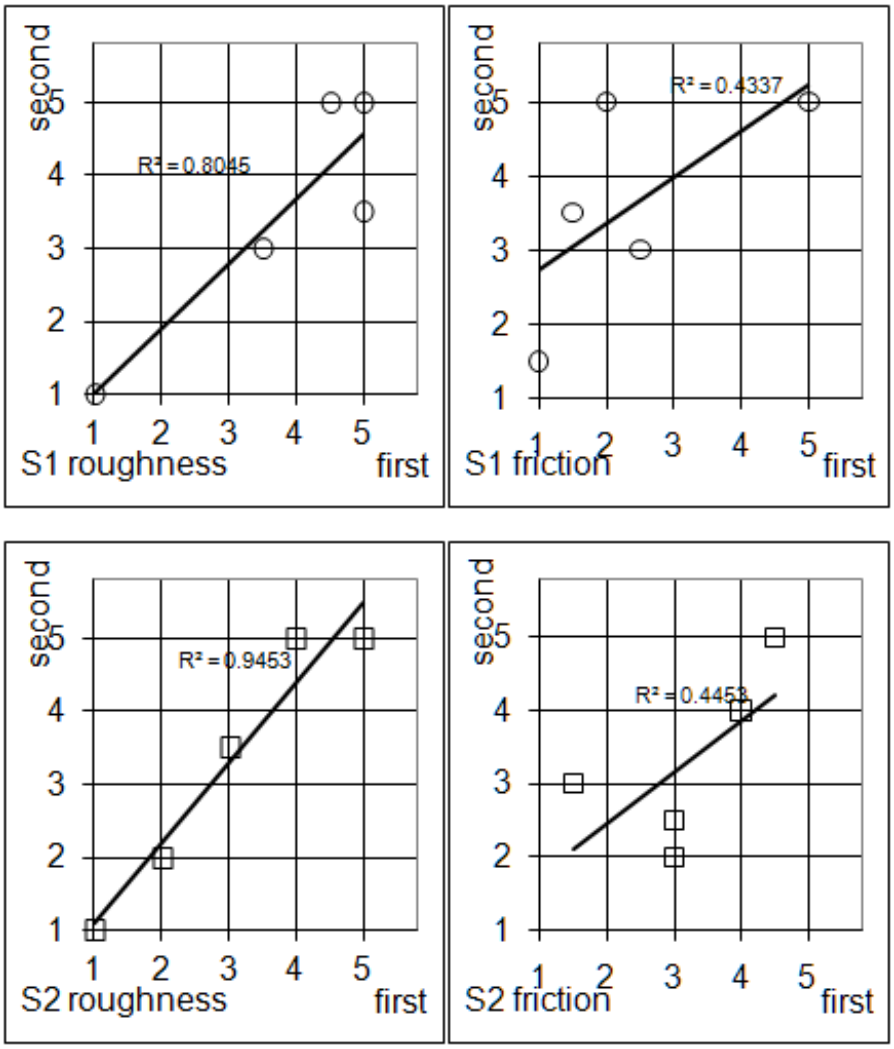

Figure 6.36: Relation of 1st and 2nd assessments for S1 (upper panels) and S2 (lower panels).The correlation coefficient R is also shown.

assessment of surface roughness, and less good for assessment of surface friction. The repeatability reflects the ease with which the user can make the assessment

Figure 6.37 shows comparisons between mean ratings from S1 and S2. Again, the correspondence is good for assessment of surface roughness and less good for assessment of surface friction.

Figure 6.38 shows the relation between the subjective ratings (averaged over S1 and S2) and the corresponding physical values of surface roughness and surface friction. (These are the values incorporated into the software models, derived from measurements on real textiles). The physical values are represented on logarithmic

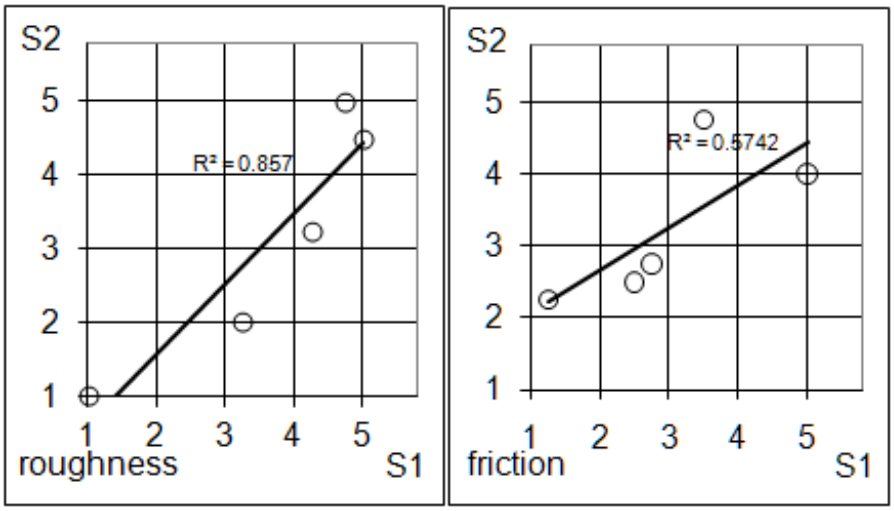

Figure 6.37: Comparisons between mean ratings from S1 and S2. The correlation coefficient R is also shown.

scales, in accordance with Weber's law[8]. It can be seen that there is a good correspondence between the ratings of the virtual textiles and the physical parameters of the software models. This suggests that the system is delivering appropriate cues to the users, i.e., the virtual textiles are a good representation of the real textiles.

Corresponding data for the manipulation of real textiles were obtained in Tampere from two assessors: S3 from MIRALab (with experience in the fashion industry) and S4 (an expert from the textile industry, recruited by SmartWear Lab). Figures 6.39 and 6.40 show the consistency and comparison of means, while 6.41 shows the relation between their subjective ratings (averaged over S3 and S4) and the corresponding physical values of surface roughness and surface friction (from measurements on the real textiles). It can be seen that there is quite good correspondence between the ratings of the real textiles and the measured physical parameters. The roughness and friction manipulations were performed "without

[8]More strictly this is the Weber-Fechner law, which states that the change Δp in subjective magnitude of a signal is proportional to the fractional change in stimulus $\Delta S/S$; by integration, this can be expressed as $p = kln(S/S0)$, where p is subjective magnitude, k is a constant and S and S_0 are the stimulus amplitude and threshold stimulus amplitude, respectively.

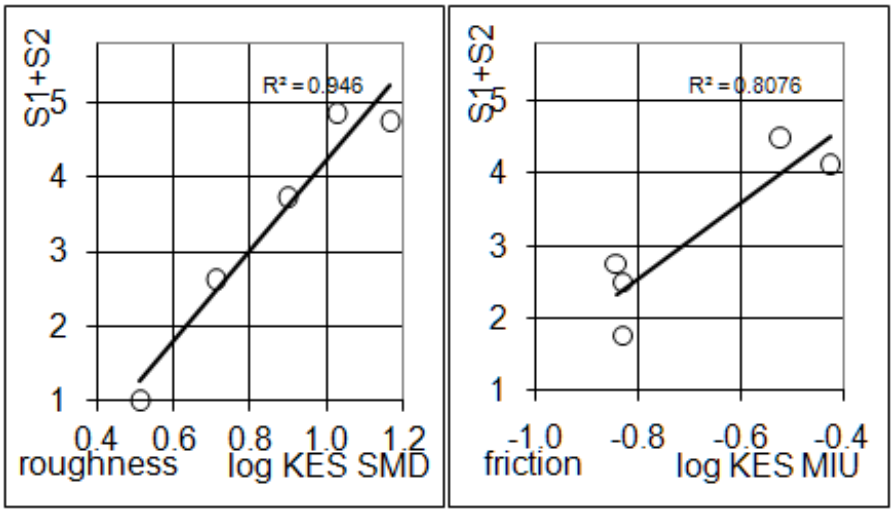

Figure 6.38: Relation between subjective evaulation of virtual textiles (mean of S1 and S2 data) and the corresponding physical values. The correlation coefficient R is also shown.

vision" so as to remove any potential visual cues. For the real textiles this was achieved by blindfolding the assessors, while in the virtual case the graphics were presented in "wire-frame" mode (i.e. the bitmapped texture rendering was disabled so that only the underlying mesh elements were visible).

Perhaps the most informative comparison is between subjective ratings of virtual textiles and subjective ratings of the corresponding real textiles. This is shown in figure 6.42. It can be seen that there is a good correspondence between the ratings of the virtual textiles and the real textiles, providing further evidence that the virtual textiles are a good representation of the real textiles and that the system is delivering appropriate cues to the user.

6.6 Summary

The tactile component of the HAPTEX system, based on designs and techniques developed by the author, was successfully implemented in terms of both hardware and software. Not only was the tactile component of HAPTEX successful in itself,

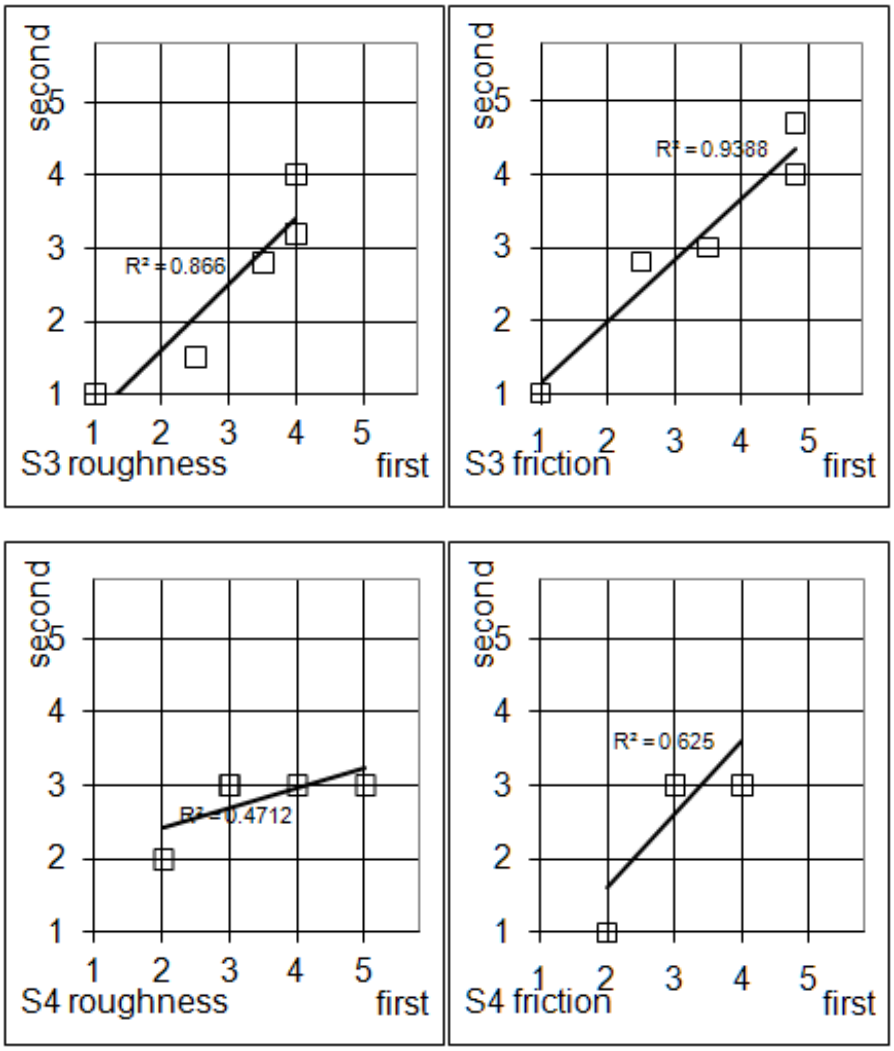

Figure 6.39: Relation of 1st and 2nd assessments for S3 (upper panels) and S4 (lower panels). The correlation coefficient R is also shown.

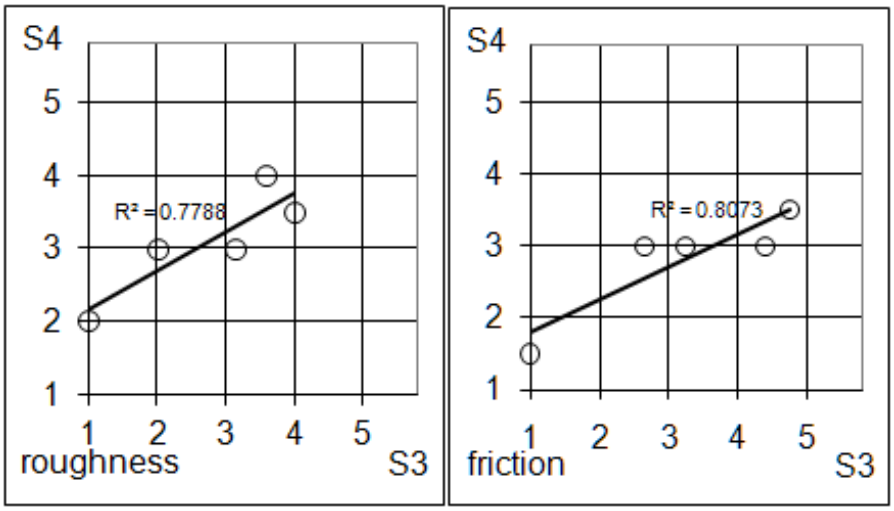

Figure 6.40: Comparisons between mean ratings from S3 and S4. The correlation coefficient R is also shown.

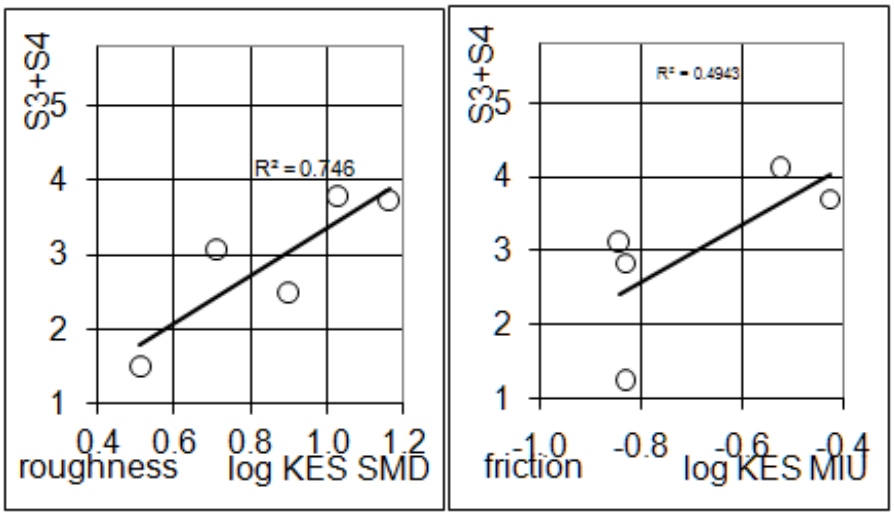

Figure 6.41: Relation between subjective evaulation of real textiles (mean of S3 and S4 data) and the corresponding physical values. The correlation coefficient R is also shown.

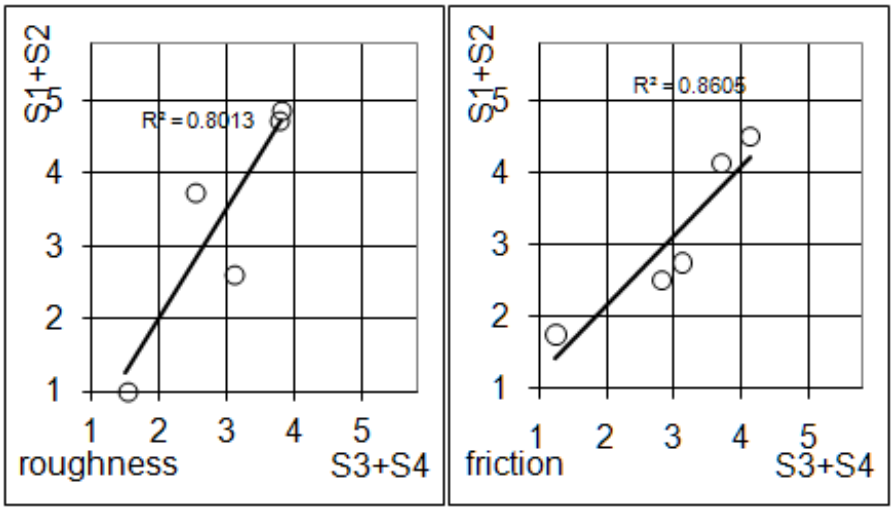

Figure 6.42: Comparison between subjective ratings of virtual textiles (mean of S1 and S2 data) and the corresponding real textiles (mean of S3 and S4 data). The correlation coefficient R is also shown.

Figure 6.43: The author using the HAPTEX system using the HAPTEX system at the HAPTEX 2007 Conference in Hannover in 2007.

but also its hardware and software design allowed successful integration with the other hardware and software components within the overall HAPTEX system. In

the authors view, the successful integration of the different components of HAPTEX into a multimodal interface which performed reliably in real time was a major achievement in its own right, and the appropriate design of the tactile component was a significant contributor to this achievement.

The tactile sensations produced by the system have multiple perceptual dimensions: spatial distribution (over the fingertip), overall intensity and spectral balance. However, in the assessment of surface properties described above, the user is asked to address only one of these dimensions the roughness assessment is essentially based on only the intensity dimension of the perceived sensation. To obtain a true impression of the potential of the tactile component, it is necessary to look at the possibilities offered by the other perceptual dimensions.

In summary, the results from chapter 5 suggest that the intended perceptual dimensions (spatial distribution, overall intensity and spectral balance) are all available to test subjects. For uniform stimuli (i.e., stimuli with no spatial variation over the surface), the spectral dimension appears relatively weak changes in spectral balance at constant subjective intensity tend to be less noticeable than changes in subjective intensity at constant spectral balance. (There are perhaps 4 to 5 discriminable steps of spectral balance along an equal-intensity contour.) There is a strong interaction between the perceived spatial aspects of the texture and the stimulation frequency. If the stimulation frequency is changed from 40 Hz to 320 Hz, the perceived sensation during active exploration changes much more if the texture is spatially non-uniform than if it is spatially uniform. It is clear that the spectral and spatial dimensions provide a significant enhancement to the available range of tactile sensations, i.e. overall intensity is not the only significant dimension. As mentioned above, time constraints within the HAPTEX project did not allow a complete evaluation to be carried out consequently the full potential of the HAPTEX system remained to be explored when the author left that project. At present, the complete HAPTEX system is no longer in operation, but fortunately the tactile renderer survives in a 2D implementation which is currently

the subject of further evaluation by a PhD student in Exeter.

The HAPTEX system described here was almost certainly the first time that distributed tactile stimulation was combined with force feedback in any kind of integrated way; it was even more groundbreaking in its use of a tactile rendering strategy which was designed to reproduce the sensation of a real surface.

The tactile array hardware developed by the author for the project is a major development in its own right. It manages to produce performance comparable to earlier devices into a smaller, lighter package, and the integrated electronics have greatly reduced the computational overhead required to drive the device in real time. Perhaps most significantly, it is designed for use on the finger in a more natural way in a 3 dimensional environment. By supporting natural gestures and manipulations, it makes a significant step towards moving tactile displays which are capable of delivering "rich" distributed content out of the lab context and into the arena of wearable devices.

Chapter 7

Conclusions

This thesis has documented the development of the tactile array over a number of years and a range of different projects. During this time it has evolved from a pure research tool into a usable desktop device and a component of virtual reality systems, and along the way much has been learnt about the role of touch perception in manual tasks and how tactile displays can be integrated into useful devices.

7.1 Tactile displays

Three similar yet contrasting tactile arrays were constructed and successfully trialed.

In chapter 4 the basic requirements for a tactile array were discussed. It was shown how a simple device with cheap, modular hardware can be capable of generating high quality stimuli. Active touch experiments were described which demonstrated how real-time tactile feedback can be incorporated into "desktop" type virtual environments.

By bridging the gap between pure research devices such as Chanter's array and usability of simple commercial Braille displays, this device, with its ease of use and facility for rapid development of real time and interactive tasks, offers the ability to explore the possibilities of distributed tactile displays in hitherto untapped ways.

Chapter 5 described the construction of a versatile tool for active touch experiments. This combined the simple modular construction and real-time control from the previous device with optimised actuators and broadband control to create a high performance device capable of providing rich tactile sensations (comparable with that of Chanter's static 100 pin array), but in an active, real-time setting. Alongside the hardware, a toolkit was developed which allows for the rapid development of experiments, making this device a very versatile research tool.

This is probably the first distributed tactile display device to offer full broadband capability across the entire spectrum of tacile sensistivity in real time, and coupled with absolute positioning within its workspace it is the first such device to be suited for virtual reality applications.

Finally in chapter 6 the geometry underlying vibrotactile pin-arrays was completely re-imagined, making important steps towards the miniaturisation of tactile displays. This along with improvements made to the drive electronics which allowed some of the computational load to be moved into hardware, was a key factor leading to the realisation of a device combining fingertip tactile displays with force-feedback hardware, using a rendering strategy based on the physical properties of real fabrics.

This device represents a step-change in tactile display technolgies, bringing the rich and powerful capabilities of broadband vibrotactile pin arrays from the lab bench to a place where they can support more natural interactions with the real, three-dimensional world.

7.2 Vibrotactile stimulation

Successful trials were performed on shape identification and line following tasks suggesting that tactile arrays are capable of addressing the perceptual channels associated with edge detection.

Earlier work had suggested that the observation of discrete tactile channels operating in different frequency bands could mean that the balance of these channels

(i.e. the spectral content of stimuli) might constitute a perceptual dimension. For uniform stimuli (i.e., stimuli with no spatial variation over the surface), the spectral dimension appears relatively weak - changes in spectral balance at constant subjective intensity tend to be less noticeable than changes in subjective intensity at constant spectral balance. (In practice there are perhaps 4 to 5 discriminable steps of spectral balance along an equal-intensity contour.) There is a strong interaction between the perceived spatial aspects of the texture and the stimulation frequency. If the stimulation frequency is changed from 40 Hz to 320 Hz, the perceived sensation during active exploration changes much more if the texture is spatially non-uniform than if it is spatially uniform. It is clear that the spectral and spatial dimensions provide a significant enhancement to the available range of tactile sensations, i.e., overall intensity is not the only significant dimension.

7.3 Future work

All of the devices described in this thesis have shown themselves to be capable and useful displays for both pychophysics research and for user focused display applications; unfortunately project priorities and funding constraints have meant that only the surface of their potential has been scratched. Lots more characterisation and experimentation is therefore highly desirable.

The development of compact, profile arrays, or indeed larger or higher resolution devices, is effectively limited by the availability of suitable actuators. Whilst technology is moving on all the time through improved materials and miniaturisation, there is an approach worth exploring using existing actuators. From the results presented here in Chapters 3 and 5 it seems reasonable to suggest that a high density of discrete actuators is only required for the high frequency channel, and that therefore it might be better to implement an array using more than one type of actuator. The lower frequency channel requires relatively large amplitudes, but only at a coarse resolution. The higher frequency channel could make use of much smaller actuators placed at intermediate sites. Such an approach might also

provide a mechanism for implementing a component of surface curvature (perhaps via a lateral skin stretching mechanism).

It could quite reasonably be argued that the tactile renderer described in chapter 6 was based on a fairly crude model with many untested assumptions. Perhaps the greatest concern is the way in which the surface texture is handled, i.e. the way that surface profile measurements are passed through multiple processing steps to generate drive waveforms for the presumed perceptual channels. There is clearly the potential for a project dedictated purely to developing this

It might be profitable to take advantage of friction measurements, which are in principle another source of input data for a tactile renderer. These are taken using a contactor made of a set of wire bands which form a "virtual finger", replicating the way in which skin ridges on the fingertip interact with a surface. A renderer based on both surface profile and friction is an attractive possibility, but work remains to be done to establish the most effective way to incorporate the friction data. A rather different strategy would involve a more fully featured "virtual finger", made from an elastomer and equipped with multiple strain gauges, with which it might be possible to generate the drive signals directly from the real surface.

In the HAPTEX implementation, the tactile model was only combined with force in a very basic manner. In doing so, it missed the ability to represent the local curvature of a surface or the softness of an object (for which directional force-feedback at fingertip is critical). Further work is required to investigate how this can best be represented; a prototype for just this type of experiment (consisting of a HAPTEX array fixed onto a PHANTOM Omni haptic device from SensAble technologies) is shown in figure 7.1.

A further refinement that could be introduced to tactile displays is one that could have a big impact for virtual reality applications. One of the major cues that one receives about the material that an object is made of comes from its temperature and thermal conductivity. Fitting a tactile display with programmable heating or

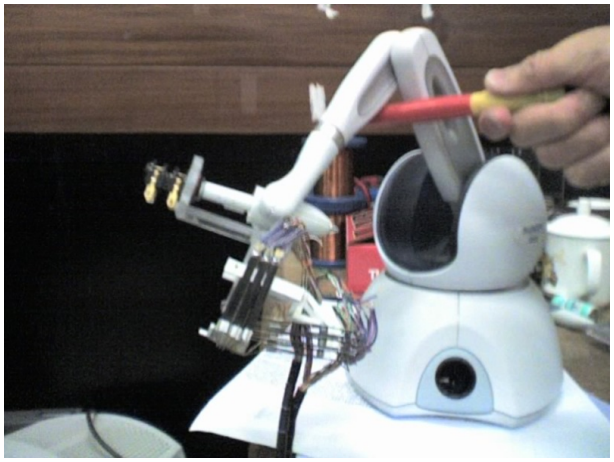

Figure 7.1: Trial of a simple one-finger integrated device: a HAPTEX array mounted on a PHANTOM Omni

cooling elements is a logical next step for VR devices.

7.4 Final remarks

The work described in this thesis has made a significant contribution to the movement to transform distributed tactile displays from being lab tools and curiosities into ubiquitous technology incorporated into a whole range of real-world situations, from teleoperation to everyday hand-held electronic devices.

Both the encouraging experimental results and the range of effective devices point to the success of the ongoing tactile array project. The implementation of a HandExos type device (see section 6.3.1) equipped with the next-generation of tactile array will be a great leap forward in fully interactive virtual reality. On a more practical level, improved actuator technology and the knowledge gathered from experiments performed on tactile arrays should lead to new forms of interaction with the ever expending range of powerful handheld devices. Haptic feedback for the most part still seems to mean a vibrating buzzer fixed to the case of the device, but the field now seems to be at a tipping point. The future of tactile display technology looks very bright, and tactile arrays are a key tool to drive their development.

Appendix A

Publications and conference presentations

I R Summers, C M Chanter, A L Southall and A C Brady *Results from a Tactile Array on the Fingertip*, Proceedings of Eurohaptics 2001, Birmingham, 2001: 26-28.

I R Summers, A C Brady, M K Syed and C M Chanter *Design of Array Stimulators for Synthetic Tactile Sensations*, Proceedings of WH05 (IEEE World Haptics Conference), Pisa, 2005: 586-587.

D Allerkamp, G Böttcher, AC Brady, J Qu, IR Summers and F-E Wolter *Tactile rendering: a vibrotactile approach*, Proceedings of Haptex05, Hannover (2005) 30-42.

AC Brady, IR Summers, J Qu and C Magnusson *Discrimination of tactile rendering on virtual surfaces*, Proceedings of ENACTIVE06, Montpelier (2006) 107-108.

D Allerkamp, G Böttcher, F-E Wolter, AC Brady, J Qu and IR Summers *A vibrotactile approach to tactile rendering*, The Visual Computer **23** 2007: 97-108.

N Magnenat-Thalmann, P Volino, U Bonanni, IR Summers, AC Brady, J Qu, D Allerkamp, M Fontana, F Tarri, F Salsedo, M. Bergamasco *Haptic Simulation, Perception and Manipulation of Deformable Objects*, Proceedings of Eurographics07, Prague, 2 2007: 1-22.

AC Brady, J Qu, S Carr and IR Summers *Tactile rendering of virtual objects*, Proceedings of Enactive/07, Grenoble, 2007: 45-48.

M Fontana, S Marcheschi, F Tarri, F Salsedo, M Bergamasco, D Allerkamp, G Böttcher, F-E Wolter, AC Brady, J Qu, IR Summers *Integrating Force and Tactile Rendering Into a Single VR System*, Proceedings of Cyberworlds 2007, Hannover, 2007: 277-284.

Appendix B

The ROSANA Project

The ROSANA project (IST-2001-34892) set out to investigate the relation between external stimuli, activity patterns of the afferent fibres and neural activity in the somatosensory pathway. It was hoped that this would lead to the development of mathematical models which would provide the capability to reproduce the activity generated by skin stimulation in the somatosensory system.

The project abstract states:

> The main objective of the ROSANA project is to provide the theoretical knowledge and the experimental tools to artificially stimulate the peripheral nerves in such a way that the elicited responses of the neural populations of the somatosensory system are similar to those generated by natural stimuli. Specific objectives are:
>
> 1. to determine how the interactions between sensory inputs and the activity of CNS neurons are used for creating the internal representation of real-world stimuli in the first stations of the somatosensory system, and
> 2. to develop mathematical models of neural signal processing which are capable to reproduce the activity generated by specific stimulation of the skin surface and to provoke the equivalent neural activity in the target stations of the somatosensory system.

To achieve the above mentioned objectives we need to know

1. the relations between peripheral stimulation patterns (stimuli to the skin) and the electrical activity of the sensory nerves and
2. the normal activity of the processing neurons and the interactions between incoming electrical signals and processing neurons in an early station of the somatosensory system.

Specifically this was to be achieved by implanting a sieve micro-electrode (to record neural activity and electrically stimulate small numbers of individual sensory fibres) in a sensory nerve of subject animals (rats and cats). After complete regeneration of the nerve fibres, a small region of the skin would be stimulated. The intention was to record the activity of small ensembles of nerve fibres (5–10) which had regenerated through the sieve holes (10-100), the activity in the cuneate nucleus (8–12 simultaneous extracellular single-unit recordings), and the activity in the somatosensory cortex (3–4 electrodes designed for unitary recordings).

The intention was then to use data analysis to establish categories for the most important mechanical stimuli according to the responses of the processing neurons. Relevant stimuli could then be artificially replicated by means of direct stimulation of the sensory nerve through the implanted micro-electrode.

The project partners were:

- Universidad Complutense de Madrid (UCM) – Dept Matematica Aplicada, Spain
- Universidad Autonoma de Madrid – Facultad de Medicina, Spain
- Frauhofer Institut fr Biomedizische Technik, Germany
- Instituto de Biologia Molecular e Celular – IBMC, Univ Porto, Portugal
- University of Exeter, School of Physics, United Kingdom

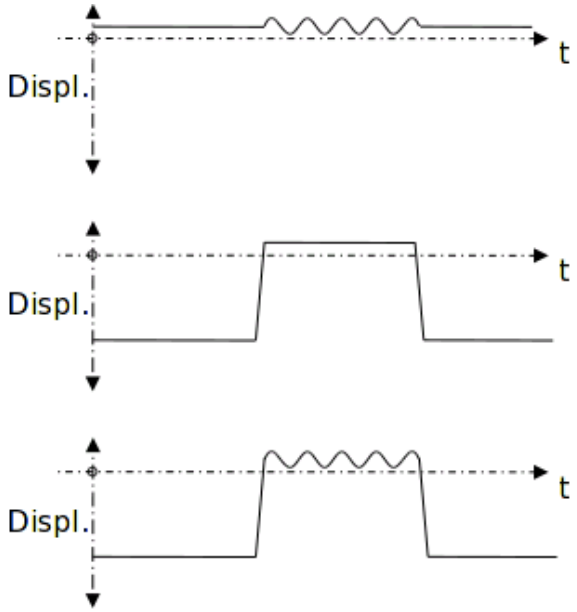

Figure B.1: In the ROSANA project, the contactor pins had to withdraw from the skin when not active.

The author's role as part of the Exeter team was to develop the hardware capable of producing the complex, tightly controlled stimulation patterns required for the mathematical analysis.

B.1 Stimulator hardware

A major difference between the stimulators developed for the ROSANA project and those described elsewhere in this thesis is that the contactors have to lifted away from the skin in the absence of stimulation; this ensures that there is no stimulation of any mechanoreceptors in that region of skin except when the array element is active. Furthermore the primary stimulation is provided by the pressure of contactor moving into contact with the skin, although the hardware has been designed so that vibratory stimulation can also be added.

This was achieved by switching the bimorphs between two oppositely poled voltages as shown in figure B.1 – this also shows how a vibratory signal could be superimposed onto the signal. The effect was increased by fitting extension arms

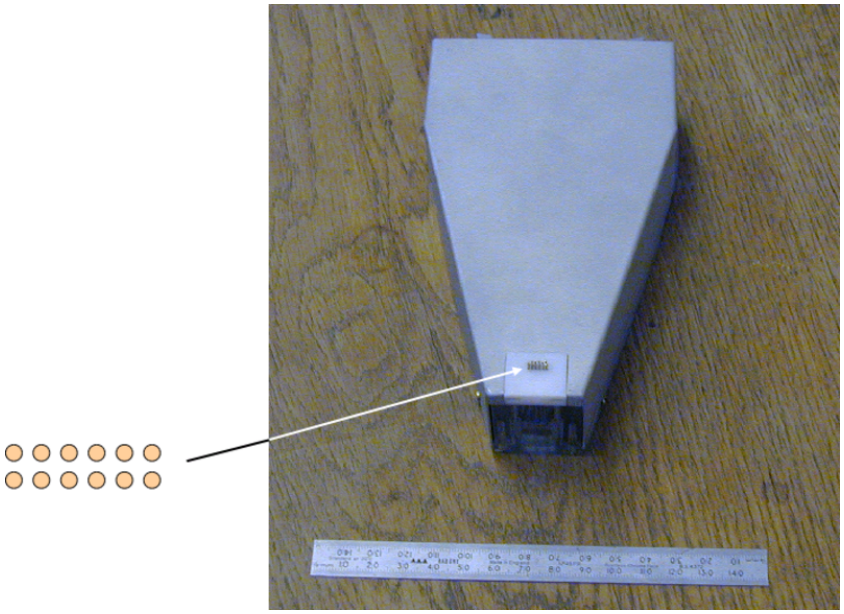

Figure B.2: The first version of the ROSANA stimulator, showing the contactor surface and the aluminium housing which provides electrical screening.

to the piezoelectric bimorph cantilevers[1], magnifying their displacement amplitude. This gain was at the expense of blocked force; this was not a problem as the 10 mm wide actuators used (the same actuators described in chapter 4) are sufficiently powerful that they can cause skin deflections in excess of 1 mm with a contactor fixed at the end of a 50 mm extension lever.

Three stimulator designs were developed during the project. The first of these is shown in figure B.2.

It has:

- 12 contactors arranged in an equispaced rectangular matrix
- 0.6 mm diameter contactors
- 1.2 mm between contactor centres
- 3.0 mm displacement for 80 V input
- Working bandwith ¿ 50 Hz

[1]These can clearly be seen in figure B.3

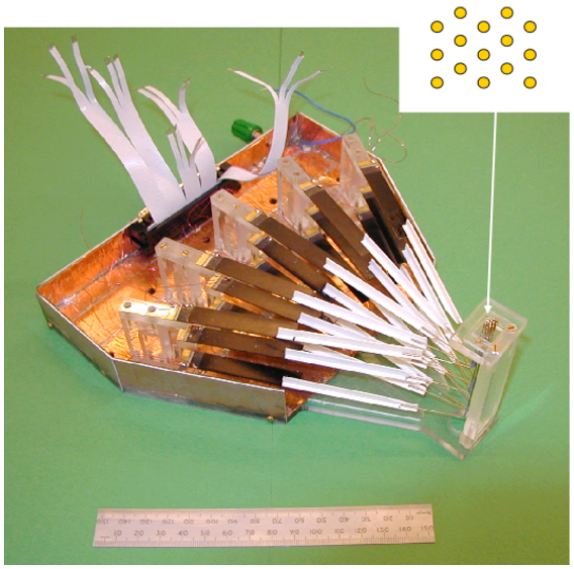

Figure B.3: The final version of the ROSANA stimulator.Mechanism consists of piezoelectric bimorphs with plastic and wire extensions.

This design performed well, but was limited by its linear contactor layout. The space available around the test animal is very limited; arranging the equipment to place the entire array surface in a position in which it could address the skin was very problematic.

A second design with the pins arranged in equilateral triangles (i.e. the contactor pad forms a hexagonal matrix) and streamlined electrical connections was developed to allow more complex stimuli to be delivered (there are 3 possible directions of movement possible as opposed to effectively one with the previous design) and to provide some degree of flexibility of the placement of the stimulator (figure B.3).

This device has:

- 15 contactors arranged in a hexagonal matrix
- 0.6 mm diameter contactors
- 1.5 mm between contactor centres
- 5.0 mm displacement for 68 V input (±5.0 mm for ±68 V input range)

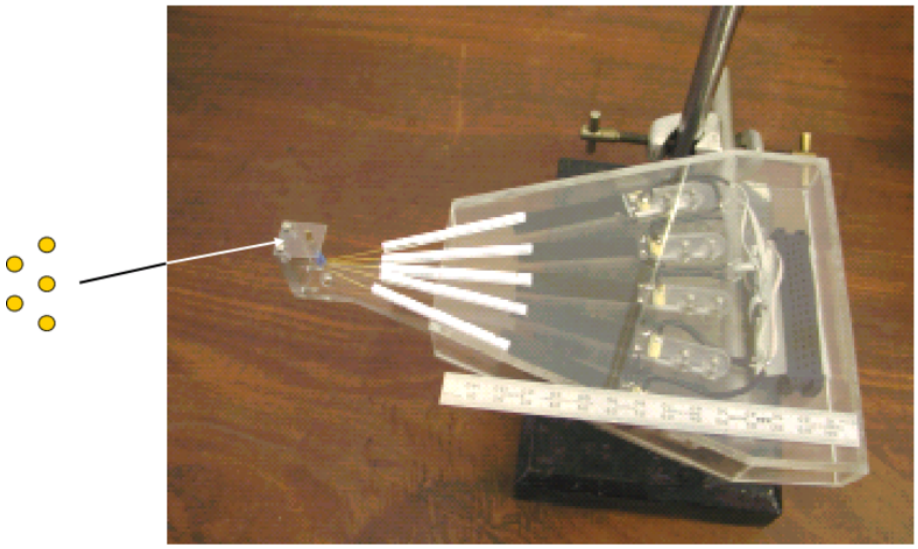

Figure B.4: The cut-down final version of the ROSANA stimulator.

This design worked well, but its large size meant that it was still cumbersome to use. Because of this, a third cut-down stimulator was developed. This is intended to take up as little space as possible so that it can be used for measurement on the rat forefoot, around which the UCM experimental set-up offers very limited room for manoeuvre. The depth of the stimulator has been reduced by using only a single layer of bimorph drive elements, and the plastic beams are shorter in order to reduce the overall length at the expense of some reduction in output displacement.

The specifications of the cut down device are:

- 5 contactors arranged in a hexagonal matrix
- 0.6 mm diameter contactors
- 1.2 mm between contactor centres
- 4.0 mm displacement for 68 V input ($\pm$4.0 mm for $\pm$68 V input range)

All three versions of the stimulator have been used successfully in investigations on rats.

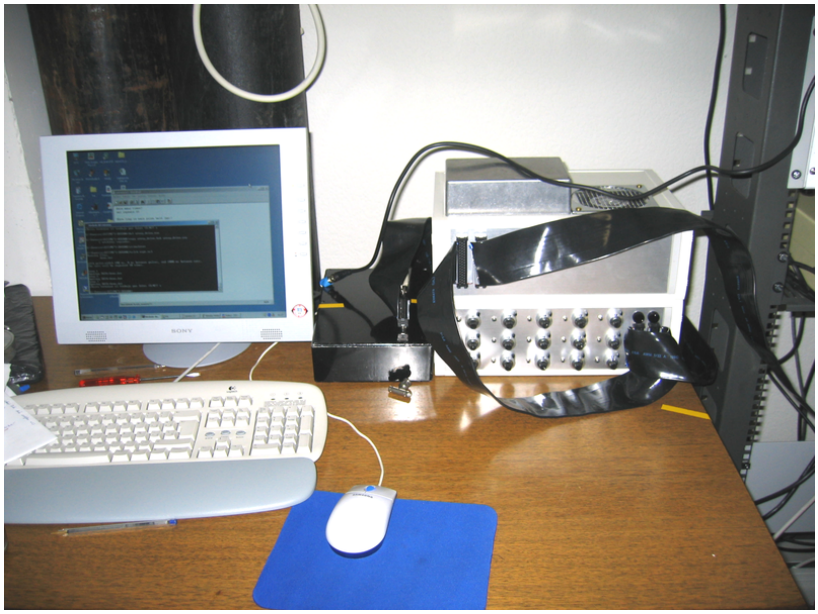

Figure B.5: The ROSANA control system in place in Madrid.

B.2 Control system

A controller (pictured in figure B.5) was developed which generates drive waveforms for the stimulator in 15 channels. It has the following key features:

- The quiescent voltage can be preset in each channel, to conform to skin topology.
- It allows variation of distance that contactors are retracted from the skin.
- It allows variation of indentation force that contactors apply to the skin.

The contactor movement is controlled by 15 TTL logic inputs, and is driven by sequencing software on a PC/laptop. Opto-isolation is used to minimise any electrical noise in the recording electrodes. The controller has a TTL output (connected to the latch on the output buffer in the interface hardware) which allows the timing of the stimulator output to be recorded in the time-line of the experimental measurements

A dedicated laptop is used to control the drive hardware. A user friendly graphical user interface was written to facilitate this. A further piece of software (figure B.6

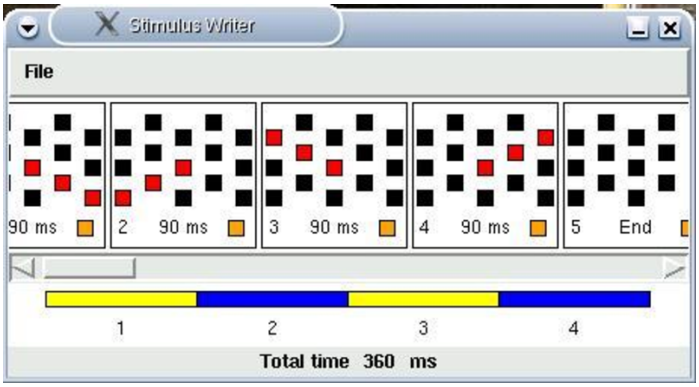

Figure B.6: Screen shot of the ROSANA stimulus programming software interface.

shows a screen shot) was also provided to simplify stimulus generation.

In this, the stimuli are designed as a sequence of frames. Each frame is specified in terms of its duration and spatial distribution. Sequences of frames can be repeated at specified intervals to produce extended stimulation patterns.

B.3 Results

The project was very ambitious and was beset by numerous delays and technical issues with the sieve-electrode system. Nevertheless, the stimulator hardware performed well, and neural recordings were achieved in a number of studies.

The stimuli sets used in one such study is shown in figure B.7. A range of timing protocols was used in these experiments, with duration T1 of the active phases in the range 10–100 ms and duration T2 of the inactive phases in the range 0–50 ms. Examples of the neural recordings obtained in this experiment are shown in figure B.8. The figure shows the average frequency of firing (events / s) as a function of time (ms) in each sequence of stimulation (A-B-C and C-B-A).

These results and their analysis was presented at a meeting of the Spanish Society for Neuroscience (SENC) in Torremolinos.

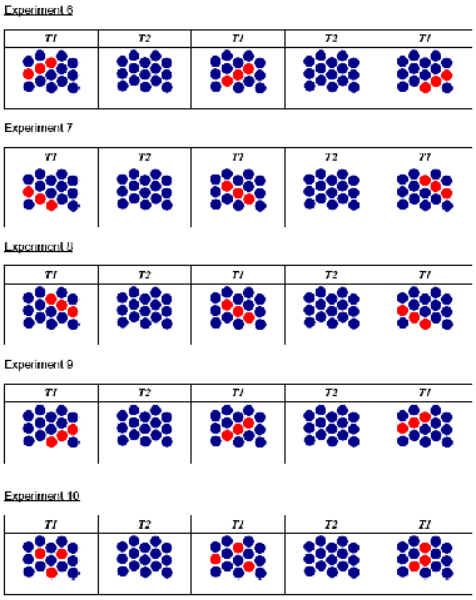

Figure B.7: Examples of stimulus patterns which were implemented for experiments at UCM in April 2006. In each frame, the red circles indicate the active pins.

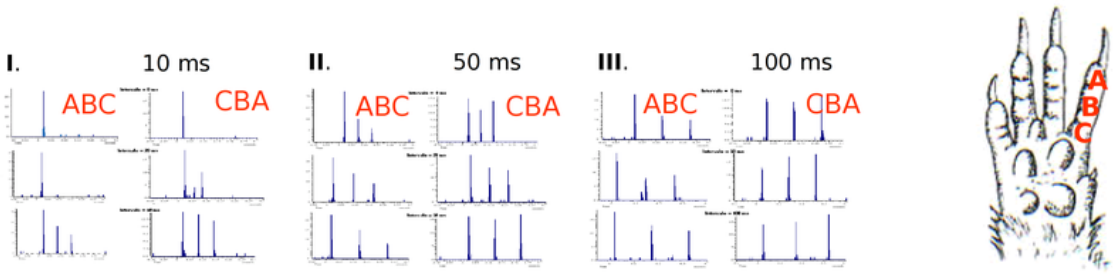

Figure B.8: Examples of neural spike recordings made during experiments performed at UCM. The traces show the electrical activity from a single neuron in the motor cortex recorded as three part stimuli were applied. The letters "A", "B" and "C" show the position and order of the stimulus constituents. The active duration T_1 is shown at the top of the three groups; the rows correspond to three variations of the inactive duration T_2.

Appendix C

Measurement of frequency response

A study was performed to validate the modelling exercise described in chapter 3. Piezoelectric bimorphs were mounted (either singly or in parallel sets) in a test jig, clamped to a known (but variable) length. An accelerometer was fitted to the free end of the actuator; a pin was also fitted to evaluate the effect of finger loading — see figure C.1.

To perform the test, the actuator assembly was driven with a sinusoidal signal of known fixed amplitude. This drive signal was swept across the frequency spectrum, with the peak amplitude of acceleration from the measurement electronics noted

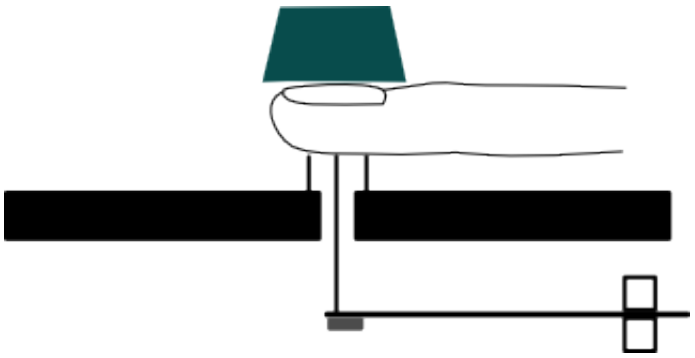

Figure C.1: Experimental configuration for measuring the frequency response of a piezoelectric bimorph

Figure C.2: BU series Knowles Accelerometers

at each step. The measurements were recorded both with no additional load on the bimorph and with a finger load in place. The finger-pad was supported by a ring of fixed pins and a mass was placed on top of the finger in an attempt to keep the effective mass and stiffness loads constant.

C.1 Accelerometer

The measurements were performed using a Knowles BU 7135 uniaxial accelerometer. This device is essentially a BU 1771 (as used for similar studies by Irwin and Chanter) repackaged into a smaller case. As with the BU 1771, it consists of a stainless steel can containing a miniature piezoelectric element and a FET, and has output ranging from ∼20 Hz to above 10 kHz. It is small and light (∼8× 5×2 mm and weighing 0.28 g) enough to be fitted to a bimorph without significantly altering the frequency response[1] — the effect of the additional mass-loading has been ignored for the purposes of this study.

The BU 7135 was used in source-follower configuration (illustrated in figure C.3);

[1]This assumption has been tested by observing the frequency response of the cantilever with additional small weights (with masses of the same order as that of the accelerometer) fixed to its end.

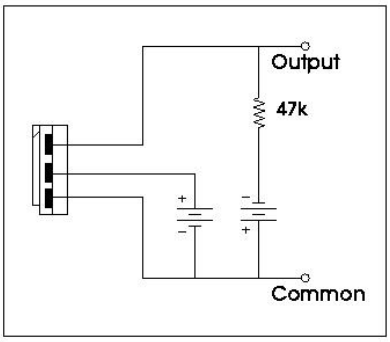

Figure C.3: Knowles Accelerometer in source-follower configuration

this set-up is recommended by the manufacturers as it gives increased output stability and is most suited to measurement of high accelerations.

The power was supplied from alkaline cells to minimise electrical noise on the output signal.

The Knowles technical specifications state that the BU 7135 has an output sensitivity of 0.411 mV/ms^2 – knowing this, the peak amplitude can be read off an oscilloscope to give a direct measure of the acceleration. Since the signals being measured are sinusoidal, the displacement waveform will also be sinusoidal and the peak displacement can be calculated directly using the relationship $x = \frac{\ddot{x}}{(j\omega)^2}$.

C.2 Example Results

The following plots show the effect of increasing the power of the transducer achieved by adding additional piezoelectric bimorphs in parallel. Notice the principal resonance at around 100 Hz and a higher mode at around 1 kHz. The peak near 300 Hz is believed to be a resonance of the wire link.

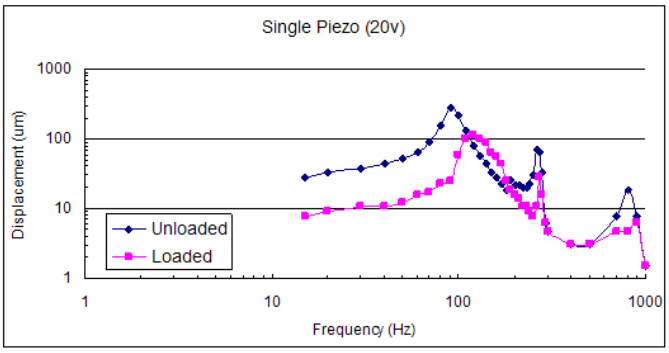

Figure C.4: Frequency response of a single 40 mm × 2.1 mm piezoelectric bimorph in loaded and unloaded conditions

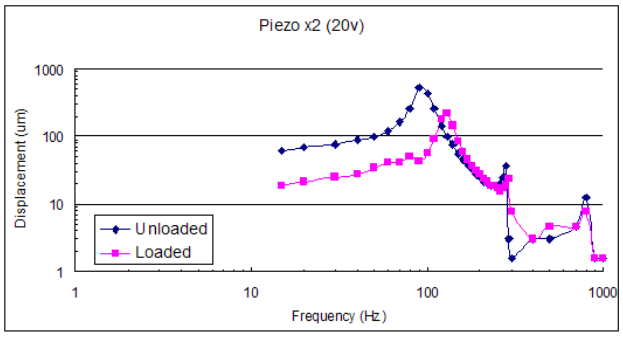

Figure C.5: Frequency response of two parallel 40 mm × 2.1 mm piezoelectric bimorphs in loaded and unloaded conditions

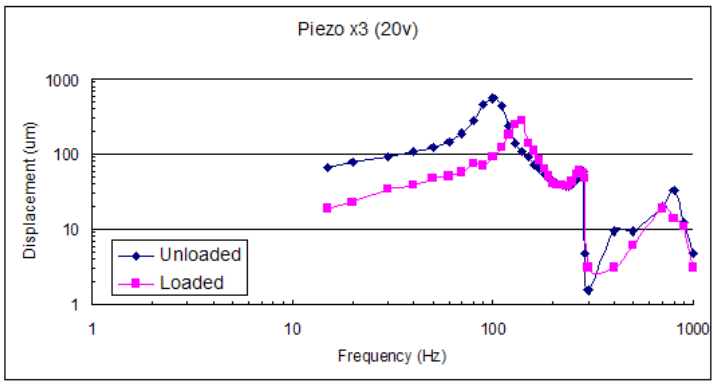

Figure C.6: Frequency response of a three parallel 40 mm × 2.1 mm piezoelectric bimorphs in loaded and unloaded conditions

Appendix D

Subjective experince of vibrotactile stimuli across the frequency spectrum

This appendix is an attempt to catalogue users' comments about their subjective experience when presented with sinusoidal vibratory stimuli using a tactile array at various frequencies across the perceptual range.

Whilst the immediate preconception might be that any such signal would feel like the tactile analogue of a buzzing sound, this is not in fact what the majority of subjects report. Whilst the higher frequencies of the perceptual range do indeed feel like a buzz, the lower end is altogether more interesting. At a few Hertz, the movement of the stimulator is perceptible and the experience is a throbbing sensation which is not clearly localised. As the frequency increases into the realm of a few tens of hertz, the feeling of oscillatory movement becomes less distinct, passing through a frequency band described by many subjects as "lumpy". This sensation becomes smoother as the frequency increases, and gradually becomes a more noticeable "buzz". In this region, moving line patterns on a tactile array feel almost like real objects moving across the skin. As the stimulus moves into the higher frequency regime, around peak of sensitivity (around 300 Hz), there is an

Frequency	**Sensation**
10 Hz	Throbbing
20 Hz	Lumpy but realistic
30 Hz	Rough real object
40 Hz	Slightly rough real object
60 Hz	Starting to feel buzzing
120 Hz	No longer a realistic sensation
200 Hz	Hard to localise the sensation
250 Hz	Buzzing more localised
300 Hz	A sharp edge within a buzzing background
400 Hz	More diffuse buzzing
600 Hz	Sensation getting weaker
1000 Hz	Upper boundary of human tactile perception

Table D.1: Subjective sensations as a function of frequency

increased sense of localisation. Beyond this point both the buzzing and the sense of localisation fade away as the stimulus moves towards the limits of perception. This perceptual spectrum is summarised in table D.1.

Appendix E

Other Experiments

The following work was performed using the tactile mouse by Caroline Pouya as part of her MPhys project work [106], with technical support from the author.

Fifteen individuals took part in a study in which four main scenarios were investigated. Two of the experiments were performed via passive touch perception and two by active touch.

The passive experiments were designed to examine subject's tactile perception of various sized "bars" (A "bar" comprises one or more rows or columns of vibrating pins on the array with stationary pins either side of it.) on the 25 pin tactile array, and to compare this to the inverse (i.e. rows or columns of stationary pins in a vibrating background) at frequencies of both 40 and 100 Hz (targeting non-Pacinian and Pacinian touch receptors respectively). This was compared to active experiments at 40 Hz and 100 Hz to determine whether the negative shapes were perceived best in an active set up or a passive set-up, and which frequency produced the best response in each case.

The results show that a bar made from vibrating pins with a stationary background (positive shape) was trivial to detect at widths of 2 mm-12 mm, yet the inverse shape was considerably harder to perceive. Negative bars were found to be perceived more accurately at a frequency of 40 Hz (targeting Non-Pacinian touch receptors) when compared with a frequency of 100 Hz. There seemed to be no frequency preference in the perception of positive shapes.

The active experiments showed no distinct frequency preference in the perception of negative shapes. All negative bars were accurately perceived except for the bars of smallest width (2 mm). This showed a very obvious preference of active perception over passive perception of negative shapes. Stripes of all widths of bars were perceived accurately for all widths, implying that is the Pacinian touch receptors that are utilised in detecting such shapes in active touch perception.

Appendix F

Details of software

The software is called "ActiveArray". Versions of it have been implemented on both Windows and Linux. Functionally the different versions of the applications are the same; the main difference is that not all of the device drivers have been implemented under Windows.

By default, the ActiveArray executable looks for the file "experiment1.xml", so this is the file that will be read if the programme icon is double-clicked. This can be overridden by running the programme from the command prompt with a filename as an argument:

```
C:\> cd Desktop\ActiveArray
C:\Desktop\ActiveArray> ActiveArray.exe myfile.xml
```

When the programme is running, the active frame is selected using the up and down arrow keys (the Space Bar also advances the frame). To exit the programme, press the Escape key. NB this is the only way to exit the Windows version of the program because the mouse is locked to the window.

F.1 Input files

All of the input files use xml, i.e. they have the format:

```
<tag1>
  <tag2 flag1="something" flag2=""...> Body </tag2>
</tag1>
```

Here follows a brief description of the structure of the files. All measurements are in millimetres (this assumes that the screen scale has been set correctly).

Experiment file

The file has the form:

```
<?xml version="1.0" encoding="ISO-8859-1"?>
<tactile_experiment title="Tactile Array Experiment">
  <tactile_display>
    device (including cursor)
  </tactile_display>
  window
  <graphics>
    background
    foreground + text
  </graphics>
  <map_data>
    input files
  </map_data>
  <experiment>
    frames
  </experiment>
</tactile_experiment>
```

A device is defined thus:

```
<device  type="pin_array" label="Digit 1" def_file="array24_1.def.xml">
  <cursor>
    <rectangle  width="8" height="12" outline="black" colour="cyan" label="d1c"></r
  </cursor>
  <input_device type="mouse"></input_device>
  <output_device type="parallel" config="standard"></output_device>
</device>
```

This section selects the array definition file (the mapping between channel and pin position), the shape/colour of the cursor (as described in "graphics", below) and the type of input and output device.

The allowed input devices are "mouse", "file" and "tablet" (the Wacom graphics tablet — not yet available in the Windows version of the code). The output devices currently available are "parallel" (as in chapter 4) and "simplesocket" for

the interface described in chapter 5 — the latter requires an additional argument to define the IP address of the slave PC in the form:

```
config="144.173.229.99"
```

Although it has not yet been implemented, it should be very straightforward to add a USB interface for the Haptex controller described in chapter 6.

"Window" sets the physical size of the workspace on the screen:

```
<window  win_width="280" win_height="190" title="Tactile experiment"></window>
```

Within "graphics", items can be placed in one of two layers — "foreground" or "background".

```
<background >
  <rectangle x="50" y="40" width="200" height="130" outline="black" colour="grey"
</background>
```

Each item is constructed and stored in memory using the label — it is this which is used to add an element to a frame.

The allowed items are:

rectangle — x, y, width, height, outline, colour, label(*x and y are the coordinates of the top left corner. Outline is the colour of the border, whereas colour is the fill.*)

ellipse — x, y, width, height, outline, colour, label(*x and y are the coordinates of the centre point.*)

line — x,y,x1,y1, colour, label(*x and y are the start coordinates, x1 and y1 are the end coordinates.*)

text — x, y, size, label (*Allowed sizes are tiny, small, medium, large or huge. The actual text goes in the body i.e. between the beginning and end tags.*)

```
<text>  Text goes here </text>
```

For all items, the allowed colours are:

white, black, red, green, blue, cyan, magenta, yellow , grey, darkGrey, lightGrey

An "input_file is handled in a similar way to a graphics item in that they are loaded into memory along with a label, and it is this label that is used to add the data to a frame.

```
<input_file  filename="A1.xml" data_type="ascii" label="file1"></input_file>
```

The "data_type" argument is present to allow very large input files to be encoded in binary format.

Each frame can contain a mixture of graphics_items and files:

```
<frame>
  <file class="xy" label="file1"  freq="40" x="75" y="85"></file>
  <file class="xy" label="file1" freq="40" x="130" y="85"></file>
  <file class="xy" label="file1" freq="320" x="185" y="85"></file>
  <graphics_item label="b1"></graphics_item>
  <graphics_item label="f1"></graphics_item>
  <graphics_item label="f2"></graphics_item>
  <graphics_item label="f6"></graphics_item>
  <graphics_item label="l3"></graphics_item>
</frame>
```

Note that the graphics_items have already been placed on the screen, but that data files can be placed anywhere (x and y are the coordinates of the top left corner of the data), and can be used as many times as necessary. The "freq" argument sets the operating frequency for the data set — this is not used by the parallel interface.

Definition file

This file is very straightforward. It has the form:

```
<?xml version="1.0" encoding="ISO-8859-1"?>
<pin_data>
  <description>
    Haptex prototype Array, with channels for PCI7200
  </description>
```

```
  <pin chan="0" weight="11" x="0" y="10"></pin>
  <pin chan="1" weight="11" x="2" y="10"></pin>
  <pin chan="2" weight="11" x="4" y="10"></pin>
  ...
</pin_data>
```

chan is the output channel number, and x and y describe the position offset of the pin in mm.

Data file

This file is also straightforward. Each data point represents a 1 mm grid square. A non-zero value means that location will activate the array. The value used should correspond to value in the frequency look-up table in appendix G. For the parallel interface, all non-zero values are equivalent.

```
<?xml version="1.0" encoding="ISO-8859-1"?>
<data_set x="10" y="10" type="ascii">
1 1 1 1 1 1 1 1 1 1
1 0 0 0 0 0 0 0 0 1
1 0 0 0 0 0 0 0 0 1
1 0 0 0 0 0 0 0 0 1
1 0 0 0 0 0 0 0 0 1
1 0 0 0 0 0 0 0 0 1
1 0 0 0 0 0 0 0 0 1
1 0 0 0 0 0 0 0 0 1
1 0 0 0 0 0 0 0 0 1
1 1 1 1 1 1 1 1 1 1
</data_set>
```

Here “x” and “y” refer to the size of the data set.

Appendix G

Amplitude scales

The amplitude levels used in the texture array control software are based on logarithmic intervals. Initially, the 7 bit peak amplitudes (i.e. values ranging from 0 to 127) were split into twenty 1 dB increments numbered 0 to 19, with 0 representing "no signal" and 19 corresponding to an amplitude of 127. as shown in table G.

This range proved insufficient to provide the dynamic range required by some experiments. However, for backward compatibility it was decided to leave the existing scale untouched and to add the additional points on to the end — see table G.2.

Following the pilot experiments described in section 5.8.1, it was felt necessary to add intermediate increments to the scale. Once again, these were appended onto the end of the scale, as shown in table G.3.

Intermediate points were also required at the lower end of the scale (table G.4).

Level index	Amplitude	dB "level"
0	0	–
1	16	1
2	18	2
3	20	3
4	23	4
5	25	5
6	28	6
7	32	7
8	36	8
9	40	9
10	45	10
11	51	11
12	57	12
13	64	13
14	71	14
15	80	15
16	90	16
17	101	17
18	113	18
19	127	19

Table G.1: The basics amplitude scale used in the texture experiments.

Level index	Amplitude	dB “level”
20	14	0
21	12	-1
22	11	-2
23	10	-3
24	9	-4
25	8	-5
26	7	-6
27	6	-7
28	6	-8
29	5	-9
30	5	-10

Table G.2: Additional amplitudes added at the lower end of the scale.

Level index	Amplitude	dB "level"
31	15	1/2
32	17	1 1/2
33	19	2 1/2
34	21	3 1/2
35	24	4 1/2
36	27	5 1/2
37	30	6 1/2
38	34	7 1/2
39	38	8 1/2
40	43	9 1/2
41	48	10 1/2
42	54	11 1/2
43	60	12 1/2
44	67	13 1/2
45	76	14 1/2
46	85	15 1/2
47	95	16 1/2
48	107	17 1/2
49	120	18 1/2

Table G.3: Additional (1/2 dB step) points in the amplitude scale.

Level index	Amplitude	dB “level”
50	13	-1/2
51	12	-1 1/2
52	11	-2 1/2
53	10	-3 1/2
54	9	-4 1/2
55	8	-5 1/2
56	7	-6 1/2
57	6	-7 1/2
58	5	-8 1/2
59	5	-9 1/2
60	4	-10 1/2

Table G.4: 1/2 dB increments at the lower end of the amplitude scale.

Appendix H

An example texture of a texture file

The following is an example of a "texture" block such as that used in chapter 5.

```
<?xml version="1.0" encoding="ISO-8859-1"?>
<!--
Random SD 2.0
2x2 average
-->
<data_set x="40" y="40" type="ascii">
13 13 15 16 16 17 17 17 16 12 11 15 16 14 15 12 11 17 18 15 15 13 14 15 11 12 13 12 14 16 15 17 18 15 15 16 13 13 14 13
17 17 16 17 17 16 15 13 14 12 11 16 16 14 13 12 13 16 16 13 15 15 16 16 12 13 14 14 13 13 16 16 15 15 17 18 16 12 11 13
18 17 14 15 16 14 13 11 12 13 14 17 18 17 15 14 15 13 11 12 16 18 15 15 15 14 16 18 15 14 16 15 15 16 16 12 13 14 11 11
15 17 13 12 14 16 17 16 17 17 18 17 15 14 15 16 16 14 11 12 15 16 14 14 17 17 16 14 14 16 14 14 14 13 13 11 14 18 15 11
11 15 17 14 13 15 18 19 18 18 17 15 11 11 15 16 14 13 13 11 13 14 17 16 15 19 17 11 13 13 13 17 18 14 13 14 16 18 15 14
14 16 16 14 13 13 16 18 14 15 15 14 14 14 15 15 11 14 13 12 13 15 17 17 15 16 14 12 15 12 13 17 17 16 13 13 14 14 14 14
18 19 15 14 13 12 16 13 11 14 16 15 18 17 15 14 14 18 15 14 13 15 16 14 14 14 15 13 15 14 14 15 13 13 13 11 11 11 13 14
14 18 18 17 15 14 17 14 11 14 16 15 17 19 18 16 17 15 12 13 14 16 16 12 12 16 16 13 13 14 13 17 14 11 11 11 11 13 15 15
11 13 15 13 12 15 18 17 17 14 14 17 17 19 19 14 14 11 12 13 15 19 18 16 15 16 16 13 13 14 15 16 15 15 15 13 13 14 15 15
12 12 14 14 13 15 16 17 19 15 13 17 17 18 16 12 11 12 14 14 14 18 17 17 17 16 18 18 15 14 14 14 19 19 16 13 14 16 16 17
14 15 19 19 16 13 13 15 16 16 12 12 13 13 13 15 17 16 14 12 14 15 12 12 13 12 14 15 14 14 13 13 19 19 15 12 13 19 18 18
15 14 15 16 13 12 13 13 15 15 13 12 11 12 15 17 19 18 15 12 11 13 13 12 11 12 15 14 14 14 16 17 19 18 15 16 14 18 18 19
16 14 15 17 16 16 16 17 18 17 16 16 15 16 17 14 12 15 15 13 12 14 15 16 15 15 17 14 11 11 17 17 16 17 15 14 13 13 15 18
19 19 18 15 17 15 16 18 15 15 17 16 15 17 16 15 13 13 13 12 13 16 18 19 19 15 13 13 11 13 18 16 15 18 16 13 15 14 14 17
16 18 16 12 14 15 14 13 11 11 14 17 17 16 17 17 15 15 16 15 12 14 17 18 17 14 15 16 15 15 16 16 15 16 14 13 14 17 17 17
13 13 13 13 14 16 12 11 13 12 15 19 19 17 17 14 12 16 17 14 14 13 15 16 16 14 15 16 15 13 11 14 17 14 12 12 12 16 16 14
11 11 12 13 13 13 12 11 14 15 17 18 17 18 14 11 11 16 14 14 17 17 17 16 18 14 14 16 15 14 13 14 18 16 15 14 13 16 13 11
12 11 14 14 15 13 12 12 13 14 14 14 15 16 15 14 14 15 14 15 16 16 13 14 17 11 12 15 14 15 16 15 15 15 17 16 14 15 14 11
13 11 14 16 16 15 12 15 15 14 13 12 15 15 17 17 16 14 15 17 12 13 13 16 18 11 11 14 15 13 14 15 13 13 16 17 14 15 18 17
11 11 13 15 17 15 13 17 16 15 15 14 15 13 14 16 17 16 16 16 13 13 15 19 18 13 14 15 15 13 12 17 15 11 15 17 17 18 18 17
13 15 16 17 19 16 16 18 14 13 15 13 11 14 15 15 16 15 14 13 15 15 16 19 18 13 15 15 15 15 12 16 16 14 15 15 18 17 15 13
15 13 16 17 15 14 17 18 15 14 14 14 12 13 15 15 17 15 12 13 15 14 16 19 19 14 13 14 16 15 11 11 13 15 15 13 14 15 17 14
13 11 14 13 13 16 16 15 15 15 15 17 15 12 13 16 17 14 15 16 13 13 16 16 18 17 14 14 16 16 13 12 12 14 16 14 14 18 19 17
11 11 14 12 12 15 16 15 16 15 14 16 16 13 12 18 15 13 18 15 14 15 17 15 15 18 15 13 16 17 14 16 15 15 15 13 16 18 16 16
14 13 14 13 14 14 15 18 19 14 11 12 13 12 15 16 16 19 17 14 14 15 16 15 16 18 16 13 15 17 16 16 15 13 13 13 15 18 17 15
16 14 12 14 17 17 14 15 16 13 11 13 13 13 14 13 15 17 16 14 12 13 17 16 15 16 15 12 11 14 17 15 15 15 15 17 16 14 15 16
16 15 13 11 12 16 14 12 13 14 14 17 19 18 14 12 12 15 17 15 12 14 18 17 13 15 15 12 11 13 15 15 16 16 13 13 13 11 14 18
16 17 18 12 11 14 14 13 13 12 15 17 17 16 15 14 13 13 14 13 13 16 16 13 16 16 14 14 15 16 16 15 13 12 11 11 11 16 18
14 18 19 15 15 18 15 15 15 14 17 15 11 12 14 15 15 14 14 15 14 13 17 15 13 16 17 15 14 14 17 15 14 14 13 13 12 12 13 15
14 15 19 16 16 17 14 16 17 14 14 14 15 15 11 13 17 19 17 16 16 14 15 15 12 15 17 15 14 13 15 15 16 15 13 13 14 13 11 13
14 15 17 16 16 14 12 15 16 12 11 13 16 15 13 14 16 19 17 16 16 14 15 14 12 16 17 16 16 18 19 15 16 16 14 12 11 12 11 14
11 16 17 15 15 14 14 13 14 14 14 14 14 15 17 16 14 14 16 16 15 13 14 16 15 18 18 15 17 19 18 12 12 16 13 11 11 12 16 16
11 12 15 12 15 17 13 12 12 15 15 15 17 17 17 15 14 14 14 14 15 15 14 16 17 18 17 14 17 18 15 13 14 17 16 12 12 15 16 15
12 14 16 14 16 16 12 12 14 17 15 15 17 15 16 15 15 15 13 11 15 18 15 15 17 18 17 15 15 15 16 17 17 19 19 15 12 17 16 13
13 15 18 16 14 13 14 15 17 17 14 14 13 11 17 17 13 13 13 12 16 19 14 16 17 15 17 16 14 14 16 18 16 16 16 14 14 18 18 16
13 14 15 15 15 15 14 14 15 16 13 13 15 14 17 17 12 14 17 16 17 18 15 14 15 17 19 17 15 14 14 16 16 14 11 13 16 17 18 17
12 12 11 15 17 16 15 12 11 12 14 11 15 18 15 15 15 15 16 14 16 16 14 15 17 18 16 16 16 13 11 12 15 13 11 15 19 17 16 16
14 11 11 13 14 14 15 15 11 11 14 15 15 15 13 15 17 17 12 14 16 13 15 17 19 17 15 16 17 16 13 14 16 14 12 14 18 18 16 15
17 12 13 15 13 14 14 15 16 13 13 16 17 16 16 16 15 16 16 18 16 14 16 14 14 17 15 15 18 15 14 16 15 13 13 13 15 16 15 15
17 14 15 19 15 15 14 12 16 16 12 12 16 15 16 15 14 17 18 19 18 16 16 14 12 15 12 14 17 16 13 13 14 14 13 13 16 17 14 15
</data_set>
```

Appendix I

Details of the Kawabata Evaluation System

The Kawabata Evaluation System (KES-F) [104] is a systematic method of measuring the mechanical and surface properties of fabrics using very sensitive testing devices developed at Kyoto University in the 1970s.

KES-F is composed of four different machines on which a total of six tests can be performed. These machines and their respective tests are:

- Tensile & Shear Tester – Tensile parameters, Shear parameters
- Pure Bending Tester – Pure Bending parameters
- Compression Tester – Compression parameters
- Surface Tester – Surface friction parameters & Roughness parameters

In addition, the complete set of of Kawabata parameters includes measurements of "weight" (mass per unit area) and average thickness (under a standard load).

Table I summarises these characteristic values together with their physical units[1]. Tensile, bending, shearing and compression parameters relate to the fabric's overall

[1]The KES-F standard uses the unusual unit gram-force (gf) which is defined as the magnitude of the force exerted on one gram of mass by standard gravity (9.80665 m/s2). Thus, 1 gf is equal to 0.00980665 N.

elasto-mechanical behaviour, while surface properties, weight and thickness relate to specific aspects of manual interaction with the fabric.

Parameters		**Definition**	**Unit**
Tensile	LT	Linearity	-
	WT	Tensile energy	$gf \cdot cm/cm^2$
	RT	Resilience	%
	EM	Max. extension	%
Bending	B	Bending rigidity	$gf \cdot cm^2/cm$
	2HB	Hysteresis	$gf \cdot cm/cm$
Shearing	G	Shear stiffness	$gf/cm \cdot \deg$
	2HG	Hysteresis at 0.5 deg	gf/cm
	2HG5	Hysteresis at 5 deg	gf/cm
Compression	LC	Linearity	-
	WC	Compressional energy	$gf \cdot cm/cm^2$
	RC	Resilience	%
Surface	MIU	Coefficient of friction	-
	MMD	Mean deviation of MIU	-
	SMD	Geometrical roughness	μm
Weight	W	Mass/unit area	mg/cm^2
Thickness	T	Thickness at $0.5gf/cm2$	mm

Table I.1: The characteristic values of the KES-F properties

In the tests, a standard specimen size of 20×20 cm is used in three replications. All of the measurements are directional (except for compression); they are made in both the lengthwise direction and in the crosswise direction of the sample, and are performed on both sides. (The measurements are nominally made in the warp (longitudinal yarns) and weft (crosswise yarns) directions, but these descriptions are not appropriate for some classes of fabric.)

Of particular relevance to the tactile aspect of the HapTex project are the measurements of surface profile and friction performed by the surface test machine shown in figure I.1. In these tests the fabric sample is supported by a smooth steel plate and is moved at a constant rate of 1 mm/s under a contact probe; the tension of the fabric is kept at 20 gf/cm along the measurement direction. In both cases the raw data (which is sampled at 1 kHz) is electronically filtered to generate the characteristic values; details of the individual tests and the filters used are given below.

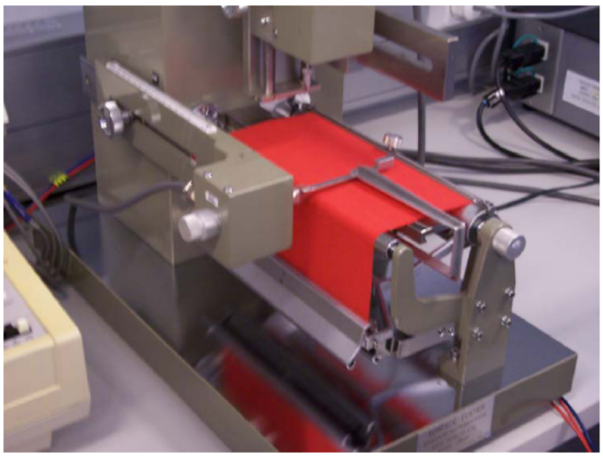

Figure I.1: The KES-F surface tester

The KES-F roughness tester measures a one-dimensional height profile along a segment of length 2 cm. The contactor of the sensor is a steel piano wire of diameter 0.5 mm, bent as shown in Figure I.2. The sensor is pressed onto the fabric with a contact force of 10 gf by a spring with stiffness 25 gf/mm. For the computation of the characteristic SMD value by the tester the analogue signal is first passed through a high-pass filter with a transfer function of the form

$$G(j\omega) = \frac{(j\omega)^2}{(j\omega)^2 + 2(j\omega)\xi\omega_n + \omega_n^2}$$

where ω is the angular frequency. In this instance, $\omega_n = 2$ rad/s, $\xi = 0.6$, giving a filter which allows signals of wavelength smaller than 1 mm to pass. The SMD value is the mean deviation of the surface in μm and is calculated as

$$SMD = \frac{1}{X} \int_0^x \mid T(x) - \overline{T} \mid dx$$

where $X = 2$ cm, x is the position of the contactor on the fabric, $T(x)$ is the thickness of the fabric at position x and $\overline{T}$ is the mean value of T. (In fact, because the mechanical response of the probe is that of a low-pass filter, the overall response of the measurement system is that of a band-pass filter. The signal processing in the HapTex software – see below – is similar, but uses two bandpass filters.)

Figure I.2: The profile probe head for the Kawabata surface tester

The surface friction is measured on the same test apparatus as the surface roughness, but with a different sensor. This consists of ten of the same piano wires used for the surface profile measurement, giving a sensor with a larger contact area as shown in figure I.3. The contactor is pressed onto the fabric by a weight with a compressional force of 50 gf.

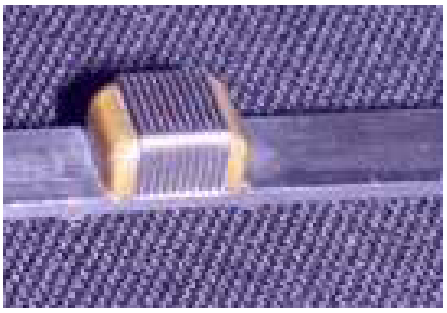

Figure I.3: The friction probe head for the Kawabata surface tester

The MIU (presumably *mu*, i.e. the coefficient of friction) and MMD values are calculated by the tester. As with the SMD value the measured signal first passes

the high-pass filter. MIU is the mean value of the coefficient of friction and MMD is its mean deviation. The definitions of both values are

$$MIU = \frac{1}{X}\int_0^x \mu(x)dx$$

$$MMD = \frac{1}{X}\int_0^x \mid \mu(x) - \overline{\mu} \mid dx$$

where $X = 2\text{cm}$, x is the position of the contactor on the fabric, $\mu(x)$ is the frictional force at position x divided by the compressional force and $\overline{\mu}$ is the mean value of μ.

Appendix J

Initial evaluation of the renderer

The work in this section was carried out by Dennis Allerkamp and his coworkers at Hanover, and is summarised from his PhD thesis [107].

J.1 The HAPTEX Tactile Renderer

As described in the main text, the raw data derived directly from the weave textures (from the surface profile data obtained during the KES-F measurements) were preprocessed to generate the appropriate small scale surface model of the given fabrics in the spatial domain.

In order to obtain a spatial frequency spectrum at different points on the fabric's surface a Fast Fourier Transform, using a Hamming window of length 4096 (corresponding to a length of 4.37 mm on the fabric), was applied at 1 mm intervals along the surface profile. As the Kawabata measurements are one-dimensional (in warp and weft direction) a two-dimensional surface has to be reconstructed (in practice, by superposition of 1D models). A very similar method for the generation of a small scale surface model is described in [108] and in more detail in [109]. It should be noted that the pre-processing is not a real-time operation – the preprocessed fabric libraries are loaded at run-time.

During manipulation of the virtual fabric, it is necessary to convert these spatial patterns back into temporal signals before they can be processed into output

signals. Remember the renderer runs in a 40 Hz loop – for each contactor in the array, data for position (on the fabric) and speed (over the fabric, weft and warp components) are obtained by the renderer every 25 ms. If the surface is represented locally as spatial frequency spectra $\overline{F_e}(k)$ and $\overline{F_a}(k)$ in weft and warp directions respectively a corresponding temporal frequency spectrum $F(\omega)$ has to be computed. When the finger moves over a surface, spatial frequency k and temporal frequency ω are related by $\omega = v \cdot k$ where v is the velocity of the finger on the surface. This results in the following conversion

$$F_e(\omega) = \overline{F_e}(\frac{\omega}{v_e})$$

$$F_a(\omega) = \overline{F_a}(\frac{\omega}{v_a})$$

where v_e and v_a denote the component of the velocity in weft and warp directions, respectively. Assuming that the vibrations in the two orthogonal directions can be simply combined by addition we obtain

$$F(\omega) = F_e(\omega) + F_a(\omega) = \overline{F_e}(\frac{\omega}{v_e}) + \overline{F_a}(\frac{\omega}{v_a})$$

The previous steps result in a frequency spectrum $F(\omega)$, which now has to be converted to a reduced spectrum, with components only at the base frequencies used to drive the tactile stimulator. We use 40 and 320 Hz as base frequencies as in the work described in the preceding chapters, and the amplitudes A_{40} and A_{320} of these frequency components are obtained by filters $F(\omega)$ into bandpass channels, centred at 40 Hz and 320 Hz. The bandpass filter functions H_{40} and H_{320} are chosen to give a tactile sensation that is similar to the sensation which would result from reproducing the whole spectrum on the tactile stimulator. (This approach is analogous to the approach used for multicolour video displays which produce almost infinite colours as mixture of only three fundamental components.) The filtering operations can be represented by

$$A_{40} = \int H_{40}(\omega) \cdot F(\omega) d\omega$$

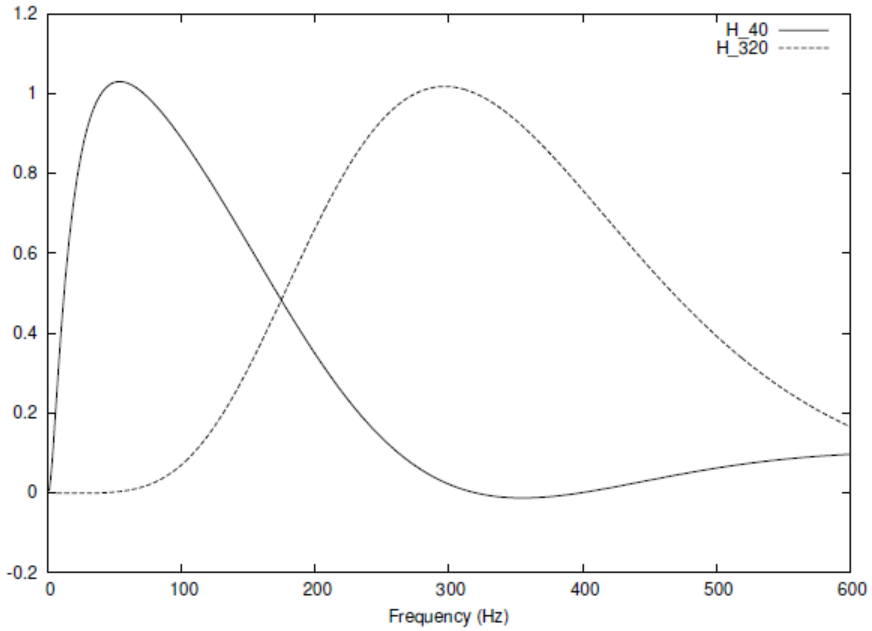

Figure J.1: The filter functions used to reduce the calculated stimulus spectrum into 40Hz and 320Hz drive amplitudes

$$A_{320} = \int H_{320}(\omega) \cdot F(\omega) d\omega$$

The functions H_{40} and H_{320} shown in figure J.1 are derived from the subjective response curves for pacinian and non-pacinian channels described in chapter 2. Whilst it could be argued that these curves are not strictly applicable they are probably the best data available and as such are a good starting point for investigation[1].

J.2 Evaluation of the renderer

A preliminary study was performed at Hanover to test the performance of the drive electronics and the tactile renderer. a tactile array of the type described in Chapter 5 (supplied by the author) coupled to an optical mouse.

[1]The test conditions under which these data were obtained were very different to those in the current scenario – a subjective response experiment using a small contactor with a rigid surround on the fingertip could conceivably be better.

Five subjects were presented with a series of real fabric samples. After each one, they were asked to examine two virtual fabrics using a texture array connected to a standard PC mouse.

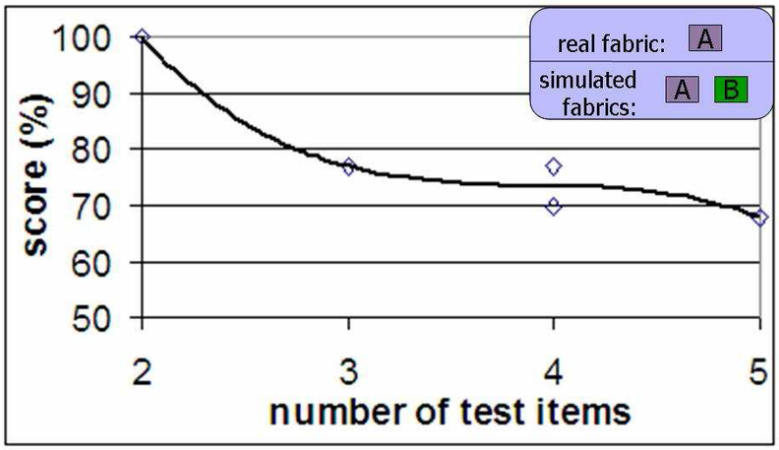

Figure J.2: Initial evaluation of the renderer

The mean scores from the 5 subjects for matching real and virtual textiles as a function of the number of textiles in the overall stimulus set are shown in Figure J.2. Chance scores are 50% in all cases. When only two textiles are involved (these having been chosen to be clearly distinguishable in the real case) all subjects score 100%. When additional "intermediate" textiles are added to the set, the task becomes more difficult and scores fall progressively. This is an encouraging result – it demonstrates that it is possible to achieve a correspondence between subjects' perceptions in the real and virtual cases. It should be noted that time constraints within the HAPTEX project allowed little time for "tuning" the renderer. The initial implementation of the rendering strategy remained essentially unchanged. It seems likely that better performance is possible with further development.

Bibliography

[1] L. Kinsler, A. Frey, A. Coppens, and J. Sanders, *Fundamentals of Acoustics*, p. 84. John Wiley & Sons, 4th ed., 2000.

[2] C. Sherrick and R. Cholewiak, *Handbook of Perception and Human Performance*, ch. Cutaneous sensitivity, pp. 1–58. New York: Wiley, 1986.

[3] A. C. Newberry, M. J. Griffin, and M. Dowson, "Driver perception of steering feel," *Proceedings of the Institution of Mechanical Engineers, Part D: Journal of Automobile Engineering*, vol. 221, no. 4, pp. 405–415, 2007.

[4] J. Cui, S. Tosunoglu, R. Roberts, C. Moore, and D. Repperger, "A review of teleoperation system control," in *Proceedings of the Florida Conference on Recent Advances in Robotics*, (Florida), May 2003.

[5] R. McCloy and R. Stone, "Clinical review: Science, medicine, and the future: Virtual reality in surgery," *British Medical Journal*, vol. 323, Oct. 2001.

[6] I. Summers, M. Peake, and M. Martin, "Field trials of a tactile acoustic monitor for the profoundly deafpeake mamartin mc," *British Journal of Audiology*, vol. 15, no. 3, pp. 195–199, 1981.

[7] P. Cooper, *Vibrotactile transducers.* PhD thesis, School of Physics, University of Exeter, 1994.

[8] P. Wright, *Instrumentation and procedures for measurements on tactile perception.* PhD thesis, School of Physics, University of Exeter, January 1997.

[9] I. Summers and C. Chanter, "A broadband tactile array on the fingertip," *Journal Of The Acoustical Society Of America*, vol. 112, pp. 2118–2126, Nov 2002.

[10] G. Robles-De-La-Torre, "The importance of the sense of touch in virtual and real environments," *IEEE Multimedia*, vol. 13, pp. 24–30, 2006.

[11] G. Jansson and L. Monaci, "Identification of real objects under conditions similar to those in haptic displays: providing spatially distributed information at the contact areas is more important than increasing the number of areas.," *Virtual Reality*, vol. 9, pp. 243–249, 2006.

[12] R. H. Gault, "Recent developments in vibro-tactile research," *Journal of the Franklin Institute*, vol. 221, pp. 703–719, 1936.

[13] F. A. Geldard, "Some neglected possibilities of communication," *Science*, vol. 131, pp. 1583–1588, 1960.

[14] H. Tan, N. Durlach, C. Reedr, and W. Rabinowitz, "Information transmission with a multifinger tactual display," *Perception and Psychophysics*, vol. 61, no. 6, pp. 993–1008, 1999.

[15] J. Bliss and J. Linvill, "A direct translation reading aid for the blind," *Proceedings of the IEEE*, vol. 54, pp. 40–51, Jan. 1966.

[16] J. B. F. van Erp, "Presenting directions with a vibrotactile torso display," *Ergonomics*, vol. 48, no. 3, pp. 302–313, 2005.

[17] A. Wing, ed., *Spatial factors in vibrotactile pattern perception*, July 2001.

[18] L. M. Brown, *Tactons: Structured Vibrotactile Messages for Non-Visual Information Display*. PhD thesis, University of Glasgow, 2007.

[19] A. Chan, K. MacLean, and J. McGrenere, "Designing haptic icons to support collaborative turn-taking," *Int. J. Human-Computer Studies*, vol. 66, pp. 333–355, 2008.

[20] J. Pasquero, V. Levesque, Q. Wang, V. Hayward, and K. E. MacLean, "Haptically enabled handheld information display with distributed tactile transducer.," *IEEE Transactions on Multimedia*, vol. 9, no. 4, pp. 746–753, 2007.

[21] ISMRM, *Cortical activation associated with tactile movement in attentive subjects*, May 2006.

[22] B. Forslind and M. Lindberg, eds., *Skin, Hair, and Nails: Structure and Function*. CRC Press, 2003.

[23] J. Manschot and A. Brakkee, "The measurement and modelling of the mechanical properties of human skin in vivo – ii. the model," *J. Biomechanics*, vol. 19, no. 7, pp. 517–521, 1986.

[24] R. Johansson and Å. Vallbo, "Tactile sensibility in the human hand: Relative and absolute densities of four types of mechanoreceptive units in glabrous skin," *Journal of Physiology*, vol. 286, pp. 283–300, 1979.

[25] J. A. Kiernan and M. L. Barr, *Barr's the Human Nervous System: An Anatomical Viewpoint*. Lippincott Williams and Wilkins, 2008.

[26] B. C. Paré M and C. O., "Paucity of presumptive ruffini corpuscles in the index finger pad of humans.," *Journal of Comparative Neurology*, 2003.

[27] M. Mendelson and W. R. Loewenstein, "Mechanisms of receptor adaptation," *Science*, vol. 144, pp. 554–555, May 1964.

[28] Mosby, *Mosby's Medical Dictionary*, ch. K. Elsevier, 8th ed., 2009.

[29] K. O. Johnson, T. Yoshioke, and F. Vega-Bermudez, "Tactile functions of mechanoreceptive afferents innervating the hand.," *Journal of Clinical Neurophysiology*, vol. 17, pp. 539–558, 2000.

[30] R. Hallin, "Microneurography in relation to intraneural topography: somatotopic organisation of median nerve fascicles in humans.," *Journal of*

Neurology, Neurosurgery and Psychiatry, vol. 53, pp. 736–744, September 1990.

[31] K. O. Johnson and G. Lamb, "Neural mechanisms of spatial tactile discrimination: Neural patterns evoked by braille-like dot patterns in the monkey.," *Journal of Physiology*, vol. 310, pp. 117–144, 1981.

[32] R. Lamotte and J. Whitehouse, "Tactile detection of a dot on a smooth surface: Peripheral neural events.," *The American Psychological society*, vol. 86, pp. 1109–1128, 1986.

[33] J. Philips, R. Johansson, and K. O. Johnson, "Responses of human mechanoreceptive afferents to embossed dot arrays scanned across fingerpad skin.," *Journal Of Neuroscience*, vol. 12, pp. 827–839, 1992.

[34] E. Gardner, C. Palmer, H. Hämäläinen, and S. Warren, "Simulation of motion on the skin v. effect of stimulus temporal frequency on the representation of moving bar patterns in primary somatosensory cortex of monkeys.," *Journal of Neurophysiology*, vol. 1, pp. 37–63, 1992.

[35] E. Gardner and B. Sklar, "Discrimination of the direction of motion on the human hand: a psychophysical study of stimulation parameters.," *The American Physiological Society*, vol. 6, pp. 2414–2429, 1994.

[36] S. Ruiz, P. Crespo, and R. Romo, "Representation of moving tactile stimuli in the somatic sensory cortexof awake monkeys.," *The American Physiological Society*, vol. 3, pp. 525–537, 1995.

[37] G. Gescheider, *Psychophysics: the fundamentals.* Lawrence Erlbaum Associates, 3rd ed., 1997.

[38] D. D. and, *Conciousness explained.* Penguin Books, 1991.

[39] S. Oldfield and J. Phillips, "The spatial characteristics of tactile form perception.," *Perception*, vol. 12, no. 5, pp. 615–626, 1983.

[40] D. Liddle and B. Foss, "The tactile perception of size: Some relationships with distance and direction.," *The Quarterly Journal of Experimental Psychology*, vol. 15, pp. 217–219, September 1963.

[41] M. Rinker and J. Craig, "The effect of spatial orientation on the perception of moving tactile stimuli.," *Perception and Psychophysics*, vol. 56, no. 3, pp. 356–362, 1994.

[42] S. Lederman, "Auditory texture perception," *Perception*, vol. 8, pp. 93–103, 1979.

[43] K. Dandekar and M. Srinivasan, "Tactile coding of object curvature by slowly adapting mechanoreceptors.," *Advances in Bioengineering.*, vol. 28, pp. 41–42, 1994.

[44] S. Lederman, "The perception of surface roughness by active and passive touch.," *Bulletin of the Psychonomic Society*, vol. 18, no. 5, pp. 253–255, 1981.

[45] S. Lederman and M. Taylor, "Fingertip force, surface geometry and the perception of roughness by active touch.," *Perception and Psychophysics*, vol. 12, no. 5, pp. 401–408, 1972.

[46] M. Taylor and S. Lederman, "Tactile roughness of grooved surfaces - model and effect of friction," *Perception and Psychophysics*, vol. 17, pp. 23–36, 1975.

[47] K. Tanaka, T. Ifukube, and C. Yoshimoto, "Some characteristics of the tactile recognition of patterns with raised dots.," *Japanese Journal of Medical Electronics and Biological Engineering*, vol. 20, no. 5, pp. 301–306, 1982.

[48] G. Lamb, "Tactile discrimiantion of textured surfaces: psychophysical performance measurements in humans.," *Journal of Physiology*, vol. 338, pp. 551–565, 1983.

[49] R. Irwin, *Measurements relating to the tactile discrimination of paper.* PhD thesis, School of Physics, University of Exeter, September 1998.

[50] C. Connor and K. O. Johnson, "Neural coding of tactile texture: comparison of spatial and temporal mechanisms for roughness perception.," *Neurosciences*, vol. 12, no. 9, pp. 3414–3426, 1992.

[51] D. Katz, "Der aufbau der tastwelt.," *Zeitschrift für Psychologie*, vol. 11, 1925.

[52] S. Bensmaia and M. Hollins, "The vibrations of texture," *Somatosensory and Motor Research*, vol. 20, pp. 33–43, 2003.

[53] J. Yau, M. Hollins, and S. Bensmaia, "Textural timbre: the perception of surface microtexture depends in part on multimodal spectral cues," *Communicative and Integrative Biology*, vol. 2, pp. 1–3, 2009.

[54] J. Gibson, "Observations on active touch.," *PsychologyReview*, vol. 69, pp. 477–491, 1962.

[55] S. Lederman and M. Taylor, "Fingertip force, surface geometry and the perception of roughness by active touch.," *Perception and Psychophysics*, vol. 12, no. 5, pp. 401–408, 1972.

[56] J. Craig, "Vibrotactile letter recognition: The effects of a masking stimulus.," *Perception and Psychophysics*, vol. 20, pp. 317–326, 1976.

[57] S. Bolanowski Jr, G. Gescheider, R. Verrillo, and C. Checkosky, "Four channels mediate the mechanical aspect of the sense of touch.," *Journal Of The Acoustical Society Of America*, vol. 84, pp. 1680–1694, 1988.

[58] C. Van Doren, "A model of spatiotemporal tactile sensitivity linking psychophysics to tissue mechanics.," *Journal Of The Acoustical Society Of America*, vol. 85, pp. 2065–2080, 1989.

[59] R. Verrillo, A. Fraioli, and R. Smith, "Sensation magnitude of vibrotactile stimuli.," *Perception and Psychophysics*, vol. 6, pp. 366–372, 1969.

[60] C. Van Doren, "The effect of a surround on vibrotactile threshold: Evidence for spatial and temporal independence in the non-pacinian (np-i) channel.," *Journal Of The Acoustical Society Of America*, vol. 87, pp. 2655–2661, 1990.

[61] J. Craig, "Vibrotactile spatial summation.," *Perception and Psychophysics*, vol. 4, pp. 351–354, 1968.

[62] R. Verrillo, "Effects of contactor area on the vibrotactile threshold.," *Journal Of The Acoustical Society Of America*, vol. 37, pp. 843–846, 1963.

[63] H. Mujiser, "An inidcation for spatial integration in a non-pacinian mechanoreceptor system?," *Journal Of The Acoustical Society Of America*, vol. 96, pp. 781–785, August 1994.

[64] J. Scheibert, S. Leurent, A. Prevost, and G. Debrégeas, "The role of fingerprints in the coding of tactile information probed with a biomimetric sensor.," *Science*, vol. 323, pp. 1503–1506, January 2009.

[65] I. Summers, C. Chanter, A. Southall, and A. Brady, "Results from a tactile array on the fingertip," in *Proceedings of Eurohaptics 2001*, 2001.

[66] J. C. Stevens, E. Foulke, and M. Q. Patterson, "Tactile acuity, aging, and braille reading in long-term blindness," *Journal of Experimental Psychology: Applied*, vol. 2, no. 2, pp. 91–106, 1996.

[67] J. Zwislocki, "Theory of temporary auditory summation.," *Journal Of The Acoustical Society Of America*, vol. 32, pp. 1046–1060, 1960.

[68] R. Verrillo and G. Gescheider, "Enhancement and summation in the perception of two successive vibrotactile stimuli," *Perception and Psychophysics*, vol. 18, pp. 128–136, 1975.

[69] G. Gescheider and R. Verrillo, "Contralateral enhancement and suppression of vibrotactile sensation.," *Perception and Psychophysics*, vol. 32, no. 1, pp. 69–74, 1982.

[70] S. Lederman, *Skin and touch.*, vol. 7 of *Encyclopedia of human biology*, pp. 51–63. Academic Press, 1991.

[71] P. Bach-y Rita, C. Collins, F. Sauders, B. White, and L. Scadden, "Vision substitution by tactile image projection," *Nature*, vol. 221, pp. 963–964, 1969.

[72] D. Sparks, L. Ardell, M. Bourgeois, B. Wiedmer, and P. Kuhl, "Investigating the mesa (multipoint electrotactile speech aid): The transmission of connected discourse.," *J. Acoust. Soc. Am.*, vol. 65, no. 3, pp. 810–815, 1979.

[73] Kajimoto, Kawakami, and Tachi, "Optimal design method for selective nerve stimulation and its application to electrocutaneous display," in *Proceedings of the Tenth Symposium on Haptic Interfaces for Virtual Environment and Teleoperator Systems*, pp. 303–310, March 2002.

[74] K. Hirota and M. Hirose, "Surface display: Concept and implementation approaches," in *Proceedings of the International Conference on Artificial Reality and Tele-Existance*, pp. 185–192, November 1995.

[75] D. Kontarinis, J. Son, W. Peine, and R. Howe, "A tactile shape sensing and display for teleoperated manipulation.," in *Proceedings of the IEEE International Conference on Robotics and Automation*, pp. 641–646, 1995.

[76] P. Taylor, A. Hosseini-Sianaki, and C. Varley, "An electrorheological fluid-based tactile array for virtual environments," in *Proceedings of the IEEE International Conference on Robotics and Automation*, (Minnesota), April 1996.

[77] Y. Liu, R. Davidson, and P. Taylor, "Touch sensitive electrorheological fluid based tactile display," *Journal of Smart Materials and Structures*, vol. 14, pp. 1563–1568, December 2005.

[78] Y. Liu, J. Ngu, R. Davidson, and P. Taylor, "Tactile display array based on magnetorheological fluid," in *Proc. SPIE 6173*, 2006.

[79] A. Yamamoto, B. Cros, H. Hashimoto, and T. Higuchi, "Control of thermal tactile display based on prediction of contact temperature," in *Proceedings of the IEEE International Conference on Robotics and Automation*, pp. 1536–1541, April 2004.

[80] T. Nara, M. Takasaki, T. Maeda, T. Higuchi, S. Ando, and S. Tachi, "Surface Acoustic Wave (SAW) tactile display based on properties of mechanoreceptors," in *Virtual Reality Conference*, pp. 13–20, March 2001.

[81] T. Iwamato, D. Akaho, and H. Shinoda, "High resolution tactile display using acoustic radiation pressure," in *Proceedings of the SICE Annual Conference*, pp. 1239–1244, August 2004.

[82] N. Asamura, N. Yokoyama, and H. Shinoda, "Selectively stimulating skin receptors for tcatile display.," *IEEE Computer Graphics and Applications*, vol. 18, no. 6, pp. 32–37, 1998.

[83] SICE, *A cutaneous feeling display using suction pressure.*, vol. 3, 2003.

[84] C. Moy, C. Wagner, and R. Fearing, "A compliant tactile display for teletaction," in *Proceedings of the IEEE International Conference on Robotics and Automation*, pp. 3409–3415, 2000.

[85] W. Schneider, *The tactile array stimulator*, vol. 9 of *John Hopkins APL Technical Digest*, pp. 39–43. John Hopkins Universiy Applied Physics Laboratory, 1988.

[86] P. M. Taylor, A. Moser, and A. Creed, "A sixty-four element tactile display using shape memory alloy wires," *Displays*, vol. 18, pp. 163–168, May 1998.

[87] M. Hafez, M. Benali Khoudja, J.-M. Alexandre, and G. Hamon, "Electromagnetically driven high-density tactile interface based on a multi-layer approach.," in *Proceedings of DSV-IS*, June 2003.

[88] J. Streque, A. Talbi, R. Viard, P. Pernod, and V. Preobrazhensky, "Elaboration and test of high energy density magnetic micro-actuators for tactile display applications," in *Proceedings of the Eurosensors XXIII conference*, vol. 1, pp. 694–697, 2009.

[89] K.-U. Kyung, M. Ahn, D.-S. Kwon, and M. Srinivasan, "A compact broadband tactile display and its effectiveness in the display of tactile form.," in *Proceedings of World Haptics Conference*, pp. 600–601, IEEE Computer Society, March 2005.

[90] A. Shigeki and I. Yasushi, "Generation methods of various tactile sensations by variable frequency stimulation on the texturedisplay2r," in *Proceedings of the Virtual Reality Society of Japan Annual Conference*, pp. 2C2–2C6, 2005.

[91] C. Van Doren, D. Pelli, and R. Verrillo, "A device for measuring tactile spatiotemporal sensitivity.," *Journal Of The Acoustical Society Of America*, vol. 81, pp. 1906–1915, 1987.

[92] J. Bliss, "The optacon," in *Proceedings of the 1974 Conference on Engineering Devices in Rehabilitation*, 1974.

[93] J. Craig and C. Sherrick, *Tactual perception: A source book*, ch. Dynamic tactile displays., pp. 209–233. New York: Cambridge University Press, 1982.

[94] V. Levesque, J. Pasquero, V. Hayward, and M. Legault, "Display of virtual braille dots by lateral skin deformation: Feasibility study.," *ACM Transactions on Applied Perception*, vol. 2, pp. 132–149, April 2005.

[95] Q. Wang, V. Levesque, J. Pasquero, and V. Hayward, "A haptic memory game using the stress2 tactile display," in *CHI '06 extended abstracts on Human factors in computing systems.*, 2006.

[96] C. M. Chanter, *Design and Development of a vibrotactile stimulator array for the fingertip.* Doctoral thesis, University of Exeter, Sep 1999.

[97] L. Bernstein, S. Eberhardt, and M. Demorest, "Single channel vibrotactile supplemants to visual perception of intonation and stress.," *Journal Of The Acoustical Society Of America*, vol. 85, pp. 397–405, 1989.

[98] R. Cholewiak and A. Collins, "Vibrotactile localization on the arm: effects of place, space and age," *Perception and Psychophysics*, vol. 65, pp. 1058–1077, 2003.

[99] P. B. y Rita, K. A. Kaczmarek, M. E. Tyler, and M. Garcia-Lara, "Form perception with a 49-point electrotactile stimulus array on the tongue: A technical note," *Journal of Rehabilitation Research and Development*, vol. 35, pp. 427–430,, 1998.

[100] N. V. Garcia-Hernandez, N. G. Tsagarakis, and D. G. Caldwell, "Feeling through tactile displays: A study on the effect of the array density and size on the discrimination of tactile patterns," *IEEE T. Haptics*, vol. 4, no. 2, pp. 100–110, 2011.

[101] A. Kappers, "Intermediate frames of reference in haptically perceived parallelity," in *Proceedings of World Haptics Conference*, pp. 3–11, IEEE Computer Society, March 2005.

[102] R. Verrillo, "Comparison of vibrotactile threshold and suprathreshold responses in men and women.," *Perception and Psychophysics*, vol. 26, pp. 20–24, 1979.

[103] D. Allerkamp, G. Böttcher, F.-E. Wolter, A. Brady, J. Qu, and I. Summers, "A vibrotactile approach to tactile rendering," *The Visual Computer*, vol. 23, pp. 97–108, 2007.

[104] S. Kawabata, *The standardization and analysis of hand evaluation.* The hand evaluation and standardization committee, Osaka, 2nd ed., 1980.

[105] I. Summers, "Final demonstrator and final integration report," Tech. Rep. 5.2, Haptex Consortium, 2007.

[106] C. Pouya, "Tactile perception of spatiotemporal cues and their inverses across the fingertip," Master's thesis, University of Exeter, 2008.

[107] D. Allerkamp, *Generation of Stimuli Supporting Tactile Perception of Textiles in a VR System.* PhD thesis, University of Hannover, June 2009.

[108] G. Huang, D. Metaxas, and M. Govindaraj, "Feel the "fabric": an audio-haptic interface.," in *SCA '03: Proceedings of the 2003 ACM SIGGRAPH/Eurographics Symposium on Computer animation*, pp. 52–61, Eurographics Association, 2003.

[109] G. Huang, *Feel the "fabric" via the phantom.* PhD thesis, University of Pennsylvania, 2002.